DEVELOPMENT OF NOVEL NMR PULSE SEQUENCES

VOLUME 2

PAUL CHRISTOPHER DOUGLAS

Doctor of Philosophy

ASTON UNIVERSITY

September 2003

APPENDICES

Table of Contents

Table of Figures

Appendix A1

Appendix A2

Appendix A3

Appendix A4

Appendix A5

Appendix A6

Appendix A7

Appendix A8

Appendix A9

Appendix A10

Appendix A11

Appendix A1 Fundamental theory of Nuclear Magnetic Resonance Spectroscopy

Nuclear magnetic resonance spectroscopy (NMR) exploits the interactions that occur between the naturally occurring magnetic fields of nuclei and artificially created magnetic fields of the NMR spectrometer. In common with all branches of spectroscopy, NMR yields spectra, which are comprised of spectral lines, the intensity, shape and frequency of which are diagnostic of the molecular surroundings of the nucleus. However, NMR is limited to the study of nuclei that possess spin angular momentum from which the magnetic properties of the nucleus are derived.

A1.1 Spin angular momentum

The atomic nucleus is comprised of neutrons and protons which both intrinsically possess spin angular momentum. The composition of the nucleus, in terms of the numerical weighting of protons and neutrons, determines whether spin angular momentum is imparted to that isotope. The spin angular momentum of the isotope, characterised by the nuclear spin quantum number **I**, takes on integer values (**I** = 0, 1, 2,...,) when the atomic mass number is even and half-integer values (**I** = 1/2, 3/2,...,) when the atomic mass number is odd. The following stipulations also apply to isotopes with even atomic mass numbers:

- when the number of protons and neutrons are both even, the isotope is devoid of spin angular momentum (**I** = 0) and is invisible to NMR.
- When the number of protons and neutrons are both odd, the isotope possesses spin angular momentum and the value of **I** takes integer values greater than zero.

Figure A1.1 specifies some isotopes that possess spin angular momentum and their corresponding spin quantum numbers and relative isotopic abundances. It is useful that most nuclei have isotopes that possess spin angular momentum and are hence observable by NMR techniques. For example, protons (^{1}H) have a spin quantum number **I** = ½ and a natural isotopic abundance of approximately100%. However, the approximately 98.9% abundant ^{12}C isotope, is devoid of spin angular momentum (**I** = 0) and is hence invisible to NMR. However the ^{13}C isotope, which is only 1.1% abundant, does possess spin angular momentum (**I** = ½) and provides a basis for the study of carbon nuclei by NMR.

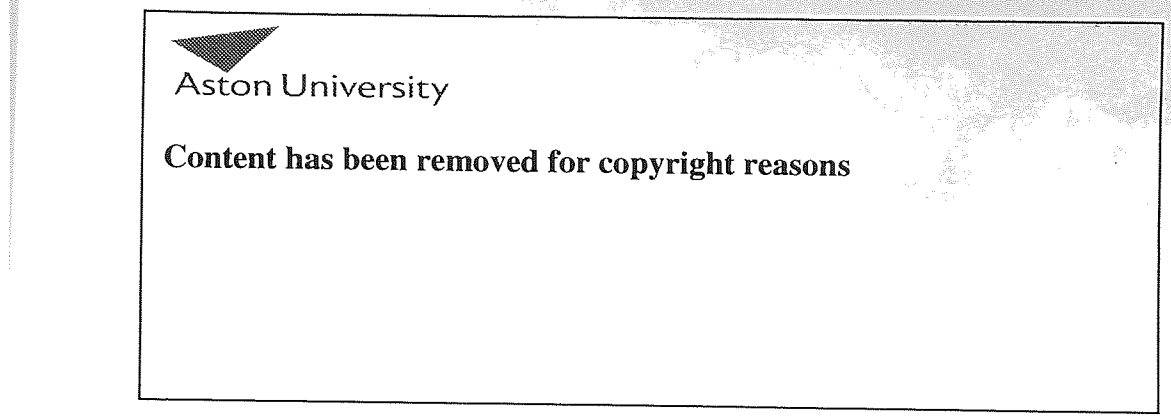

Figure A1.1 **Table of common isotopes and their magnetic properties. Taken from publication by Levitt [52]**

The total magnitude of the spin angular momentum, **P**, of a nucleus is given by:

$$P = \hbar\sqrt{I(I+1)} \qquad \text{A1- 1.1}$$

where $\hbar$ is the reduced Planck's constant, $h/2\pi$.

Spin angular momentum is quantised and may only take discrete observable values of magnitude $m\hbar$, where m is the magnetic quantum number, which takes the values **I**, **I**-1, **I**-2,…,-**I**. Therefore there are 2**I**+1 total number of observable values of spin angular momentum, which corresponds to 2**I**+1 separate and equally spaced spin angular momentum states.

Spin angular momentum is a vector quantity and its direction is similarly quantised (*space quantised*). Therefore, along an arbitrarily chosen axis, i.e., the Z-axis, there are 2**I**+1 Z-components of **P**. For a **I** = ½ nucleus this corresponds to $P_z = +m\hbar$ *and* $-m\hbar$, which corresponds to $+1/2\hbar$ and $-1/2\hbar$ respectively.

The quantisation of angular momentum necessitates the quantisation of energy. In the absence of an external influence, the $2\mathbf{I}+1$ magnitudes and directions all have the same energy.

A1.2 The nuclear magnetic moment μ

The action of spin angular momentum **P** upon a charged nucleus imparts a magnetic property quantified as the magnetic moment **μ**. Consequently, **μ** is also a vector quantity and is necessarily related to **P** by a proportionality constant called the gyromagnetic ratio γ, which is unique to each nucleus:

$$\mu = \gamma P \qquad \text{A1- 1.2}$$

The magnetic moment is parallel to the spin angular momentum vector. The sign of γ is dependant on the mutual orientation of the magnetic moment vector and spin angular momentum vector: negative values account for anti-parallel orientations and positive values account for parallel orientations.

The magnitude of γ is a convenient measure of the strength of the magnetic moment and is valuable for the comparison of nuclei. It will be shown that the magnitude of γ dictates the sensitivity of a nucleus to NMR. ^{13}C, which has a small γ and poor natural isotopic abundance, is therefore inherently disadvantaged to observation by NMR. Indeed many methods have been developed to enhance the spectra of ^{13}C and other *dilute* (poor natural isotopic abundance) insensitive nuclei, upon which work reported in this thesis relies.

A1.3 Types of magnetic nuclei: Dipolar and Quadrupolar

Nuclei of spin $\mathbf{I} = ½$ that possess the same number of protons and neutrons are assumed to be perfectly spherical as a result of the symmetrical distribution of charge at the nucleus. Consequently, $\mathbf{I} = ½$ nuclei are dipolar with respect to the magnetic moment **μ**.

In contrast, nuclei of $\mathbf{I} > ½$ that possess unequal numbers of protons and neutrons possess an asymmetric distribution of charge at the nucleus and are non- spherical. Consequently, $\mathbf{I} > ½$ nuclei exhibit a local electric field gradient, or electric quadrupole moment, in addition to the magnetic moment. The behaviour of dipolar and quadrupolar nuclei in terms of their

interactions with external magnetic fields is vastly different. Work detailed in this thesis is focused upon $\mathbf{I} = ½$ nuclei and so quadrupolar nuclei are not considered further.

A1.4 The effect of an external magnetic field $\mathbf{B_0}$ on $\mathbf{I} = ½$ nuclei

When introduced to a strong external static magnetic field of a NMR magnet, $\mathbf{B_0}$, the degeneracy of the spatial quantisation of $\boldsymbol{\mu}$ is removed. The quantisation axis is no longer arbitrary and coincides with the direction of $\mathbf{B_0}$, which is assumed to be coincident with the z-axis of a set of Cartesian co-ordinates. The magnetic moment can align itself with respect to the direction of $\mathbf{B_0}$ according to the $2\mathbf{I}+1$ allowed orientations, as defined earlier by m. As the spatial degeneracy has been removed, the energetic degeneracy is similarly removed. The energy of the nucleus in a magnetic field of magnitude $\mathbf{B_0}$ is therefore given by:

$$E = -\gamma m \hbar B_0 \qquad \text{A1- 1.3}$$

There are $2\mathbf{I}+1$ non-degenerate energy levels corresponding to the $2\mathbf{I}+1$ values of m, which are each separated by $\gamma\hbar\mathbf{B_0}$. Therefore, for a $\mathbf{I} = ½$ nucleus the spin energy levels are $+1/2\gamma\hbar\mathbf{B_0}$ ($\boldsymbol{\alpha}$) and $-1/2\gamma\hbar\mathbf{B_0}$ ($\boldsymbol{\beta}$), which correspond to the alignment of $\boldsymbol{\mu}$ with and against $\mathbf{B_0}$ respectively (Figure A1.2). The $\boldsymbol{\alpha}$ spin state is considered to be the lowest energy and the $\boldsymbol{\beta}$ spin state the highest energy. The terms $\boldsymbol{\alpha}$ and $\boldsymbol{\beta}$ are the corresponding wavefunctions of the states (Appendix A12) and the energies $+1/2\gamma\hbar\mathbf{B_0}$ ($\boldsymbol{\alpha}$) and $-1/2\gamma\hbar\mathbf{B_0}$ ($\boldsymbol{\beta}$), are corresponding eigenvalues. The $\boldsymbol{\alpha}$ and $\boldsymbol{\beta}$ spin states are sometimes referred to as the Zeeman states [4].

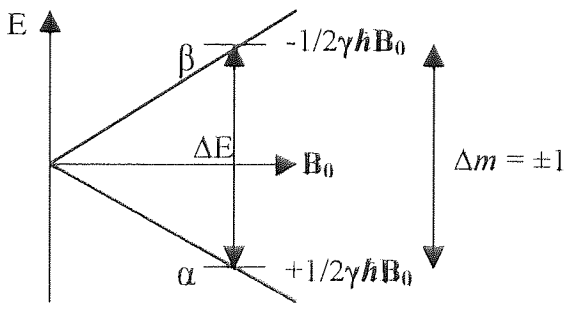

Figure A1.2 Quantisation of energy of the nucleus in the static magnetic field $\mathbf{B_0}$

A1.4.1 The resonance condition

Spectroscopic transitions can be stimulated by application of energy, which is equal to the energy difference ΔE, between the $2\mathbf{I}+1$ spin energy levels (figure A1.2). According to the conservation of momentum, observable transitions can only be stimulated between the $2\mathbf{I}+1$

energy states that correspond to a change of one quantum in the magnetic quantum number $\boldsymbol{m}$ ($\Delta\boldsymbol{m} = \pm 1$). Such transitions are called single quantum transitions (SQT).

Expressed in terms of the Bohr frequency condition the energy separation, ΔE, between the spin energy levels is given by

$$\Delta E = \frac{1}{2}\gamma\hbar B_0 - \left(-\frac{1}{2}\gamma\hbar B_0\right) = \gamma\hbar B_0 \Delta m = h\upsilon . \qquad \text{A1- 1.4}$$

Spectroscopic transitions in NMR are achieved by the application of magnetic fields in the form of radio-frequency energy in the megahertz range. The comparatively small energy difference between spin states, lends to the inherent insensitivity of NMR, with respect to other branches of spectroscopy. Since the sensitivity of spectroscopic techniques relies on the energy gaps between energy states, a major thrust in the development of NMR is to increase the static magnetic field strengths $\mathbf{B_0}$.

A1.4.2 The Larmor frequency and nuclear precession

When exposed to $\mathbf{B_0}$, a torque is exerted on the magnetic moment of the nucleus. Consequently, the nucleus precesses about the axis of $\mathbf{B_0}$, such that the magnetic moment traces out a path upon the surface of a cone of half angle $\cos\theta = \boldsymbol{m}/[\mathbf{I}(\mathbf{I}+1)]^{1/2}$. Precessional motion preserves the z-component of $\boldsymbol{\mu}$ according to the $2\mathbf{I}+1$ allowed values, however, the transverse components to the field are continuously modulated according to the frequency of precession. The magnetic moment precesses at a constant angular velocity of $-\gamma\mathbf{B_0}$, which rather misleadingly is commonly termed the Larmor frequency, $\boldsymbol{\omega}$.

$$\omega = -\gamma B_0 \qquad \text{A1- 1.5}$$

Of course, one should restate the equation above as $\boldsymbol{\omega} = -\gamma\mathbf{B_0}/2\pi$ to express a frequency, however, to remain consistent with popular convention, the earlier will be used hereafter.

It is evident that the Larmor frequency is in fact equal to the energy difference between the spin states, $\boldsymbol{h\nu}$. Therefore, to cause resonance one must apply radio-frequency radiation at the Larmor frequency of the nucleus under scrutiny.

The sign of ω depends upon the sign of γ, and refers to the sense of precession about $\mathbf{B_0}$: for positive γ, the sense of precession is considered to be left-handed and for nuclei with negative γ, is considered to be right-handed. Figure A1.3 illustrates precessional motion for a $\mathbf{I} = ½$ nucleus with $\gamma > 0$

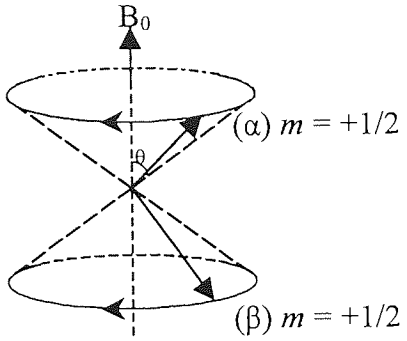

Figure A1.3 Nuclear precession in $\mathbf{B_0}$ for a $\mathbf{I} = ½$ nucleus with $\gamma > 0$.

The classical motion of nuclear precession is central to a basic understanding of NMR experiments. Indeed, the rest of this rather classical treatment of NMR relies upon it. More mathematical descriptions of NMR can be obtained from the following references [4, 53-54].

A1.5 An ensemble of I = ½ nuclei

Thus far, only a single nuclear isotope has been considered. When an ensemble of $\mathbf{I} = ½$ nuclei is introduced to $\mathbf{B_0}$, the individual nuclei adopt one of the two allowed angular momentum energy states α or β. The corresponding *populations* or number of nuclei that occupy one of the two spin states are, N_α and N_β respectively, and the relative occupancy of the states at thermal equilibrium obeys a Boltzmann distribution.

$$\frac{N_\alpha}{N_\beta} = e^{-\frac{\Delta E}{kT}} \qquad \text{A1- 1.6}$$

Where $\mathbf{T}$ is the absolute temperature in Kelvin and k is the Boltzmann constant.

A small excess of the total number of nuclei in the system populate the more energetically favourable α spin state. For protons at 300K, in a magnetic field, $\mathbf{B_0}$, of 9.4 Tesla (which corresponds to a proton Larmor frequency of 400MHz) the corresponding population excess

in α spin state is one proton in 300000. $\mathbf{B_0}$ is usually quoted in terms of the proton Larmor frequency that it invokes.

A1.6 Longitudinal magnetisation

The small excess of nuclei that populate the α spin state causes the sample to develop a longitudinal magnetisation, which is a coherent summation of the z-components of the magnetic moment vectors (μ_z) of the individual nuclei. Described in terms of classical vectors, $\mathbf{M_z}$ lies coincident with $\mathbf{B_0}$ and at thermal equilibrium is called the equilibrium longitudinal magnetisation $\mathbf{M_0}$ (Figure A1.4).

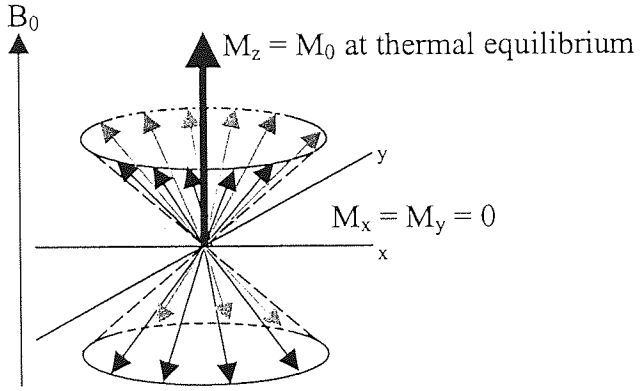

Figure A1.4 Longitudinal magnetisation

The time varying incoherent transverse components of the magnetic moment μ_{xy}, caused by continual precession, do not give rise to a coherent summation. Consequently, the transverse magnetisations, $\mathbf{M_x}$ and $\mathbf{M_y}$, are zero at equilibrium.

NMR spectroscopy relies on the manipulation and detection of longitudinal magnetisation. The sensitivity of NMR is therefore dependent upon the population excess in the lower spin states, which is dependent upon the inherent properties of the nucleus, e.g., the magnitude of γ and isotopic abundance. Furthermore, to maximise sensitivity one must use large magnitudes of $\mathbf{B_0}$, work at reasonably low temperatures, and use concentrated analytical samples.

A1.7 Radiofrequency (*r.f.*) pulses

NMR transitions are induced by applying radio-frequency (*r.f.*) energy at the Larmor frequency of the nuclei. It is shown in appendix A3 that nuclei of the same isotopic species

do not exhibit the same Larmor frequency, and a range of frequencies exist. Indeed, the Larmor frequency of a nucleus is diagnostic of the surrounding molecular environment, which is manifested in spectra as the chemical shift. Consequently, to observe simultaneously the spectra of nuclei of a given isotope, the radio frequency field, $\mathbf{B_1}$, must encompass the entire 'bandwidth' of Larmor frequencies. This is achieved using non-frequency selective 'hard-pulses', hence the name, pulse FT NMR. FT represents, Fourier transform, which is the specific mathematical transformation of the experimental data that gives rise to the frequency spectrum. This is described in terms of a basic pulse FT NMR experiment in Appendix A2.

Hard pulses are assumed to be short high power square wave pulses, which have infinitely short build-up times to the maximum field amplitude and then fall to zero in an infinitely short time. The duration of the pulse, τ_p, is often called the pulse width or pulse length and is typically of the order of microseconds (μs).

The Fourier transform (FT) of a perfect short square wave pulse, which obeys the condition ($\gamma\mathbf{B_1} << \gamma\mathbf{B_0}$), contains frequency components over a large bandwidth according to the function sinx/x (Figure A1.5).

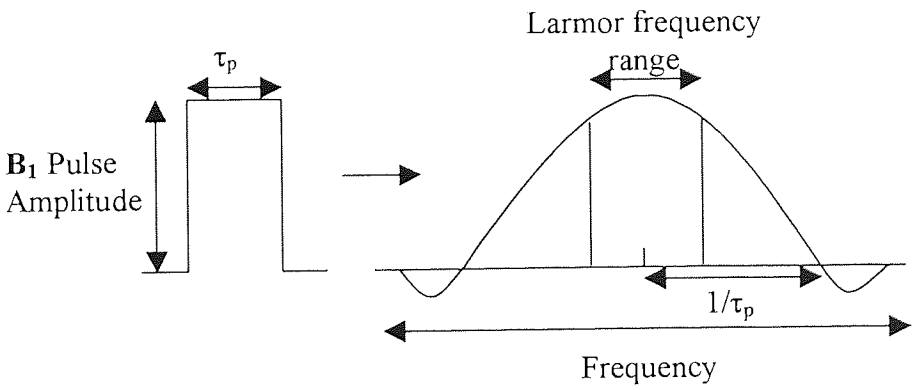

Figure A1.5 Hard pulse and corresponding frequency bandwidth over which the pulse acts

The effective bandwidth of Larmor frequencies encompassed by the pulse, or the selectivity of the pulse, is proportional to $1/\tau_p$. As typical hard pulse lengths are of the order of microseconds, the amplitude of the pulse over most Larmor frequency ranges of nuclei is considered to be near constant. Uniform excitation over the entire bandwidth of Larmor frequencies would be desirable however, this is impossible to achieve since it would require a pulse width, which was infinitely small.

$\mathbf{B_1}$ can be thought of as being composed of two contra-rotating magnetic vectors. When applied along the x-axis the magnetic vectors rotate in the x-y plane away from the x-axis with frequencies +ν and –ν (Figure A1.6).

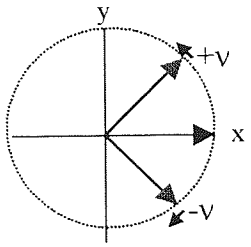

Figure A1.6 Schematic representation of contra-rotating magnetic vectors of $\mathbf{B_1}$

Only the component rotating with the same precessional sense as the nuclear magnetic moment vectors can cause resonance while the other is considered ineffective. Subsequently, nuclei with $-\gamma$ and $+\gamma$ interact with opposite components of $\mathbf{B_1}$.

The magnetic field of $\mathbf{B_1}$ produces a torque upon the precessing nuclear magnetic moment causing precession about the $\mathbf{B_1}$ field at an angular frequency $-\gamma\mathbf{B_1}$ while simultaneously precessing about $\mathbf{B_0}$ at an angular frequency $-\gamma\mathbf{B_0}$. This rather intangible motion is called nutation and results in the tipping of the individual magnetic moments and hence $\mathbf{M_z}$ toward the x-y plane.

A1.8 The rotating frame of reference

The complexity of movement of $\mathbf{M_z}$ due to nutation is suitably minimised by the incorporation of a rotating coordinate system called the rotating frame of reference.
One can replace the static Cartesian axes x, y and z with a Cartesian frame of reference that rotates with angular frequency ω_0 about $\mathbf{B_0}$ with axes x′, y′ and z′.

Viewed from the rotating frame, a magnetic moment vector, $\boldsymbol{\mu}$ with Larmor frequency $\boldsymbol{\omega}$ will precess with angular frequency $(\omega_0 - \omega)$. The apparent precession frequency viewed in the rotating frame has been reduced and is tantamount to the application of a fictitious field of magnitude ω_0/γ opposing $\mathbf{B_0}$. Consequently, the magnetic moment vectors precess in the rotating frame about a reduced static magnetic field $\mathbf{B_r}$ of magnitude $(\omega - \omega_0) / \gamma$. Therefore, when $\omega_0 = \omega$, $\mathbf{B_r}$ is zero, $\boldsymbol{\mu}$ appears to be stationary in the rotating frame.

The rotating frame of reference is integral to the execution of modern NMR experiments. Moreover it provides the means to describe more simplistically, the motion of magnetisations in terms of classical vectors.

A1.8.1 Application of B_1 in the rotating frame

The description of the rotating frame is couched in terms of the precession of individual magnetic moments. However, the concept holds for the description of the passage of magnetisation acting under the influence of $\mathbf{B_1}$. Although the $\mathbf{B_1}$ pulse is designed to bring all nuclei to resonance simultaneously, one defines a particular frequency, or *carrier frequency,* at which $\mathbf{B_1}$ is applied. The carrier frequency, which is the rotational frequency of the rotating frame, is set equal to the frequency of rotation of one of the magnetic components of $\mathbf{B_1}$. Consequently $\mathbf{B_1}$ appears to be stationary in the rotating frame along the axis of which it is applied.

When the carrier frequency is set to the Larmor frequency, ω, of the nucleus, $\mathbf{B_1}$ is considered to be 'on-resonance'. When the carrier frequency is not set to the Larmor frequency of the nucleus, $\mathbf{B_1}$ is considered to be 'off-resonance'.

A1.8.2 Application of B_1 on-resonance

If $\mathbf{B_1}$ is applied exactly on-resonance ($\omega = \omega_0$) with a phase x, the reduced magnetic field, $\mathbf{B_r} = 0$, and the magnetic moment vector precesses around $\mathbf{B_1}$ alone with an angular frequency $-\gamma\mathbf{B_1}$. Subsequently $\mathbf{M_z}$ is nutated toward the x′ y′ plane in the z′ y′ plane, which creates transverse magnetisation M_y (Figure A1.7).

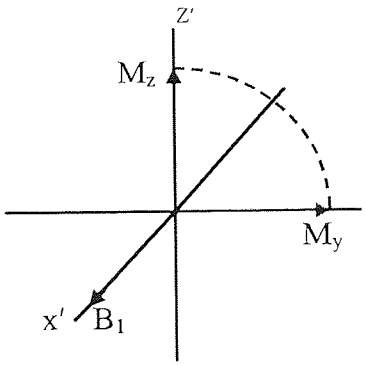

Figure A1.7 **A $\pi/2_x$ pulse exactly on resonance in the rotating frame. M_z is converted to pure transverse magnetisation M_y**

The magnitude of transverse magnetisation, $\mathbf{M_y}$, created, or indeed the magnitude of $\mathbf{M_z}$ that remains, is proportional to the nutation angle, θ. The nutation angle is dependent upon, $\boldsymbol{\tau_p}$, and is given by:

$$\theta = -\gamma B_1 \tau_p . \qquad \text{A1- 1.7}$$

Therefore, one can manipulate the magnetisation of a sample in terms of both phase and magnitude by judicious setting of $\boldsymbol{\tau_p}$ and the pulse phase. In the example given in figure A1.7, the duration of $\mathbf{B_1}$ necessitated the passage of magnetisation through 90 degrees, (hereafter stated, $\pi/2$,) such that it lies coincident with the y′ axis.

A1.8.3 Application of B_1 off-resonance: Off-resonance effects

When $\mathbf{B_1}$ is off-resonance ($\omega \neq \omega_0$), the reduced static magnetic field $\mathbf{B_r} = \omega - \omega_0/\gamma$. Consequently, $\mathbf{M_z}$ precesses about an effective field, $\mathbf{B_{eff}}$, which is the resultant of $\mathbf{B_1}$ and $\mathbf{B_r}$, which is tilted at an angle of $\tan\theta = \mathbf{B_1/B_r}$ to the z-axis. For the same pulse length and phase ($(\pi/2)_x$) as described previously for the on-resonance condition, $\mathbf{M_z}$ is nutated toward the x′ y′ plane, however does not lie coincident with the y' axis. Transverse magnetisation has both x and y components, $\mathbf{M_{xy}}$ (Figure A1.8).

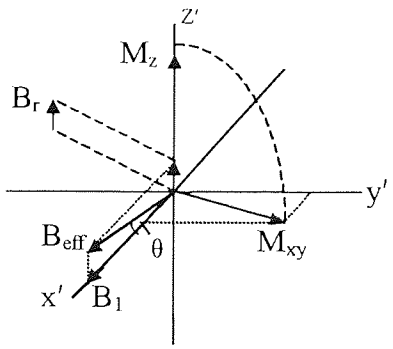

$$B_r = (\omega - \omega_0)/\gamma$$

Figure A1.8 **A pulse applied off-resonance and the corresponding off-resonance effect upon nutation angle and phase of the resultant transverse magnetisation.**

The effective nutation angle, θ_{eff}, of the off-resonance pulse is given by:

$$\theta_{eff} = -\gamma B_{eff} \tau_p \qquad \text{A1- 1.8}$$

The corresponding phase-shift, φ, of the transverse magnetisation component, $\mathbf{M_{xy}}$, from the y′ axis, with respect to the on-resonance pulse is given by:

$$\tan\varphi = \frac{M_y}{M_x} = \frac{(1-\cos\theta_{eff})\sin\theta}{\sin\theta_{eff} - \gamma B_1} \times B_r \qquad \text{A1- 1.9}$$

The nutation of magnetisation has been subject to an *off-resonance effect*, as it is generically termed. The nutation angle and subsequent phase and magnitude of the resulting transverse magnetisation components are proportional to the difference between the Larmor frequencies and the carrier frequency: generally speaking, the greater the offset from resonance, the more severe the off-resonance effect.

As illustrated in figure A1.8, (π/2) pulses are reasonably self-compensating in terms of nutation angle. Close to complete conversion of $\mathbf{M_z}$ into transverse magnetisation, $\mathbf{M_{xy}}$ occurs, and when this is the sole purpose of a π/2 pulse, the off-resonance effects are broadly considered unimportant. However, off-resonance effects of π/2 pulses often prove problematic when one wishes to manipulate nuclei with precise phases.

For pulses that are designed to yield 180° (π) nutation angles (π-pulses), the off-resonance effect is generally more severe, since the nutation angle as well as the phase of the magnetisation is effected (Figure A1.9).

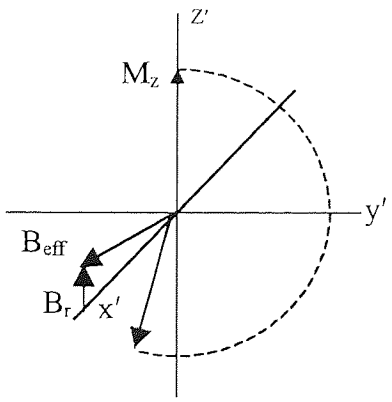

Figure A1.9 Off-resonance effect for a π-pulse

Off-resonance effects are inevitable when studying nuclei of the same isotopic species with different Larmor frequencies, because one cannot set the carrier frequency on resonance for each nucleus during one pulse. Off-resonance effects obviously increase in severity for isotopes that inherently possess greater Larmor frequency ranges. In organic molecules, the typical Larmor frequency range of ^{13}C in comparison to ^{1}H is approximately 20 times greater and subsequently, off-resonance effects are more severe for the precise manipulation of ^{13}C nuclei. Indeed, off-resonance effects are a serious problem when pulse sequences are designed to manipulate magnetisations in a precise fashion. Consequently, composite pulses are often used instead of single hard pulses to compensate for off-resonance effects (Appendix A9).

It is the very precision with which magnetisation can be manipulated that sets NMR apart from all other branches of spectroscopy. Magnetisations can be manipulated to reveal a plethora of important features of the nuclear spin system, for which an enormous variety of experiments have been designed. The experiments range from simple one-pulse experiments, like the one shown above, to complex sequences of pulses, generically termed *pulse sequences*. These so-called *pulse sequence* experiments are introduced later in appendix A2.

A1.9 Coherence

According to the quantum mechanical selection rule, observable spectroscopic transitions occur between the $2\mathbf{I}+1$ energy states, which differ by one quantum ($\Delta \boldsymbol{m} = \pm 1$). However, extra energy states exist, called *superposition states*, which are conceptually supported by quantum mechanics, [4,52-53] and are intermediate energy states between the $2\mathbf{I}+1$ energy levels.

When the spin system is at thermal equilibrium, most of the nuclei are in superposition states between the Zeeman states $\boldsymbol{\alpha}$ and $\boldsymbol{\beta}$, while a minority will occupy or be very close to $\boldsymbol{\alpha}$ or $\boldsymbol{\beta}$. However, the ensemble average of the superposition states allows one to define the energy of the nuclei as either $\boldsymbol{\alpha}$ or $\boldsymbol{\beta}$. It has been shown previously (Figure A1.4) that at thermal equilibrium the ensemble average of the transverse phase components of magnetic moments is zero and the sum of their z-components gives rise to the macroscopic longitudinal magnetisation $\mathbf{M}_z$.

When $\mathbf{B}_1$ is applied, a perturbation of the energy of the nuclei occurs, causing a coherent superposition of the Zeeman energy states, which is simply called *coherence*. The energy of the nuclei is no longer attributed to α or β but is intermediate between the two. When the spins exist in superposition states between α and β, which correspond to a single quantum transition where $\Delta m = \pm 1$, the coherence is called single quantum coherence (SQC).

The physical manifestation of single quantum coherence is observable transverse magnetisation, which has been previously described on a macroscopic level. On a microscopic level, the application of $\mathbf{B}_1$ at thermal equilibrium induces the individual magnetic moments (spins) to precess with a common phase, which is transverse to $\mathbf{B}_0$. The spins are said to be *phase-coherent* with one another and an external axis, and the vector resultant of the latter causes a transverse magnetisation (Figure A1.10).

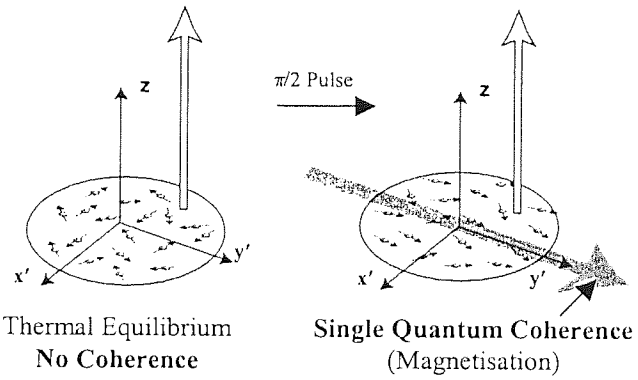

Figure A1.10 **Diagram Illustrating Coherence. Z-components of μ are not shown. Modified from publication by [52]**

Figure A1.11 illustrates diagrammatically, the populations of the α and β states at equilibrium and the single quantum coherence that exists between α and β after application of a $\pi/2$ pulse: the corresponding populations of the spin energy levels, which are represented by balls, are considered equal and all spins are in superposition states.

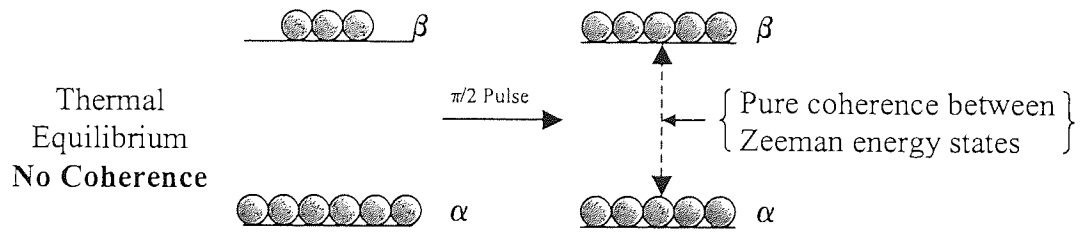

Figure A1.11 **Crude conceptual illustration of populations and coherence between the single quantum energy levels, α and β.**

Coherence is represented by dashed lines interconnecting the α and β states, which should not be confused with transitions, which are represented by solid lines. If the nutation angle is away from $\pi/2$, then some longitudinal magnetisation remains, which corresponds to the individual magnetic moment vectors that exhibit z-components. This would be idealised as a small excess of spins occupying the α spin energy level.

Only single quantum coherence is detectable by NMR since it corresponds to a measurable magnetisation and obeys the spectroscopic selection rule $\Delta m = \pm 1$. Coherences can also be induced between spin energy states for which $\Delta m \neq \pm 1$. These so-called multiple quantum coherences (Appendix A8.2.1) are unobservable to NMR directly, since the spectroscopic transition is forbidden ($\Delta m \neq \pm 1$).

Although multiple quantum coherences are directly unobservable to NMR, they constitute extremely important intermediary states in many interesting and important experiments. Indeed, the creation (excitation) of multiple quantum coherences is central to investigative work detailed in this thesis.

Appendix A2 leads on to describe the principles behind obtaining a NMR spectrum by pulse FT NMR and the relevant spectrum acquisition parameters.

Appendix A2 Pulse FT NMR experiments

A2.1 A basic pulse FT NMR experiment: 'Pulse and collect' experiment

A pulse and collect (direct detect) experiment is the simplest of all NMR experiments. As the name suggests, a non-frequency selective hard pulse (e.g. $\pi/2$) is applied to the nuclear isotopes under scrutiny, and the data is collected during an acquisition period, $\tau_{ac.}$ Thereafter, a frequency spectrum can be obtained by Fourier transformation of the data (Figure A2.1).

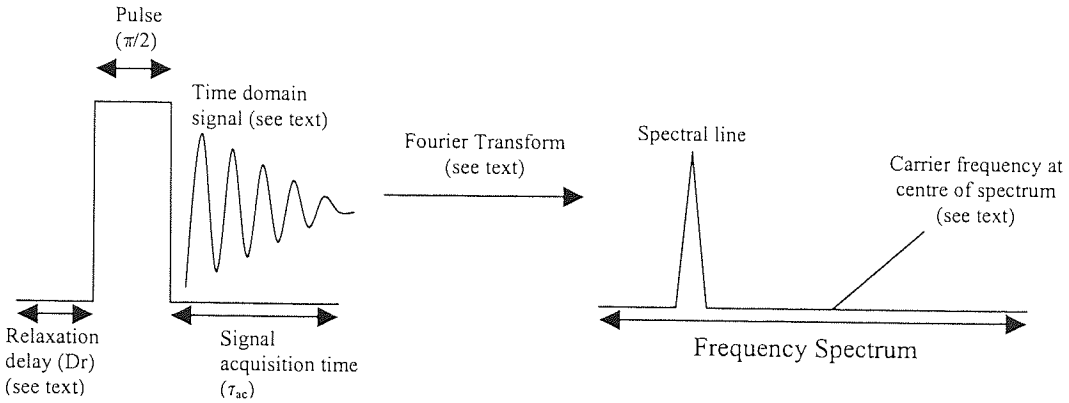

Figure A2.1 **Schematic diagram of a 'pulse and collect' experiment**

The hard pulse causes excitation of single quantum coherence of all nuclei. Subsequently, the single quantum coherences evolve or rotate in the x′y′ plane of the rotating frame about $\mathbf{B}_0$ (z-axis), with angular frequencies $(\pm\omega - \omega_0)$. As the single quantum coherence (magnetisation) evolves, an electromotive force (e.m.f.) is induced in the receiver coil of the NMR probe in which the analytical sample is positioned (Appendix A4). The receiver coil is conceptually rotated at the carrier frequency, which is the frequency of the rotating frame, ω_0, and is assumed to lie coincident with one of the rotating frame axes. Consequently the amplitude and phase of the induced signal (e.m.f.) is modulated according to the frequency $(\pm\omega - \omega_0)$ (Figure A2.2).

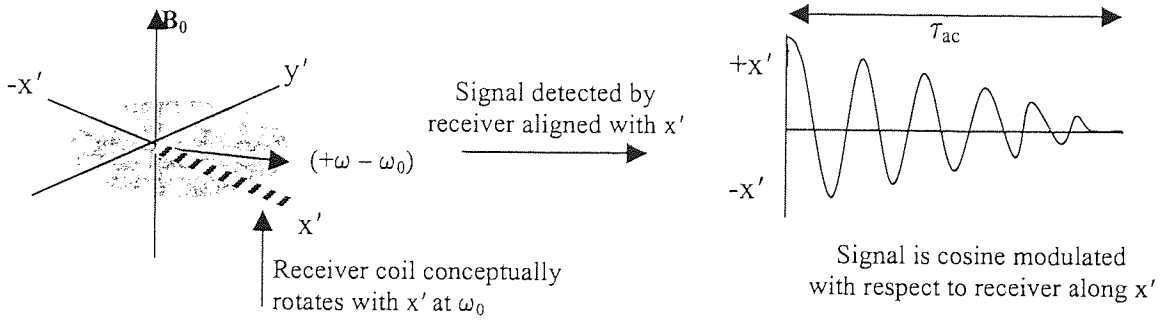

Figure A2.2 **Evolution of single quantum coherence and the NMR signal**

Coherence does not perpetually evolve, indeed it decays or de-phases due to transverse relaxation during a time $\mathbf{T_2}$, which is unique to each nuclear coherence (Appendix A6). As the name suggests, transverse relaxation acts perpendicularly to $\mathbf{B_0}$ and acts to restore the thermal equilibrium condition, $\mathbf{M_x} = \mathbf{M_y} = 0$. The coherence, and hence e.m.f., decays exponentially over the time $\mathbf{T_2}$, which is schematically shown above in figure A2.2.

The analogue signal (e.m.f.) is digitised and the amplitude and phase of the signal is plotted as a function of time. The decaying *time domain signal*, which is amplitude and phase modulated at frequencies ($\pm\omega - \omega_0$), is called the free induction decay (F.I.D.) (Figure A2.3). In order to generate the familiar *frequency domain* NMR spectrum, the time domain signal is subjected to Fourier transform.

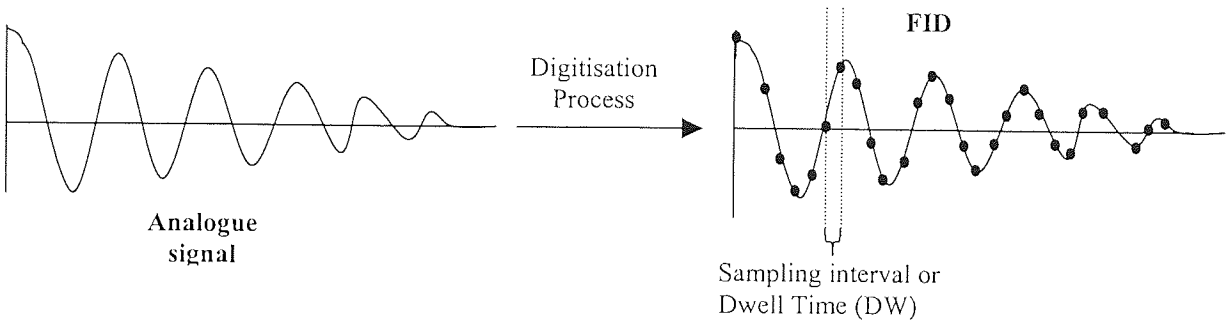

Figure A2.3 The Free Induction Decay (F.I.D)

Before progressing to the process of digitisation and Fourier transformation, the concept of longitudinal relaxation is introduced.

A2.2 Longitudinal relaxation and the inter-pulse sequence relaxation delay

It has been mentioned that transverse relaxation occurs during signal acquisition. Furthermore, longitudinal relaxation occurs simultaneously, which acts to restore longitudinal magnetisation, $\mathbf{M_z}$, and the thermal equilibrium condition $\mathbf{M_0}$ in a time $\mathbf{T_1}$. (Appendix A6).

The restoration of longitudinal magnetisation is central to the performance of pulse FT NMR experiments since detectable single quantum coherence is derived from it. The basis of pulse FT NMR is that a number of identical pulse sequence experiments are performed sequentially and their F.I.D.s coherently added. Consequently the signal intensities in the frequency spectrum are increased by a factor **n**, while the random spectral noise builds up by a factor

$\sqrt{\mathbf{n}}$, where **n** is the number of separate experiments or transients. Indeed, it is this *signal averaging* [23, 43] that partially overcomes the inherent insensitivity of NMR. However, a consequence of signal averaging is that one must wait for a suitable period of time so that sufficient longitudinal magnetisation has built-up before the next transient is executed.

Unfortunately, relaxation in NMR is generally lengthy, and varies considerably between nuclei and different isotopes. Consequently, one may have to wait seconds or even tens of seconds between transients. When compared to many pulse sequences, which are executed in fractions of seconds, the relaxation delay represents a significant proportion of overall experiment time. Of course one may not need to wait for the complete restoration of thermal equilibrium, which takes at least $5.3 \times \mathbf{T_1}$ of the nuclei in question. Instead, when sensitivity is the only issue, one usually sets the inter-pulse sequence relaxation delay, $\mathbf{D_r}$, to the approximate $\mathbf{T_1}$ of the nuclei. This allows a reasonable magnitude of $\mathbf{M_z}$ to build-up prior to the next transient.

Reducing the natural $\mathbf{T_1}$s of nuclei via artificial means has received widespread use in order to increase sensitivity in a given experimental time. Indeed, the further development of a method for the reduction in $\mathbf{T_1}$ of protons in heteronuclear polarisation transfer experiments is the subject of chapter 4.

A2.3 Digitisation of the analogue signal: The Free Induction Decay (F.I.D.)

The induced e.m.f. in the receiver coils, which constitutes the analogue signal is converted to a digital signal by the analogue-to-digital converter (Appendix A4.4.5). The analogue signal is sampled during a pre-defined signal acquisition time, τ_{ac}, over small discrete sampling periods ($\tau + \tau$+t). The time interval between the sampling periods is called the dwell time, **DW**, the inverse of which defines the frequency width of the NMR spectrum, **SW**. (Figure A2.3)

A2.4 Quadrature detection and Fourier Transformation

It is evident from figure A2.2 that the cosine modulation (or sine modulation if the receiver were conceptually aligned along the y′-axis) fails to discriminate the rotational sense or *phase* of the coherence relative to ω_0. Consequently a complex Fourier transformation (FT) yields two signals, which are symmetrically disposed about the carrier frequency at the centre of the

frequency spectrum. Hence the correct Larmor frequency, which is diagnostic of molecular environment of the nucleus, has not been distinguished and the spectrum is meaningless.

For a complex FT to distinguish the correct Larmor frequency, the data must contain real (Re) and imaginary (Im) components, i.e., the cosine and sine modulations of the coherence respectively. This could be achieved by introducing another receiver coil perpendicular to the first, which would measure the remaining cosine or sine component simultaneously.

To achieve the same aim but without introducing another receiver coil in an already crowded region of the probe, quadrature detection is employed. After the signal acquisition is finished the analogue signal is first split into two equal parts, constituting two separate channels, and are each fed into a separate phase sensitive detector. Each signal is simultaneously fed a reference signal, which is the carrier frequency, which differs in phase from the other by $\pi/2$ radians. One signal remains the same (cosine component) and the other is modified such that it is $\pi/2$ radians out of phase with the former (sine component). The two analogue signals are then filtered and digitised simultaneously. A complex fast Fourier transform (FFT) algorithm [55], (hereafter referred to simply as FT), which acts over the finite acquisition time, is applied to the digitised time domain data, and is given by:

$$f(\omega) = \sum_{-t}^{+t} f(t) e^{i\omega t} dt \qquad \text{A2- 2.1}$$

which gives

$$f(\omega) = \mathrm{Abs}(+\Delta\omega) + i\mathrm{Dis}(+\Delta\omega). \qquad \text{A2- 2.2}$$

The FT has successfully discriminated the sign (phase) of the absorption (Abs) and dispersion (Dis) mode signals, which are the real and imaginary components respectively. The absorption mode frequency spectrum shows a Lorentzian line at the correct frequency difference, $+\Delta\omega$, from the carrier. The various components and functions of the NMR spectrometer that are referred to above are dealt with in appendix A4.

A2.4.1 Aliasing of signals

The digital sampling of the F.I.D. must occur at a frequency at least twice that of the Larmor frequencies of coherences that are being digitised. This sampling frequency is known as the Nyquist frequency [43] and coherences that have frequencies that are greater than the Nyquist frequency can be sampled incorrectly. Consequently, their true Larmor frequencies are misrepresented and the corresponding signals may be *aliased* or *folded* into the spectrum at incorrect frequencies. *Aliased* signals usually exhibit different phases from properly digitised signals, which serves to identify them easily. However, aliasing does prove problematic if the signals superimpose upon genuine signals of interest or their intensities affect the dynamic range (Appendix A4.4.5) Aliasing can be prevented by increasing the frequency width of the spectrum, **SW**, which in turn reduces **DW**, and hence increases the rate at which signals are digitised.

A2.4.2 Digital resolution

The digital resolution of spectral lines depends on the number of data points, **TD**, used to digitise the F.I.D.. The digital resolution, **DR**, of the spectrum is related to the value of **SW** and **TD** by the following equality.

$$DR = 2SW / TD \qquad \text{A2- 2.3}$$

Therefore, the greater the frequency width of the spectrum, the poorer the digital resolution. The impact of poor digital resolution can be manifested in the spectrum as poor Lorentzian line shapes and the inability to resolve lines, which are closely spaced. The latter is particularly troublesome when one wishes to measure small scalar coupling constants, **J** (Appendix A3.2).

Improving digital resolution can be simply achieved by increasing the number of **TD** data points used. However, the increase in data points necessitates a larger burden upon dedicated computer memory for the storage of spectral data. Of more importance is the relationship between **TD** and the total acquisition time τ_{ac}, given by:

$$\tau_{ac} = TD \times DR . \qquad \text{A2- 2.4}$$

It is evident that better digital resolution comes at the expense of greater acquisition times and hence longer experimental times. Therefore, one usually limits the digital resolution to the minimum required in order to minimise experimental time and financial cost.

One significant advantage of pulse FT NMR is that the user can define the magnitude of **SW**. This is particularly useful for focusing on an interesting region of a spectrum, thus concentrating digitisation on genuine signals as opposed to noise. Consequently, the signal-to-noise ratio and digital resolution can be maximised.

A2.4.3 Sequential sampling quadrature detection

Sequential sampling quadrature detection mimics a single channel receiver detection system with the reference frequency situated at the edge of the spectrum, which removes the need to differentiate the sign of the frequencies.

For each sampled point the reference phase is incremented by $\pi/2$ and at a digitisation rate of 2**SW** and the signal appears to have advanced by ¼ of a cycle. The frequency of the signal appears to have increased by 2**SW**/4 or **SW**/2 and since the reference frequency is set to the middle of the spectrum, the genuine frequency range runs from +**SW**/2 to –**SW**/2. The artificial increase of +**SW**/2 shifts the frequency window to +**SW** to 0 therefore causing no requirement to distinguish negative frequencies.

Since all the digitised data are comprised of real data (Re or (Abs)), only real Fourier transforms are required for conversion to the frequency domain. The only noticeable difference in the two methods is that the simultaneous method leads to flatter baselines and a difference in how signals are aliased into the spectrum.

A2.4.4 Simultaneous sampling quadrature detection

The two-channel simultaneous sampling method described previously allows the desirable property of positioning the reference frequency at the centre of the NMR spectrum so only requiring digitisation of half the frequency range ±**SW**/2. According to the Nyquist criterion the sampling rate need only be equal to **SW** or half that required for the single channel detection method described previously. Consequently, the acquisition parameters are modified thus:

$DW = 1/TD$ and $\tau_{ac} = DW \times TD/2 = TD/2SW$,

Also $DR = SW/SI = 2SW/TD$ so $DR = 1/\tau_{ac}$. A2- 2.5

A2.5 Post acquisition treatment of the F.I.D.

Prior to Fourier transform, the F.I.D. can be treated in a number of ways in order to increase signal-to-noise ratios and/or poor digital or spectral resolution. Due to the fact that the methods are post acquisition procedures, the user does not incur any penalties in terms of extended experimental times.

A2.5.1 Zero Filling

In the common Fourier transformation algorithms used, half of the data points collected that constitute the imaginary or dispersion mode data points are discarded. Zero filling [43, 56] is used to effectively retrieve the discarded data hence increase the resolution of signals in the frequency spectrum by increasing the number of data points by a factor of 2. Zero filling is achieved by setting the total number of data points used in the FT, given by the parameter **SI**, to twice that of **TD**.

Zero filling is only usually performed once, however, if one wishes to increase digital resolution further, zero filling can be repeated any number of times. Zero filling in the latter case causes interpolation between data points giving a cosmetic benefit to the spectrum.

Zero filling can also be used to improve the resolution of signals that exhibit *sinc wiggles* as a result of truncation [23]. Truncation of the F.I.D. occurs when the coherences that have been detected have not decayed to zero before the end of acquisition. Consequently the *step function* at the end of the F.I.D. causes *sinc wiggles* to appear at the base of signals as a result of FT. Doubling the time domain data file size by zero filling helps reduce or remove truncation effects.

A2.5.2 Convolution and exponential multiplication

Convolution is another post acquisition technique that can be used to adjust the digital resolution, signal-to-noise ratio (S/N) or line shape of spectral lines. The F.I.D. is multiplied by a *weighting function* and upon FT of the modified F.I.D., causes the convolution or

broadening of the frequency spectrum by an amount proportional to the weighting function applied.

Exponential multiplication, has been used routinely in experimental work reported in this thesis to increase the S/N of ^{13}C spectra. Exponential multiplication constitutes the multiplication of an exponentially decaying Lorentzian function with the F.I.D.. Consequently, the noise from the latter stages of the F.I.D. is removed increasing the S/N in the final spectrum. A consequence of exponential multiplication is that the lines are broadened by a factor proportional to the weighting function and spectral resolution is decreased. Indeed exponential multiplication is often referred to simply as *line broadening*. One must specify an appropriate magnitude of the function when the resolution of spectral lines or scalar coupling multiplets is important. This is achieved by specifying the broadening of the lines in Hz prior to execution. Since the F.I.D. is stored, convolution may be repeated on the raw F.I.D. a number of times to gain the desired effect.

A2.5.3 Phase correction

After Fourier transform the frequency spectrum requires phase correction. All spectral lines exhibit phases such that they are not in perfect absorption mode and exhibit partial dispersion. There are two phase discrepancies inherent to all spectral lines, which require zero-order and first-order phase correction. The zero-order phase correction compensates for the phase differences between the pulse transmitter and the conceptual phase of the receiver. Consequently all signals exhibit the same zero-order phase discrepancy and are all corrected by the same zero-order correction. The first-order phase discrepancy varies according to frequency such that some lines will exhibit larger first-order phase discrepancies than others. First-order phase correction requires more care to ensure that phase correcting one signal does not adversely affect another. The work reported in this thesis has used the standard automatic phase correction routines on the NMR spectrometer and where applicable, the zero and first-order corrections were optimised by hand.

Appendix A3 The chemical shift and scalar coupling for I = ½ nuclei in organic molecules in solution

A3.1 The Chemical shift

The expression defining the Larmor frequency given previously (A1-1.5) suggests that all nuclei of the same spin quantum number **I** come to resonance at the same frequency. However, this is not the case and each resonance appears at a frequency in the spectrum that is diagnostic of the surrounding electronic environment of the nucleus.

The effect of $\mathbf{B_0}$ induces currents within the charged electron density surrounding all nuclei of the sample, which induces a localised magnetic field at the site of each nucleus. The induced local magnetic field works in opposition to $\mathbf{B_0}$ hence reducing the total magnetic field $\mathbf{B_T}$ experienced by each nucleus:

$$B_T = B_0(1-\sigma) \qquad \text{A3- 3.1}$$

The nucleus is said to have been "screened" from the full effect of $\mathbf{B_0}$ by a function called the nuclear screening constant, σ, which is largely dependent on the electron density surrounding the nucleus. The Larmor frequency of the nucleus and hence the true resonance condition therefore becomes:

$$\omega = -\gamma I B_T \equiv \upsilon = \frac{\gamma B_T}{2\pi} \qquad \text{A3- 3.2}$$

The resonance frequency is dependent on the magnitude of $\mathbf{B_0}$, and so changes between spectra acquired with different magnitudes of $\mathbf{B_0}$. Therefore the dependence on the magnitude of $\mathbf{B_0}$ is removed by defining a general empirical quantity called the chemical shift (δ).

The chemical shift of a nucleus is the difference between the resonance frequency, ν, of the nucleus in question and that of a reference standard, ν_r, and is measured on the δ-scale according to:

$$\delta = \frac{\upsilon - \upsilon_r}{\upsilon_r} x10^6 = (\sigma_r - \sigma) \times 10^6 . \qquad \text{A3- 3.3}$$

Where the fractional frequency change is the same as the difference in screening constants. Since the numerator and denominator are proportional to $\mathbf{B_0}$, the dependence of $\mathbf{B_0}$ has been removed. The value of δ is usually quoted in parts per million (ppm), hence the factor 10^6, and for a magnetic field operating at 500MHz, a chemical shift of 1.0ppm equates to a resonance frequency difference of 500Hz.

By IUPAC convention, when $\delta<0$ the resonance appears to the right-hand side of an appropriate reference and the nucleus is said to be screened; corresponding to a high degree of electron density surrounding the nucleus. When $\delta>0$ the resonance appears to the left-hand side of an appropriate reference and the nucleus is said to be de-screened; corresponding to a lack of electron density surrounding the nucleus (Figure A3.1).

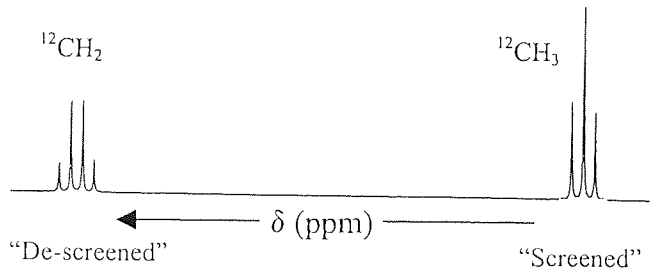

Figure A3.1 **Schematic representation of the chemical shift for the protons of a CH_3 and CH_2 group in e.g., ethanol.**

A3.1.1 The nuclear screening constant, σ, in liquid samples: The isotropic chemical shift

The induced local magnetic field at the nucleus due to surrounding electron density is dependent on the orientation of the electron density with respect to $\mathbf{B_0}$. Therefore σ is a tensor function and is anisotropic, such that its magnitude differs along Cartesian axes (x, y and z) relative to $\mathbf{B_0}$

In isotropic liquids, rapid molecular reorientations necessitate that the time average of σ is constant and is given by:

$$\bar{\sigma} = \frac{1}{3} = \left(\sigma_{xx} + \sigma_{yy} + \sigma_{zz}\right) \qquad \text{A3- 3.4}$$

Therefore the observed chemical shift in isotropic liquids is the isotropic chemical shift.

A3.1.2 The magnitudes of Chemical shifts: The magnitude of σ

The absolute values of chemical shifts and hence the magnitude of σ depends upon complex interactions between nuclei and electron density and of the electron density with $\mathbf{B}_0$.
The important information to be borne out of chemical shifts obviously relates to intra-molecular chemical environments. However, the empirical chemical shift depends on mechanisms that affect the electron density at the nucleus that originate from intra-molecular and inter-molecular effects. The solute molecules contain the nuclei of interest and mechanisms affecting the chemical shift from within the solute molecule are intra-molecular. Mechanisms affecting the chemical shift, which originate from outside the solute molecule are considered to contribute to the intermolecular effects.

In most cases, liquid state NMR is carried out in a homogenous liquid where the solvent is required for magnetic field-frequency lock purposes (Appendix A4.3). Other experiments may require the presence of a solvent(s), other than that required for field-frequency lock purposes. Therefore, intermolecular effects may be considered to originate from solute-solvent or solute-solute interactions, which are broadly considered to be *solvent* interactions hereafter. Some of the more important contributions to σ are addressed in turn for both intra-molecular and inter-molecular effects with a view to qualitatively describing the effect of each upon the chemical shift.

A3.1.2.1 Intra-molecular contributions to σ.

σ is comprised of the sum of a diamagnetic screening term, σ_d, and paramagnetic screening term, σ_p, each being opposite in sign and of similar magnitudes ($\sigma = \sigma_d + \sigma_p$). The two terms are defined quantum mechanically [49 and references therein], however, their qualitative description is only given here.

σ_d – Originates from the $\mathbf{B}_0$ induced electron currents in the ground electronic states and so is generally concerned with the amount of electron density in the inner electronic orbital.

σ_p – Is dependant upon several factors:

- the inverse of the energy separation, ΔE, between ground and excited electronic states of the molecule.
- The relative electron densities in the various p-orbitals involved in bonding, i.e., the degree of asymmetry in electron distribution near the nucleus.
- The average inverse cube distance from the nucleus to the orbitals concerned ($<1/r^3>$).

For hydrogen atoms, the electron density surrounding the nucleus is small necessitating the magnitude of σ_d to be small also. Similarly, the magnitude of σ_p is also small since s-orbitals are spherically symmetric and ΔE is large. Therefore, the range of magnitudes of σ for protons in most molecules is small, corresponding to a small chemical shift range typically of the order 0 – 20ppm.

To a good approximation the magnitude of σ for protons varies linearly with inductive effects: an element or chemical group will withdraw or donate electron density in the proximity of the magnetic nucleus hence altering the nuclear screening and the chemical shift.

Elements of higher atomic mass tend to have smaller values of ΔE and larger values of σ_p and σ_d. This is a consequence of greater electron density surrounding the nucleus in lower-lying electronic excited states. However, σ_p and σ_d increase disproportionately such that σ_p becomes the dominant term. Subsequently there is a greater variation in chemical shift of elements with higher atomic mass, e.g., ^{13}C chemical shifts range from 0 – 300ppm.
The magnitude of σ does not however, increase proportionately with atomic mass and exhibits a periodicity such that it closely follows the ($<1/r^3>$) proportionality.

A3.1.2.2 Neighbouring group contributions

The inductive effect of individual nuclei contributes a great deal to the magnitude of σ. However, the effect of groups of nuclei or chemical functions is also important: the effect of $\mathbf{B_0}$ upon the electron density surrounding these groups influences the local magnetic field at nuclei in their proximity.

For example protons in the plane of the ring in benzene experience a reinforcement of their local magnetic field, which causes a chemical shift that is indicative of de-screening. In contrast, protons out of the plane of the ring (for example in substituent groups) experience a decrease in local magnetic field, which causes a chemical shift that is indicative of screening. This so-called magnetic anisotropy of the neighbouring group (benzene ring) causes a chemical shift without having directly perturbed the electron density at the protons.

A3.1.2.3 Electric Fields

If a strongly polar group is present within a molecule, the resulting electric field can cause electron drifts in the bond directions, which alters the electronic symmetry at an adjacent nucleus. The component of σ attributed to electric field effects, σ_E, is given by:

$$\sigma_E = -AE_z - BE^2. \qquad \text{A3- 3.5}$$

Where A and B are constants, A<<B, E_z is the electric field along the bond to the nucleus in question, and E is the maximum electric field at the atom. The first term ($-AE_z$) produces an increase in screening if the electric field causes an electron drift from the bond towards the atom, and a decrease if the converse is true. The second term ($-BE^2$) always leads to de-screening. The electric field effect falls off with increasing distance so generally speaking, de-screening decreases with an increase in the number of intervening bonds. Electric field effects tend to be of more importance to nuclei of higher atomic mass with lower lying electronic ground states, e.g., ^{13}C.

A3.1.2.4 Inter-molecular contributions to σ

The effect of the solvent on the chemical shift of the nucleus contained in the solute, σ_{solv}, can be defined as the sum of the contributing factors; the bulk magnetic susceptibility, σ_b ; weak Van-der-Waals forces, σ_v; magnetic anisotropy of the solvent molecules, σ_a; electric field effects, σ_e; specific solute-solvent interactions, σ_x. Therefore, $\sigma_{solv} = \sigma_b + \sigma_v + \sigma_a + \sigma_e + \sigma_x$.

A3.1.2.5 Bulk magnetic susceptibility, σ_b

All molecular species in solution exhibit a magnetic susceptibility, which is a measure of how readily the molecule develops a magnetic moment on exposure to $\mathbf{B}_0$. Magnetic susceptibility may have a positive or negative sign according to a paramagnetic and

diamagnetic susceptibility respectively. Generally, paramagnetic susceptibility solvents tend to increase the local magnetic field at the nucleus of a solute, while diamagnetic susceptibility solvents tend to reduce it. Paramagnetic susceptibilities tend to be larger than diamagnetic, the earlier tends to distort the local external magnetic field by pulling the field inward, while the converse is true for diamagnetic susceptible species.

In a sample where the chemical shift reference is homogenously incorporated into the solvent-solute liquid, the effects of bulk magnetic susceptibility are assumed to be equal for the reference and nucleus in question. A sample that is heterogeneously referenced (a cylindrical tube, which contains the reference and is subsequently contained within the solvent-solute mixture) exhibits a chemical shift that is markedly different due to the bulk magnetic susceptibility difference.

A3.1.2.6 Van-der Waals Forces, σ_v

Van-der Waals interactions between solvent-solute and solute-solute molecules results in the distortion of the electronic environment about a given nucleus, which causes a change in σ. Rapid molecular motions in isotropic liquids tend to average this effect.

A3.1.2.7 Magnetic Anisotropy, σ_a

Effects similar to those described for ring current shifts can exist in certain solvents, e.g. benzene, imparting local magnetic fields to the nucleus in question. In analogy to ring current effects, molecular reorientation in liquids does not average this effect to zero.

A3.1.2.8 Electric Field effects, σ_e

An effect similar to that described for intramolecular electric field effects σ_E. In circumstances where the solvent is diamagnetic, a polar solute or polar group(s) in the solute molecule can induce a polarisation to the solvent, which may in turn modify the electronic environment at the site of the nucleus in question in the solute molecule.

A3.1.2.9 Specific Solvent-Solute interactions, σ_x

Semi-permanent bonds, which exist between solute or solvent and solute molecules perturb the electronic environment at the nucleus in question. The effects due to such transient interactions may not be visible if the lifetime of the state is short relative to the timescale of observation of NMR experiments.

A3.1.3 Empirical chemical shifts

To summarise, the following three contributions provide the most influence on the chemical shift in isotropic liquids.

- The paramagnetic contribution σ_p - lower-lying electronic excited states. Nuclei of greater atomic mass tend to have greater chemical shift ranges.
- Chemical shifts tend to correlate well with inductive effects of neighbouring elements or chemical groups, i.e. the electronegative atoms like O, Cl, F etc cause de-screening of nuclei.
- In rigid molecules with well-defined three-dimensional structure, magnetic susceptibility effects strongly effect the chemical shift of the nucleus whether they be intra- or intermolecular in origin.

The complexity and variation of nuclear screening effects necessitates a degree of uncertainty regarding the predictions of chemical shifts of nuclei in particular chemical environments. Consequently chemical shift correlation tables present ranges over which resonances may fall when in proximity to certain functional groups or elements.

A3.2 Mechanism of Scalar (Spin-Spin) Coupling

In isotropic liquids the *direct* or *through-space* dipolar coupling between dipolar nuclei is averaged to zero by molecular motions. However, an *indirect* dipolar coupling or scalar coupling exists between adjacent magnetic nuclei, which is not averaged to zero by molecular motions and is mediated through chemical bonds.

The dipolar interaction of an electron with an adjacent nucleus in a chemical bond is known as a *Fermi contact interaction* (**C**), which is isotropic and is not averaged to zero by molecular motions. The strength of the electron-nucleus interaction is proportional to the scalar product of the magnetic moment of each and is given by [57]:

$$\mathbf{C} \propto -\gamma_e \gamma_n \mathbf{I}.\mathbf{S} \qquad \text{A3- 3.6}$$

where **I** and **S** are the spin angular momentum vectors for the nucleus and electron, and γ_e and γ_n are the gyromagnetic ratios of the electron and nucleus respectively. The electron

gyromagnetic ratio is negative ($\gamma_e < 0$). The contact interaction energy of a nucleus with $\gamma_n > 0$ is *stabilised* when the electron angular momentum vector and the nuclear angular momentum vector (and magnetic moment vectors) are anti-parallel ($\mathbf{I.S} < 0$). Conversely, the contact interaction energy is *destabilised* when the magnetic moments are parallel ($\mathbf{I.S} > 0$) (Figure A3.2).

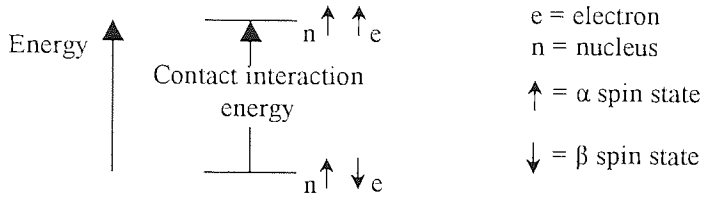

Figure A3.2 **Energy levels of an electron and (I=1/2) nucleus (with $\gamma>0$), coupled by Fermi contact interaction.**

The magnitude of the interaction energy is also proportional to the probability of finding the electron adjacent to the nucleus and hence its wavefunction. Consequently, the magnitude of the interaction energy is dependent upon the magnitude of s-character of the bonding orbital. Therefore, the electron senses the orientation of the nuclear magnetic moment and the energy of each is dependent upon the relative electron and nuclear spin states.

A consequence of stabilising the energy of the electron-nucleus interaction for anti-parallel orientations is to cause the polarisation of the electron wavefunction. For example, the probability of finding the electron in state β adjacent to a nucleus(A) in state α is higher than finding the electron in state α. Subsequently, there is a corresponding increase in the probability of finding the electron in state α at the site of another directly bonded nucleus(X).

Of course, the Pauli exclusion principle [57, 58] necessitates that the electron spin polarisations must be opposite to maintain a chemical bond. Consequently, the nucleus(X) will be energetically *stabilised* when its spin state is β (anti-parallel electron-nucleus interaction) and *destabilised* when the nucleus(X) is in spin state α. The opposite would be true if nucleus(A) had been in state α so that the electron spin state would favour β at nucleus(X), which is subsequently *destabilised* in its α state.

The entire ensemble of nuclear and electron orientation possibilities is depicted in figure A3.3, where each possibility is obviously limited to a separate molecule. The polarising

effect of $\mathbf{B}_0$ is not considered so that the α and β spin states of the nucleus are energetically degenerate.

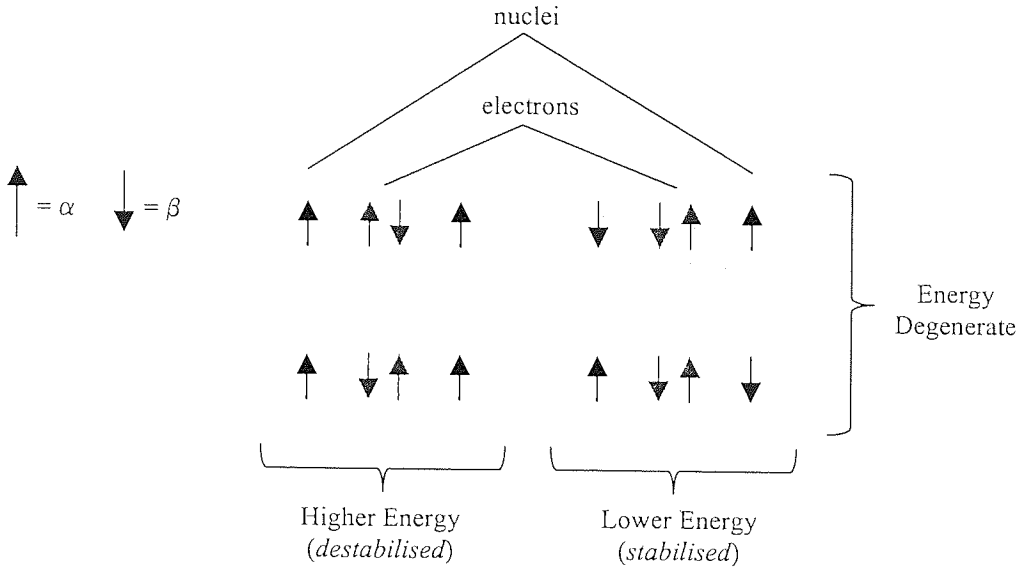

Figure A3.3 Effect of scalar coupling upon the energy stabilisation of nuclei.

Therefore, one nucleus senses, or is scalar coupled to another via Fermi contact interactions through chemical bonds. Consequently the energy of each spin state of the nucleus is perturbed (*stabilised or destabilised*) by the spin state of an adjacent scalar coupled nucleus.

The magnitude of energy perturbation or the scalar coupling interaction energy, **E**, is proportional to the scalar product of the magnetic quantum numbers, ***m***, of the nuclear spins involved:

$$E = \left(hJ / \hbar^2\right) m_A . m_X \qquad \text{A3- 3.7}$$

Where **J** is the scalar coupling constant measured in Hz. Consequently, for $\mathbf{I} = ½$ nuclei, $\mathbf{E} \propto \pm ¼\mathbf{J}$, depending on the spin state (α or β) of the involved spins. The perturbation of the energy of the nucleus in a particular spin state necessitates a proportionate change in the Larmor frequency.

The effect of scalar coupling in terms of the spin energy levels and corresponding single quantum transitions of two $\mathbf{I} = ½$ nuclei A and X are illustrated in figure A3.4 overleaf. The Larmor frequencies (chemical shifts) of A and X are assumed to be well separated.

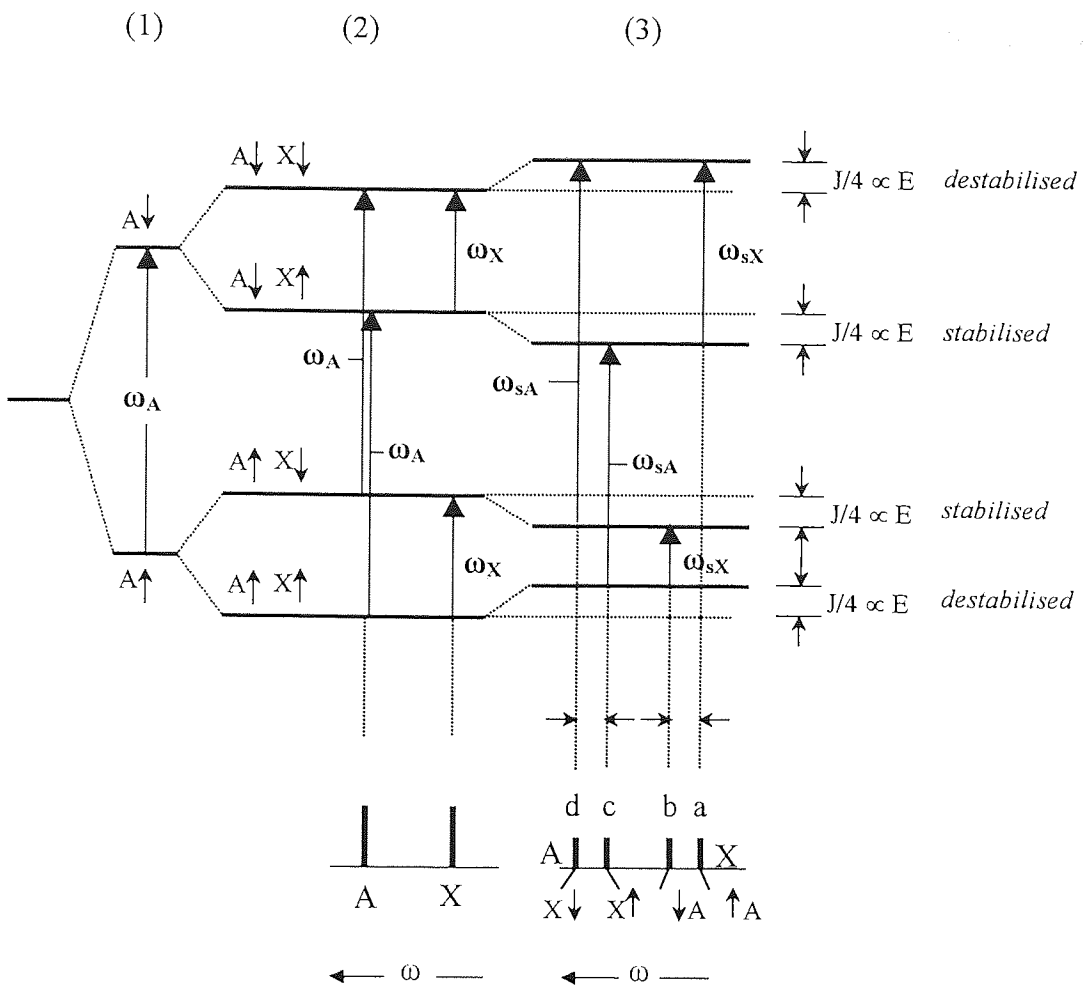

Figure A3.4 **Idealised scalar coupling energy level diagram for I = ½ nuclei A and X ($\gamma > 0$). Modified from publication by Hore [57]**

Situations (1) and (2) depict the introduction of A and X to $\mathbf{B}_0$ and the single quantum transitions, which correspond to the Larmor frequencies corrected for nuclear screening. Furthermore, scalar coupling is considered zero ($\mathbf{J}_{AX} = 0$). Situation (3) assumes scalar coupling exists ("switched-on") between the directly bonded A and X nuclei, ($\mathbf{J}_{AX} \neq 0$). To ensure clarity, the energy differences between spin energy states is greatly exaggerated.

The scalar coupling (3) of A and X leads to a loss of degeneracy of the individual $\boldsymbol{\alpha}$ and $\boldsymbol{\beta}$ spin states by the *stabilising* and *destabilising* effect of the Fermi contact interaction. Consequently, two new single quantum transitions exist for nuclei A (ω_{sA}) and X (ω_{sX}), giving rise to two resonance lines symmetrically disposed about the chemical shift of each nucleus. The scalar coupling pattern or multiplet is referred to as a *doublet* and the total

integrated intensity of both lines is equal to the intensity of the line when $\mathbf{J} = 0$. The relative intensities of the lines are approximately equal due to the Boltzmann distribution of α and β spin states in the molecular ensemble.

The spin energy level diagram e.g., figure A3.4, representing scalar couplings is more often depicted in the more simpler fashion given in figure A3.5.

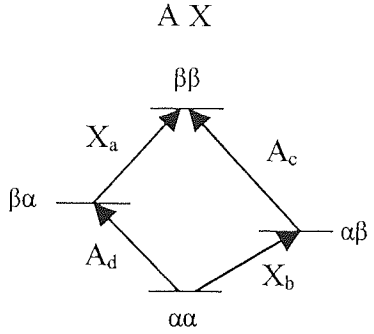

Figure A3.5 **Scalar coupling diagram. Differences between energy levels have been greatly exaggerated for ease of interpretation.**

The frequency separation between the lines is measured in Hertz and is the scalar coupling constant **J**, which unlike chemical shift, is independent of the magnitude of $\mathbf{B}_0$. The general Larmor frequency of A after scalar coupling ω_{sA} (which is valid for X after appropriate substitution of terms) is given by:

$$\omega_{sA} = -\gamma B_T - \sum_{X \neq A} J_{AX} m_X \qquad \text{A3- 3.8}$$

Where the summation extends over all spins (X), which exhibit mutual scalar coupling with (A). The simplistic model of two-spin coupling through one bond can be extended to three-spin and indeed multi-spin scalar coupling through multiple bonds.

A3.2.1 The magnitude of J

The prediction of the magnitude of **J** is not a trivial task. Explicit calculation of **J** would require the calculation of electronic wavefunctions and contact interaction energies at the site of the coupling nuclei and extended through the chemical bonds of the coupling *pathway*. Indeed the magnitudes of **J** are in some ways as equally or even more unpredictable than isotropic chemical shifts, nevertheless some qualitative trends do exist.

The magnitude of **J** crucially depends on the s-character of the molecular bonding orbitals between the coupling nuclei and hence the hybridisation of bonds [49]. Furthermore, the magnitude of **J** generally depends upon the following parameters, which are given in an arbitrary order:

- the product of the gyromagnetic ratios of the species involved in the coupling
- The number of intervening bonds between coupling nuclei
- Molecular geometry, i.e., bond angles

The only certainty in the magnitude of **J** is that one-bond scalar couplings are always larger than multiple-bond couplings. For example, $^{13}C - {}^{1}H$ one-bond scalar couplings in organic molecules typically range from 120Hz to 250Hz [50], whereas two and more bond couplings can range between 0-20Hz [10]. Generally, one-bond couplings are referred to as *short-range* couplings ($^{1}\mathbf{J}$) and multiple bond couplings are referred to as *long-range* couplings ($^{n}\mathbf{J}$) where n>1. Thereafter, in general, the magnitude of **J** decreases dramatically with increasing number of intervening bonds and is rarely resolvable over more than 5 or 6 chemical bonds. An interesting quirk generally occurs for homonuclear ($^{1}H - {}^{1}H$) [49, 52] and heteronuclear (^{13}C-^{1}H) [17] scalar couplings over 3 bonds, which tends to be larger than **J** for scalar coupling through two bonds. Furthermore, in rigid molecules the empirical $^{3}\mathbf{J}_{HH}$ values of vicinal proton-proton scalar couplings are found to vary in a predictable manner with the H-C-C-H dihedral angle according to the Karplus relations [44, 52]. Consequently one can predict structural geometry and hence conformation.

A3.2.2 The sign of J

The value of **J** may be positive or negative: for scalar coupled nuclei with $\gamma > 0$, if the anti-parallel orientation of the nuclear magnetic moments are energetically favoured or *stabilised*, then generally $\mathbf{J} < 0$. When parallel orientations are *stabilised*, then generally $\mathbf{J} > 0$. However, these conditions are reversed if one of the nuclei has $\gamma < 0$. Consequently, the scalar coupling transitions of X, **a** and **b** in figure A3.4 would be reversed for $\mathbf{J}_{AX} < 0$. Although the sign of **J** is of theoretical importance, and is necessary for the calculation of second order scalar coupling effects, (see later) it does not affect the appearance of multiplets. By analogy with the magnitude of **J**, the sign of **J** does not simply adhere to the criterion given above, and will vary depending upon bond angle and the specific electronic wavefunctions and Fermi contact interactions.

A3.2.3 Multiplicity of scalar couplings

NMR spectra usually exhibit a multitude of scalar couplings, which have different multiplicities (number of lines in the multiplets) and coupling patterns caused by scalar coupling between more than one nucleus. The type of multiplet pattern depends on the properties of the nuclei involved in the coupling, namely, their magnetic and/or chemical equivalence. Furthermore, nuclei that are magnetically equivalent mutually exhibit scalar, however, the coupling is not resolved in the spectrum.

A3.2.3.1 Chemical equivalence

A group of nuclei exhibit chemical equivalence when the following conditions are satisfied:

- the nuclei are of the same isotopic species
- A molecular symmetry operation exists which exchanges the involved spins

For example, the six protons of benzene are all chemically equivalent since reflection symmetry planes exist whereby all protons experience an exchange. Furthermore, the chemical shift of all protons are identical, however, two nuclei that exhibit identical chemical shifts may not be chemically equivalent.

The rapid rotation of chemical groups can invoke a chemical equivalence. For example, the CH_3 and CH_2 protons of ethanol experience an exchange of position due to rotation about the C-C bond. Consequently, the chemical shift of all the protons within the two groups are identical and are therefore chemically equivalent. Indeed, the protons in benzene and the protons within the CH_3 and CH_2 groups in ethanol are also *magnetically equivalent*.

A3.2.3.2 Magnetic equivalence

For a group of nuclei to exhibit magnetic equivalence, the nuclei must exhibit the same chemical shift ($\Delta\delta = 0$) and have identical mutual scalar couplings and identical scalar couplings with all other spins in the molecule. The consequence of magnetic equivalence is that the scalar couplings are not resolvable in NMR spectra.

For two magnetically equivalent $\mathbf{I} = ½$ nuclei (A_2) there are four possible spins states given by the wavefunctions (Appendix A1 and A13), $\alpha\alpha$, $\beta\beta$, $\alpha\beta+\beta\alpha$ and $\beta\alpha-\alpha\beta$. Each spin state can

be classified in terms of their total spin angular momentum I ($\mathbf{I}_A + \mathbf{I}_A$) and the total magnetic moment $\mathbf{M}$ ($m_{Az} + m_{Az}$) according to:

$I = 1$ (Spins Parallel):	$\mathbf{M} = +1$	$\alpha\alpha$
	$\mathbf{M} = -1$	$\beta\beta$
	$\mathbf{M} = 0$	$\alpha\beta + \beta\alpha$
$I = 0$ (Spins paired):	$\mathbf{M} = 0$	$\alpha\beta - \beta\alpha$

The three *parallel* spin states have non-zero spin angular momentum, ($I = 1$). In contrast, the anti-parallel or *paired* spins state, $\beta\alpha$-$\alpha\beta$, has a zero angular momentum vector resultant ($I = 0$). It can be shown that for magnetically equivalent nuclei only transitions between the spin states can occur that obey the following selection rule, $\Delta I = 0$ and $\Delta\mathbf{M} = \pm 1$. Consequently only two transitions $\alpha\alpha \rightarrow \alpha\beta+\beta\alpha$ and $\alpha\beta+\beta\alpha \rightarrow \beta\beta$ are allowed, however, they have degenerate energies and therefore produce a singlet. Therefore, magnetically equivalent nuclei do not exhibit scalar coupling in the NMR spectrum.

A3.2.4 Scalar coupling multiplicities in I = ½ nuclei

The number of component resonance lines of a scalar coupling multiplet (which correspond to the number of single quantum transitions that result due to scalar coupling) is given by n +1. Where n is the number of magnetically equivalent nuclei to which one nucleus or a group of magnetically equivalent nuclei are coupled.

The relative intensities of the component lines of the mutliplet are given by the binomial series on Pascal's triangle. Therefore, for the scalar coupling of the magnetically equivalent protons of the CH_3 with CH_2 protons in e.g., ethanol, the proton NMR spectrum comprises a triplet and a quartet, with relative intensities of the component lines of 1:2:1 and 1:3:3:1 respectively (Figure A3.6).

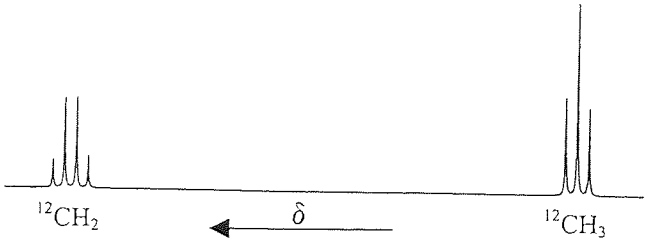

Figure A3.6 **Scalar coupling multiplicities of the magnetically equivalent protons in e.g., ethanol.**

A3.2.5 First order and second order scalar couplings

Thus far (with the exception of the scalar coupling between magnetically equivalent nuclei) it has been assumed that scalar couplings are first-order or obey the weak scalar coupling condition. The weak coupling condition occurs when the chemical shift separation of coupled nuclei is greater than the coupling constant ($\delta >> \mathbf{J}$). Species involved in weak coupling are often designated letters of the alphabet A, M and X, where the separation of the letters is large and analogous to the separation of the chemical shift. Weak coupling produces multiplets that are easily analysed in terms of their structure, and their component intensities obey that given by the binomial series on Pascal's triangle. Therefore scalar coupling in heteronuclear systems, (upon which the work detailed in this thesis relies) e.g., ^{13}C - ^{1}H, are by default first-order.

A3.2.6 Second order spectra, the strong scalar coupling condition.

Deviation from the weak coupling condition occurs when the chemical shift and **J**-coupling constants approach the same value ($\delta \geq \mathbf{J}$). Strong coupling is manifested as a distortion of the component intensities and structure of multiplet lines. Consequently **J**-values and chemical shifts often have to be determined using quantum mechanical approaches [44].

It is possible to invoke a weak coupling condition by increasing magnetic field strength, $\mathbf{B}_0$, so that $\delta >> \mathbf{J}$. Second order spectra are usually restricted to homonuclear scalar coupled systems due to the similarity of Larmor frequencies.

A3.2.7 Scalar coupling of ^{13}C and ^{1}H in organic molecules (heteronuclear spin systems)

The ^{13}C -^{1}H short-range scalar coupling multiplets in proton spectra are found symmetrically disposed about the chemical shift of the proton at ½ $\mathbf{J}_{CH}$ and are referred to as the ^{13}C proton satellites. The total integrated intensities of the satellites for molecules that have not been isotopically enriched with ^{13}C are approximately 1% of the main ^{1}H resonance. This is simply due to the relative isotopic abundance of ^{13}C ($\approx$ 1%) as compared to the ^{1}H ($\approx$ 100%): each ^{13}C proton satellite is indicative of 1% of the total ensemble of molecules in solution in which there exists the given prothe given proton to ^{13}C. Similarly, each proton resonance is indicative of the 99% of the total ensemble of molecules in solution in which there exists the given proton directly bonded to magnetically inactive ^{12}C (^{12}C-bonded protons). Consequently, ^{13}C proton satellites are difficult to distinguish without sufficient signal-to-

noise ratio and suffer from adverse dynamic range problems (Appendix A4.4.5.1). Indeed, homonuclear ^{1}H-^{1}H scalar coupling (should it exist for the given proton) further reduces the ability to resolve what would have been a simple ^{13}C-^{1}H doublet.

The scalar coupling multiplets of protons that exhibit mutual long-range scalar coupling with ^{13}C are invariably hidden beneath the intense proton resonance lines of the ^{12}C-bonded protons. This is a consequence of the similarity of homonuclear ^{1}H-^{1}H and long-range ^{13}C-^{1}H **J**-values. If one were able to remove the ^{12}C-bonded proton signals from the spectrum, one would find the long-range ^{13}C-^{1}H scalar coupling multiplets with intensities indicative of the total ensemble of molecules in which the coupling exists.

The significant differences in short-range and long-range ^{13}C-^{1}H **J**-values facilitates their individual manipulation by pulse sequence experiments. Therefore, one is able to probe separately short-range and long-range ^{13}C-^{1}H scalar couplings for means of structure elucidation. This can be achieved separately or by combination of the following two ways:

- one may exploit the differences in **J** in terms of their frequencies of evolution in the rotating frame.
- One may selectively manipulate either a short-range or long-range ^{13}C-^{1}H scalar coupling (in separate molecules) by continuous selective *r.f.* irradiation or selective *r.f.* pulses. (Appendix 10)

The latter is possible since the difference in **J**-values necessitates their different resonance frequencies. If one wanted to manipulate all protons, which exhibit long-range^{13}C-^{1}H scalar couplings, one could apply a selective pulse that encompasses the entire frequency range of long-range^{13}C-^{1}H scalar couplings. This relates to the spectral region of the ^{12}C bonded proton resonance, as detailed above. If the frequency selectivity of the pulse is maintained, the short-range coupled protons in other molecules would not be manipulated since the frequencies of the ^{13}C satellites are well removed. Indeed this is the basis of the selective 1-D heteronuclear long-range correlation experiments detailed in this thesis.

A3.2.8 Broadband proton decoupling

Scalar coupling multiplicities sometimes lead to the complication of crowded spectra and always lead to the reduction in signal-to-noise ratio. The latter is a major problem in the

spectra of insensitive nuclei, e.g., ^{13}C, and often one implements the removal of scalar couplings to all protons of the sample thereby increasing signal-to-noise ratios.

To achieve this aim one uses proton broadband decoupling utilising *composite pulse decoupling* (CPD) sequences (Appendix 9) [54, 23, 43]. Each composite pulse element contains a number of proton pulses of different phases and nutation angles, which cause a resonance offset and *r.f.* inhomogeneity-compensated proton inversion pulse.

An inversion pulse applied to protons in a spin-echo sequence causes the refocusing of scalar coupling evolution of the heteronucleus, e.g., ^{13}C, in the rotating frame (Appendix A1.8). Consequently, composite proton inversion pulses applied at a rate that is fast in comparison to J_{CH} during ^{13}C signal acquisition (trains of CP elements) effectively leads to broadband decoupling of all protons from ^{13}C.

The relative phases of pulses within the CP elements and the relative phases of the train of elements themselves are inverted in a prescribed fashion so as to achieve optimum cyclicity [43]. From a qualitative view-point, optimum cyclicity is achieved when the CPD element refocuses the component vectors of the scalar coupling exactly to the point from where they originated. In terms of the scalar coupling spin energy levels, the proton spin levels remain completely degenerate and hence the insensitive nucleus is completely decoupled from protons.

The MLEV-16 CPD sequence [22-23, 43], as the name suggests, comprises 16 CP elements:

$R\overline{R}\overline{R}R\ \overline{R}RR\overline{R}\ \overline{R}RR\overline{R}\ R\overline{R}RR$

Where R and $\overline{R}$ are the composite pulse sequence elements: $90_x180_y90_x$ and $90_{-x}180_{-y}90_{-x}$ respectively. The MLEV-16 CPD sequence achieves proton broadband decoupling over a frequency bandwidth of $1.5 \times \gamma B_1/2\pi$, which is adequate for most proton chemical shift ranges. The MLEV-16 composite pulse scheme is an example of a "super-cycle" composite pulse sequence [43, 23] of which there are now many.

Appendix A4 The NMR Spectrometer

The precise composition of NMR spectrometers depends upon the manufacturer. However, the basic elements and their general function remain consistent between most types. Figure A4.1 illustrates the typical composition of a NMR spectrometer and each of the main components, which are briefly addressed in turn.

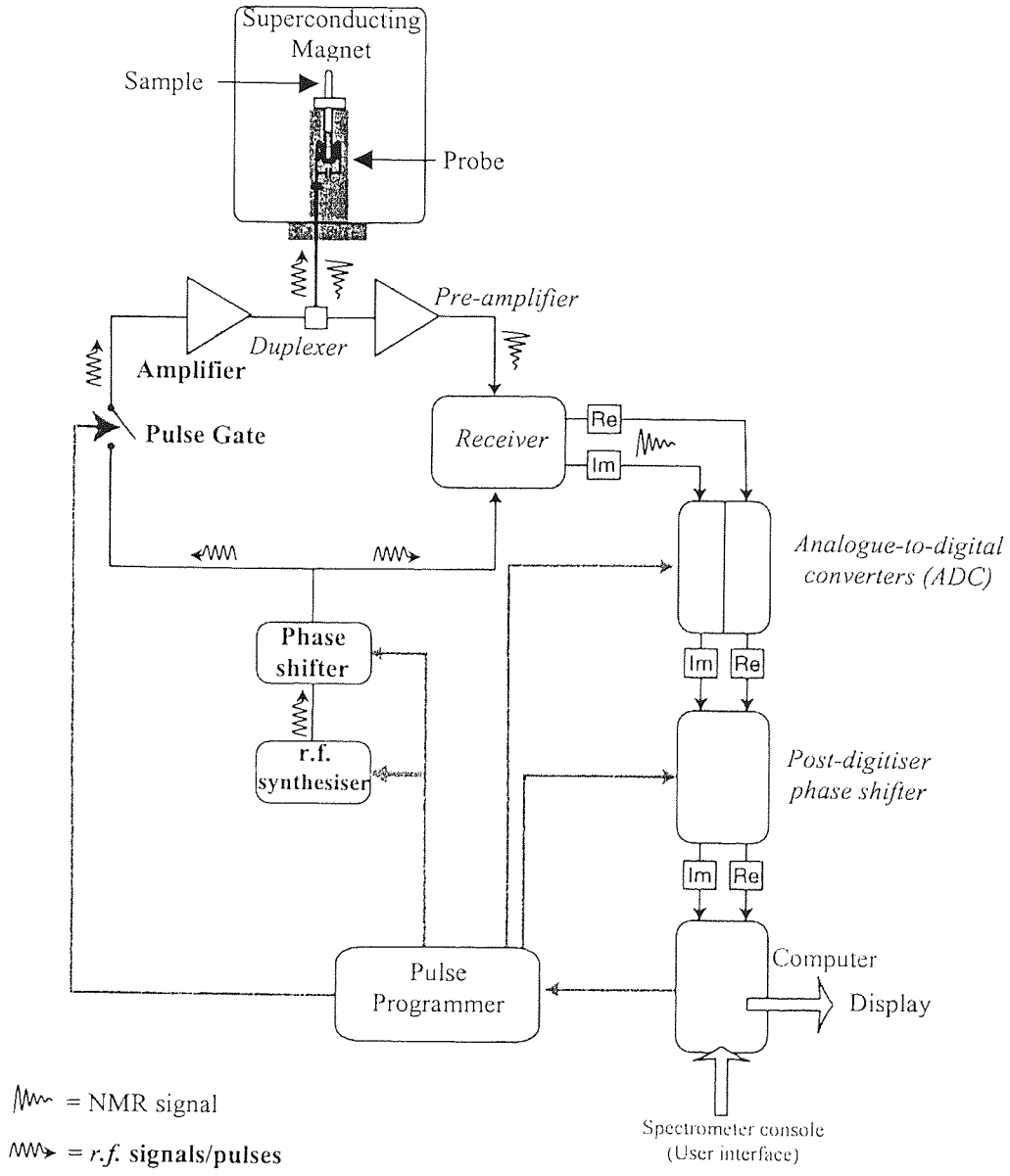

Figure A4.1 Schematic of a typical NMR spectrometer modified from Levitt [52]

Labels in *italics* indicate components of the 'receiver section' and those in bold represent the 'transmitter section', which are described later.

A4.1 The static magnetic field B_0

Most modern spectrometers except, for the recently released table–top spectrometers, utilise superconducting magnets consisting of a suitable metal alloy solenoid immersed in a bath of liquid helium, which facilitates the superconducting nature of the alloy. Once the magnet is initially charged or *energised* after installation, the superconducting magnet will run almost indefinitely. The helium bath is insulated by a liquid nitrogen reservoir, which is separated from the helium bath by a vacuum barrier to reduce thermal leakage of helium molecules. The superconducting solenoid encapsulates the central cavity, called the *bore*, which runs through the centre of the cylindrical can. The NMR probe, into which the analytical sample is positioned, is inserted into the bottom of the bore such that the sample sits in the strongest and most homogeneous part of the magnetic field $\mathbf{B}_0$. The bore is separated from the superconducting solenoid by evacuated barriers so that the probe may remain at room temperature if so desired.

It is essential to achieve optimal long-term stability and homogeneity of the magnetic field across the entire sample volume to ensure minimal inhomogeneous line broadening (Appendix A6.5.1) and to optimise spectral resolution and signal line-shape. The magnetic field will have inherent defects in its homogeneity, which are in part corrected by the cryo-shims. The cryo-shims are coils of the same superconducting material as the solenoid, which are energised at the same time as the magnet and are also immersed in the liquid helium bath. The cryo-shims are oriented such that they impart small correctional magnetic fields to $\mathbf{B}_0$ and are adjusted when the magnet is installed for the first time in order to *shim out* any major inhomogeneities.

A second set of shim coils called the *room temperature shims* are supported on a tube, which is situated inside the bore in the vicinity of the solenoid. The electrical currents in the room temperature shims, which give rise to small correctional magnetic fields, are adjusted prior to experiments to fine-tune $\mathbf{B}_0$ homogeneity and maximise signal resolution and sensitivity. The process of room temperature shimming is performed prior to the start of the experiment and is described later in section A4.4.

It is desirable for optimum sensitivity to obtain the highest possible field strengths (Appendix A1.4.1). Superconducting magnets are extremely expensive, and constitute the majority of

the cost of the NMR spectrometer and increase in price in proportion to their field strength. Magnetic field strength is measured in Tesla but for convenience is usually expressed in terms of the proton Larmor frequency that it invokes. Currently the highest field strength is 900MHz (21 Tesla).

In addition to the intrinsic cost of NMR spectrometer hardware, one must periodically top-up the liquid helium and nitrogen supplies to maintain superconductivity and magnetic field stability. Consequently, the cost of NMR in comparison to other spectroscopic techniques is very high and so necessitates efficient use of experimental time. Subsequently, one of the major thrusts of NMR pulse sequence design and NMR hardware development is to increase the sensitivity of experiments and reduce experimental time. Indeed, the reduction experimental time is one of the objectives of novel pulse sequences detailed in this thesis.

A4.2 The probe

The probe is considered the most important and sensitive piece of hardware of the NMR spectrometer and has several functions:

- the probe positions the sample in the strongest and most homogeneous part of $\mathbf{B}_0$
- It contains all of the components responsible for the application of *r.f.* pulses and detecting (receiving) the NMR signal (e.m.f.).
- It usually has a device for spinning the sample tube about its long axis to average out magnetic field inhomogeneities transverse to $\mathbf{B}_0$.
- It will contain a heating/cooling device for stabilising the temperature of the analytical sample.
- It may contain extra coils for special functions including the application of magnetic field gradients.
- The probes components and function will vary according to whether liquid or solid state NMR is being employed or depending upon the nucleus under scrutiny.

The liquid analytical sample is contained in a precisely machined glass tube since discrepancies in the tubes dimensions adversely affect the homogeneity of $\mathbf{B}_0$ across the sample volume or its magnetic susceptibility. The sample tube is inserted into the top of the bore and pneumatically positioned into the top of the probe where it is surrounded by the *r.f.* coils. In a ^{13}C- ^{1}H dual probe there are generally two coils; a transmitter/receiver coil for

manipulation and observation of ^{13}C and ^{1}H, and a second coil usually referred to as the *decoupling coil.* The decoupling coil is usually used to apply pulses or continuous *r.f.* fields to ^{1}H to remove (decouple) scalar coupling to protons during observation of insensitive nuclei (Appendix A3.2.8). Both coils are situated perpendicular to the axis of the sample tube so as to apply *r.f.* pulses transverse to $\mathbf{B}_0$. In contrast, Z-gradient coils are wound around the sample tube to impart small longitudinal magnetic field gradients that augment or detract from $\mathbf{B}_0$. (Figure A4.2).

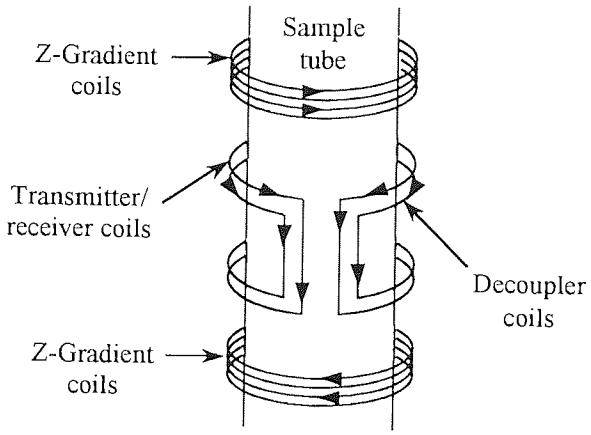

Figure A4.2 **Simplified schematic of a liquid-state dual probe with Z-gradient coils**

All probe components are made from materials, which have near zero net magnetic susceptibility.

In a pulse sequence experiment, when the *r.f.* pulses have ceased, the transmitter/receiver coil detects the tiny e.m.f. generated by the evolution of single quantum coherence, and is subsequently routed to the duplexer and receiver hardware (Figure A4.1).

The probe contains a tuneable electronic circuit consisting of a tuning and matching capacitor, which allows one to manually (or automatically in some systems) increase the sensitivity of the probe to detect the e.m.f. and increase the intensity of the *r.f.* pulses. The electrical properties of the tuned and matched circuit are affected by the sample composition and demands readjustment for every new sample. Similarly, the circuit must also be tuned and matched for the study of different nuclear isotopes.

A4.3 Field-frequency lock system

To ensure the long-term stability of $\mathbf{B}_0$, which is prone to drift, a field-frequency lock system is employed. The spectrometer computer continuously monitors the resonance condition of deuterium isotopes in the dispersion mode so that it can easily detect the natural drift of $\mathbf{B}_0$ (Figure A4.3).

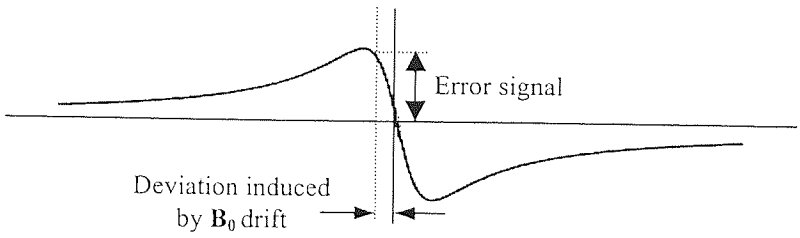

Figure A4.3 Deuterium field-frequency lock signal in dispersion mode.

The analytical sample or solute is usually dissolved in a deuterated solvent (lock solvent), so providing a homogeneous liquid, which provides the necessary deuterium isotopes. However, one can incorporate the lock material heterogeneously by inserting a capillary, which contains the lock material into the analytical sample tube. The choice of lock solvent employed obviously depends on the solubility of the solute and e.g., aggregation effects that the solvent may invoke. Thereafter, one should choose a solvent, which has a high concentration of deuterium isotopes for optimum lock sensitivity, and one with an inherently narrow line shape to ensure optimum sensitivity to $\mathbf{B}_0$ drift.

The lock system utilises a continuous feedback circuit so that when it senses a drift in $\mathbf{B}_0$ (which is manifested in the integrated lock signal having a non-zero (error) value) a proportionate compensatory electric current is applied to an extra room-temperature shim coil. The magnetic field generated in the shim coil appropriately augments or detracts from $\mathbf{B}_0$ to correct the field drift. Once activated by the user, the lock system can be considered a perpetual NMR experiment that runs in parallel to the real NMR experiment. Consequently, the lock system has dedicated *r.f.* synthesisers, receiver hardware and transmitter coils in the NMR probe.

To start the lock system it is necessary to *lock onto* the deuterium resonance, which is achieved either manually or automatically depending upon the spectrometer. Essentially the frequency of the lock transmitter is set exactly on the deuterium resonance and the lock

system is then engaged and the feedback circuit active. The lock signal can now be displayed as the integrated intensity of the signal, which remains constant so long as $\mathbf{B}_0$ remains constant. When the homogeneity of $\mathbf{B}_0$ is diminished, the height of the lock signal decreases according to a loss of spectral resolution and broadening of the NMR line.

Manual adjustment of the room temperature shims is performed to maximise the height of the integrated lock signal, which corresponds to an increase in $\mathbf{B}_0$ homogeneity. Consequently, greater signal resolution of the deuterium lock signal is achieved, which narrows the deuterium line. Since the central part of the dispersion signal is now steeper, the lock system becomes more sensitive and better corrects for subsequent drifts in $\mathbf{B}_0$.

The lock system can be optimised manually namely, the lock gain, monitoring interval and lock power, to provide increased stability of $\mathbf{B}_0$. Indeed, lock optimisation has been employed in more sensitive work detailed in this thesis, which rely upon accurate long-term $\mathbf{B}_0$ stability.

A4.3.1 Room Temperature Shimming

The room temperature shims are used to correct the day-to-day $\mathbf{B}_0$ inhomogeneities that arise due to the changing of probes, samples, temperature and pressure. Room temperature shimming is performed prior to all NMR experiments to ensure optimal spectral resolution and good line shapes. There are two main sets of shims; those that effect the longitudinal homogeneity of $\mathbf{B}_0$ (axial or Z-shims) and transverse to $\mathbf{B}_0$ (radial or X/Y shims). Each individual shim prescribes a different correctional effect upon $\mathbf{B}_0$, which interact with other subsets of shims to different orders. Consequently shimming is an iterative process requiring a great deal of insight into the inter-relationship of the sub sets of shims. However, maladjustment of certain shims, causes particular inhomogeneities, which produce well-known line shapes, which act as a guide for their subsequent correction [1].

In some high-resolution experiments the sample is spun to average out transverse (X-Y) inhomogeneities. Consequently, the radial shims are sometimes referred to as the *stationary shims* since they must be corrected when the sample is stationary. The stationary shims must be well adjusted to prevent the manifestation of *spinning sidebands*, which are miniature images of the resonance line symmetrically disposed about the chemical shift at multiples of

the spinning frequency. When the magnet has been well shimmed, usually only a select few of the axial and radial shims require adjustment prior to the experiment.

A4.3.2 The analytical sample

The analytical sample is prepared to achieve optimum spectral resolution and experiment sensitivity. Obviously one should maximise the solute concentration in solution to maximise sensitivity while maintaining a sufficiently high concentration of lock solvent. One should use sample tubes machined to the highest affordable precision in order to minimise magnetic susceptibility differences, which can reduce spectral resolution. The sample tubes should be clean and dry on both the internal and external surfaces. Cleaning and flushing with acetone usually suffices followed by drying initially on a clean vacuum line and finally in an oven to remove any remaining acetone.

The liquid sample should be free from particulates, which cause local distortions in $\mathbf{B}_0$ homogeneity. Sample tubes may simply be filled from a Pasteur pipette containing a plug of clean and dry cotton wool acting as a filter. Samples may need to be filtered through a metal chelating resin in order to remove paramagnetic impurities that lead to T_2 (Appendix A6.5) relaxation-induced losses in spectral resolution.

One must ensure that all samples are made to a minimum liquid depth as specified by the probe manufacturer. This is to ensure that the sample is fully encompassed by the coil region of the probe so preventing magnetic susceptibility differences in the sample leading to a loss of spectral resolution.

A4.3.2.1 Degassing liquid analytical samples

When performing high-resolution experiments or relaxation dependent experiments, e.g., nOe measurements, one is usually required to remove dissolved molecular oxygen from the liquid sample (Appendix A7.2.2). Three to four freeze-pump-thaw cycles is usually sufficient, to remove the majority of dissolved molecular oxygen: the liquid sample is slowly frozen over liquid nitrogen and the cavity above the liquid in the sealed sample tube is evacuated under high vacuum. The sample is allowed to thaw, and the dissolved molecular oxygen comes out of solution into the evacuated area above the liquid [24]. The tube can be sealed temporarily with a rubber septum or permanently flame sealed.

A4.4 Performing NMR experiments

In general the following actions are carried out in order to perform a basic NMR pulse sequence.

- Prepare and locate the sample in the NMR probe and allow for temperature to equilibrate if necessary.
- Tune and match the NMR probe.
- Engage the field-frequency lock system and adjust the room temperature shims
- Set the receiver gain.
- Load the pulse sequence (Pulse program) and set the acquisition parameters (see later)
- Execute the experiment.
- Process the F.I.D. and spectrum.

NMR spectrometer operations are controlled via a user interface, which maybe a stand-alone computer or a console, which is integrated with the NMR hardware. The computer or console software routines allow one to inspect and edit pulse sequences, input acquisition and processing parameters and plot spectra. Among the many other experimental parameters, the acquisition parameters define the function of the transmitter, namely the pulses and delays of the pulse sequence. The parameters pertaining to processing, i.e., the spectral width, acquisition time, digital resolution etc., have already been discussed in Appendix A2.

A4.4.1 The Transmitter Section

The transmitter section is responsible for the generation of *r.f.* pulses, which are routed to the probe for application to the analytical sample.

A4.4.2 The *r.f.* synthesiser and pulse gate

The synthesiser produces a constant oscillating *r.f.* signal B_1,which is set by the user and determines the centre of the NMR spectrum (carrier/reference frequency). The phase of the signal is set by the phase-shifter, which is controlled by the *pulse programmer*, which has interpreted the pulse sequence via a *pulse program* (The pulse program is described later).

The pulse programmer instructs the pulse gate to open and close to the continuous *r.f.* signal producing a pulse. The duration of the pulse, i.e., the period of time in which the pulse gate is opened and then closed, is defined by the acquisition parameters.

In order to obtain clean pulses, the pulse gate is usually switched open after a suitable time has been given to allow the transmitter to stabilise after switching phases and/or frequencies of $\mathbf{B_1}$. The time taken to switch pulse powers, phases and frequencies is accommodated in pulse programmes, according to the recommendations made by the spectrometer manufacturers. Usually such functions require a maximum of a few tens of microseconds.

A4.4.3 The *r.f.* amplifier

The amplifier simply amplifies the *r.f.* pulse to the power specified by the pulse program for application via the probe to the sample.

A4.4.4 The duplexer

The duplexer routes the pulses to the probe and the e.m.f. to the receiver hardware. Therefore, the former does not interfere with the sensitive receiver hardware and the latter is not lost to the transmitter hardware.

A4.4.5 Receiver Section

After the e.m.f. (NMR signal) exits the duplexer it is subsequently amplified by the pre-amplifier (pre-amp) prior to being fed into the receiver. To achieve quadrature detection (Appendix A2.4), the 'receiver' splits the NMR signal and feeds them into two separate channels each with its own phase sensitive detector. The two signals are combined with the carrier frequency (reference frequency) from the *r.f.* synthesiser so that each is $\pi/2$ radians out of phase with respect to the other, and oscillates at a relative Larmor frequency $(\omega - \omega_0)$. The two analogue signals (representing the real (Re) and imaginary (Im) parts of the NMR signal) are fed into separate analogue-to-digital converters (ADC) and the analogue signals are converted to the digitised F.I.Ds. Eventually each F.I.D. is stored in a separate memory region before being combined for a complex FT.

In order to achieve phase cycling one must be able to specify the conceptual phase of the receiver, which is tantamount to modifying the phase of the digitised F.I.D.. This can be achieved in one of two ways:

- the carrier frequency (receiver reference frequency) can be changed independently after pulsing, which would cause the phase shift of the Real (Re) and Imaginary (Im) signals prior to digitisation.
- The phase of the Re and Im F.I.D.s can be modified by a post-digitiser phase shifter.

NMR spectrometers usually employ post-digitiser phase shifters, which simply multiply the complex F.I.D. by a phase factor $\exp\{-i\varphi_{dig}\}$ before FT. For F.I.D. (receiver) phase shifts of $\varphi_{dig} = \pi$, this corresponds to changing the sign of the Re and Im signals, i.e., $\exp\{-i\varphi_{dig}\} = -1$. For phase shifts $\varphi_{dig} = \pi/2$, a combination of phase shifting and data routing is utilised: the sign of the Re signal is changed as above and the Re and Im signals are routed down the opposite channels and stored in opposite memory regions.

A4.4.5.1 Dynamic range and the receiver gain

The maximum range of frequencies that the ADC can digitise (SW) is dependent upon the rate at which the signal can be digitised, i.e., the lowest value of DW. Furthermore, the ADC limits the range of amplitudes of the NMR signals that can be measured: the digitiser represents the amplitude of the NMR signal by assigning a binary number of proportionate value, which is represented by computer bits. The number of bits available to represent the amplitude of signals is referred to as the ADC *resolution*. For example, a 16-bit digitiser is able to represent amplitudes in the range $\pm 2^{15}$-1, and the ratio between the maximum and minimum values, i.e., 2^{15}:1 is referred to as the *dynamic range* of the ADC. If the *receiver gain* (see later) is set such that the largest NMR signal is digitised using the maximum number of bits, the smallest signal must be represented by 1 bit. Consequently, NMR signals that have amplitudes that are proportionately less than that represented by 1 bit will not be digitised. Dynamic range problems are usually limited to the observation of sensitive nuclei, namely, protons. For example, the considerably more intense signal amplitudes of protonated solvents *fill* the digitiser, while the significantly less intense signals of the solute may not be digitised or suffer from low signal-to-noise ratios.

The gain of the receiver is set prior to all NMR experiments usually by using an automated system invoked by the user. Subsequently, the receiver is able to correctly digitise the most intense NMR signal so preventing *clipping* of the F.I.D., which results in baseline distortion in the NMR spectrum.

A4.5 Pulse programming

Pulse sequences are transcribed into pulse programs, which are ASCII texts consisting of a number of lines containing one or more pulse program statements. Pulse program statements are the commands that are interpreted by the pulse programmer and specify the actions to be carried out by the hardware and software in the order specified, i.e., pulses and delays. Pulse programs are written in a *program language* and syntax that is specific to the manufacturer of the NMR spectrometer.

When the user initiates a NMR pulse sequence experiment, the pulse program compiler is invoked, which converts the pulse program into a binary form that can be interpreted by the pulse programmer. The pulse sequence experiment is started and is performed according to the acquisition parameters, which have been set by the user prior to starting. If syntax errors are found in the pulse program the experiment is aborted.

Novel NMR pulse sequences have to be transcribed into pulse program language using the correct syntax. Additional to the raw transcription of the pulse sequence, pulse program statements must be entered to execute vital functions for the correct performance of the pulse sequence experiment. For example, the application of a pulse to a particular nuclear isotope requires the specification of the correct channel (transmitter or decoupler) along which it is applied.

The composition of a pulse program of a PENDANT pulse sequence for a Bruker Avance 300 spectrometer is given below. The pulse program statements, which refer to the raw pulse sequence are highlighted in **bold** and the additional spectrometer operational statements, i.e., channel specifications, power level switching commands, etc, are highlighted in *italics*. The shaded area contains the PENDANT pulse sequence and related pulse program statements.

```
;pendant avance version
;John Homer, Michael C. Perry, J. Chem. Soc. Chem. Comm. 1994,
373
;gives XH, XH3 negative and XH2 and X positive
;with decoupling during acquisition

#include <Avance.incl>
"p2=p1*2"
"p4=p3*2"
"d4=1s/(cnst2*4)"
"d15=5s/(cnst2*8)"


1 ze
2 d1 do:f2                ;d1 : relaxation delay; 1-5 * T1
  d12 pl2:f2              ;pl2 : f2 channel - power level for pulse
  (p3 ph1):f2 (p1 ph2):f1
  d4                      ;d4 : 1/(4J(XH))
  (p4 ph3):f2 (p2 ph4):f1
  d4
  (p3 ph5):f2 (p1 ph7):f1
  d15                     ;d15 : 5/(8J(XH))
  (p4 ph3):f2 (p2 ph6):f1
  d15 pl12:f2             ;power level for CPD decoupling
3 go=2 ph31 cpd2:f2 ;acquire spectrum with CPD decoupling
  d12 do:f2
  wr #0
exit
```

```
ph1=0 0 0 0 0 0 0 0
    2 2 2 2 2 2 2 2
ph2=0 0 0 0 0 0 0 0
    2 2 2 2 2 2 2 2
ph3=0 2
ph4=0 2
ph5=1 1 3 3
ph6=0 2
ph7=1 1 3 3
ph31=1 1 1 1 1 1 1 1
     3 3 3 3 3 3 3 3

;cpd2 : decoupling according to sequence defined by cpdprg2
;p1 : f1 channel - 90 degree high power pulse
;p2 : f1 channel - 180 degree high power pulse
;p3 : f2 channel - 90 degree high power pulse
;p4 : f2 channel - 180 degree high power pulse
;p31 : - 90 degree pulse for decoupling sequence
;NS : 4*n
;DS : 4 or 8
```

A4.5.1 Pulse program composition and basic syntax rules

Pulse programs are line oriented: the pulse programme statements on each line specify the actions to be taken by the NMR hardware and software.

- Statements on the same line are executed simultaneously.
- Statements on consecutive lines are executed sequentially.
- Statements within parentheses are executed sequentially.
- When more than one set of parentheses exists on the same line, the first statement within all of the parentheses are executed simultaneously. Statements within each set of parentheses thereafter are performed sequentially as usual.

Each line in the program is performed sequentially from top to bottom. Some lines one numbered, the reasons for which are defined later.

A semicolon (;) specifies that the rest of the line is dedicated to a comment used for information purposes and is not interpreted as action to be taken by the spectrometer.

The statement, #include <filename>, specifies the name of another pulse program file that is invoked at the same time as the current pulse program. For example, #include <Avance.incl> specifies basic instructions for the execution of all pulse sequence experiments.

A4.5.2 Pulse program statements

The ZE command has the following functions.

- Resets the scan counter, i.e., the number of transients of a particular experiment collected, to zero before the acquisition is started. When the user has specified that a number of dummy scans (DS) are to be executed prior to the execution of real scans, the scan counter is set to –DS. Dummy scans are identical to real transients except that the NMR signal is not acquired during the acquisition time and are used to achieve steady-state in the spin system prior to real data acquisitions. When DS = 0 no dummy scans are executed.
- Sets the phase list pointer to the first entry in the phase program lists after DS dummy scans.

- Instructs the computer to overwrite the existing F.I.D. in the current memory area with the subsequent F.I.D..

Line 2: **d1** *do:f2*

Delays are represented by the statement **dn**, where **n** is an integer. "**d1**" instructs the spectrometer to execute a delay of length **D1** defined in the acquisition parameters. In this instance, **D1** is the relaxation delay of PENDANT. Simultaneously, the pulse gate on frequency amplifier channel 2 (**f2**) is closed (**do**) and composite pulse decoupling (CPD) (Appendix A3.2.8) turned off (see below). In this example, the relaxation delay **D1** provides more than adequate time to execute, **do**, since a minimum of 20 microseconds is required. However, in other circumstances a separate delay will be specified in front of the spectrometer operation statement.

Following line 2 a similar action is taken: ***d12 pl2:f2***. During the delay of value **D12**, the power level (**pl2**) is set to the value **PL2** from the acquisition parameters for frequency channel 2 (**f2**). In this case channel 2 is the *r.f.* channel (decoupler) used for proton pulses in PENDANT and the power level is set for high power (hard) pulses. More than one spectrometer command, e.g., two power-switching commands, cannot be placed on the same lines.

The pulse program statement, **(p3 ph1)***:f2* **(p1 ph2)***:f1* executes a pulse of duration given by the acquisition parameter **P3** on channel **f2**, of phase given by the phase program list **ph1** at the bottom of the pulse program. Simultaneously, a pulse of duration given by the acquisition parameter **P1** on channel **f1**, of phase given by the phase program list **ph2** is executed. Channel **f1** in this instance is the transmitter/receiver channel used for ^{13}C pulses and signal acquisition.

The remainder of the highlighted pulse program pertain to the pulses and delays component to PENDANT.

Line 3: *go=2* ph31 *cpd2:f2*

The pulse programme statement "***go***" is a *macro* statement and initiates a number of integral functions including and relating to signal acquisition. On the Bruker Avance 300 spectrometer, 8 functions are performed, five of which are performed during the delay DE.

Each of the five functions; DE1, DE2, DERX, DEPA and DEADC are executed after each of their corresponding subdelays in an order that depends on the length of each.

1) DE1: Modifies the frequency of the receiver if a particular type of quadrature detection is employed.

2) DE2: Sets the receiver phase to 0 (+x).

3) DERX: The receiver channel is open ready for data acquisition.

4) DEPA: The pre-amplifier is set to receive the NMR signals.

5) DEADC: The digitiser is enabled.

6) After the total delay DE, digitisation of the NMR signal is started according to the acquisition parameters, **DW** and **TD** (Appendix A2.3).

7) The acquisition delay **AQ** is executed during which digitisation continues.

8) At the end of **AQ** and subsequently the end of digitisation of the F.I.D., a 3 millisecond delay is executed in which the following functions are executed:

a) The scan counter is incremented.

b) If DE1 is executed the frequency of the receiver is reset.

c) The list pointers of the phase programs (**phn**) are incremented to the next phase in the pulse sequence phase cycle.

d) The statement *go=n* initiates a loop to the statement *n*. The pulse program statements between *n* and *go* are executed DS + NS times. The numbering of pulse program lines is only required to indicate the destination of loops.

Behind the *go* statement the receiver phase is specified by the phase program **ph31**.

At the start of acquisition broadband composite pulse decoupling (CPD) of protons (**cpd2**) on channel f2 occurs simultaneously, utilising the CPD pulse program CPDPRG2, e.g., MLEV16 (Appendix A3.2.8), which is defined in the acquisition parameters. CPD decoupling continues until it is turned off by the statement, *do*, on line 2.

After the final transient has been collected, CPD is switched off by the pulse programme statement, *d12 do:f2*, which is situated after the *go* statement. The acquisition data, including the F.I.D., acquisition parameters, processing parameters, etc, are written to the default data file by the statement *wr #0*.

A4.5.3 The phase program statements

The phase programs, **phn**=, define the phases of the pulses according to the phase cycle. Each phase is taken in turn by the sequential movement of the phase list pointer by execution of step 8c in the *go* statement. The numbers 0,1,2 and 3 correspond to the phases x, y, -x, -y.

A4.5.4 User defined parameters

At the beginning of the pulse program a number of comments appear in speech marks. These are convenient methods of defining the magnitudes of delays and pulses by means of simple formulae: "d4=1s/(cnst2*4)". The acquisition parameter D4 will always take the value defined by the formula where the value of the constant (cnst2) is the average **J**-value in PENDANT, i.e., 145Hz. When a new value of <**J**> (cnst2) is defined in the acquisition parameters, the new value of D4 is automatically calculated. This facilitates routine use of the pulse program since usually only <**J**> is changed between experiments.

The lengths of delays can be specified in the pulse programs for the Bruker Avance 300 or can be set as acquisition parameters prior to the start of the experiment. For example, one can simply enter the statement, 20m, to invoke a 20 millisecond delay. Such statements are usually limited to fixed delays, e.g., power switching delays, while evolution delays, are defined by the usual "**dn**" statements can be set by the corresponding acquisition parameter without having to change the pulse program.

A4.5.5 Pulse lengths and pulse powers

Pulse power levels of (magnitudes of $\mathbf{B}_1$) are defined by the acquisition parameters (PLn) and are given by attenuation level, measured in decibels (dB), from maximum power of the amplifier being used. In general, hard pulses utilise maximum power (lowest attenuation setting), while soft selective pulses take lower values (higher attenuation settings). Since the nutation angle for a given pulse duration is proportional to the magnitude or power of $\mathbf{B}_1$, a calibration of each pulse for different pulse powers is required. The calibration of pulses is described briefly in A4.13and A4.14.

A4.5.6 Glossary of other pulse program statements

gpn – Executes a gradient pulse of length specified by the preceding pulse statement. The type of gradient is specified by the gradient program, which is an acquisition parameter, and defines the shape of the gradient pulse (See Appendix BX). The amplitudes of gradients are specified by a percentage, i.e., 100% being maximum power, and a sign + or -, indicating the phase.

UNBLKGRAD – Unblank gradient pulse amplifier and turn field-frequency lock-hold off.

BLKGRAD – Blank gradient pulse amplifier and turn field-frequency lock-hold on.

fqn – Sets the carrier frequency to the value, which is currently assigned by the frequency list pointer in the corresponding frequency list "FQLISTn" specified in the acquisition parameters. The frequency list is an ASCII text file defining a list of frequencies usually specified in Hz. When the statement, **fqn**, is encountered in the pulse program, the first value in the list is executed and the list pointer is incremented to the next value. When the last value in the list is executed the list pointer is reset to the first value.

spn – Executes a shaped selective pulse of type specified by the acquisition parameter SPn. The pulse duration, power and phase are specified by the associated acquisition parameters of the preceding pulse program statements **pn**, **pln** and **phn** respectively.

lo to n time ln – By analogy with the *go* statement, this statement executes a loop to line **n**, which is repeated **ln** times as specified in the acquisition parameters. The pulse program statements between line **n** and the loop statement are then executed **ln** times-1. Therefore, to execute the train of 200 pulses in the DANTE (Appendix A10.3) pulse for selective PENDANT, the pulse program statements pertaining to the DANTE pulse are situated on line **n** and between the loop statement (Appendix A13.3). **ln** is then set to 200 prior to execution of the pulse sequence.

A4.5.7 Initiating signal acquisition without using the '*go*' statement

In the selective PENDANT-1-D HOESY pulse sequence (Chapter 3), there are two NMR signal acquisitions within the same pulse program: the first signal acquisition corresponds to the selective PENDANT experiment and the second to the 1-D HOESY experiment. In this instance the functions 8a and 8c performed automatically by the '*go*' statement are inappropriate for the first signal acquisition: the scan counter and phase list pointers should only be incremented after the second signal acquisition. Consequently, one should omit the functions 8a and 8c from the signal acquisition process, while maintaining execution of all the other signal acquisition functions integral to the '*go*' statement. This can be achieved by specifying the 5 macro statements, DE1, DE2, DERX, DEPA and DEADC in the same line in the pulse sequence where the '*go*' statement would usually have been situated (Appendix 15). Additionally, one specifies the statements, *aq* and *DWELL_GEN* on the next line, which causes the digitisation of the F.I.D. to continue for the full length of the acquisition time **AQ** according to the value of **DW** respectively.

After signal acquisition, the statement, *eoscnp*, appears on the next line behind a minimum delay of 100 microseconds (100u), which instructs the spectrometer to carry out the functions defined by 8a, and b given previously in the description of the '*go*' statement. Unfortunately, the scan counter is incremented, which cannot be avoided with current pulse programming capabilities. As the statement *eoscnp* does not define a loop, the pulse sequence continues with the next line and the remainder of the selective PENDANT-1-D HOESY experiment.

The receiver phase cycle for the selective PENDANT acquisition must be defined by the phase list ph31, i.e., the default receiver phase list specified by the macro statement DE1.

During a NMR pulse sequence experiment the NS F.I.D.'s are stored temporarily in a memory buffer before being written to a permanent file by the '*wr* =' command. However, when two signal acquisition periods exist in the same pulse sequence one must specify into which memory buffer the F.I.D.s of each experiment are temporarily stored, otherwise the separate data sets will be combined. The number of memory buffers made available for data storage is set by the acquisition parameter NBL (NBL =2) prior to the beginning of the pulse sequence. At the beginning of the pulse sequence, the statement, *st0*, resets the memory block pointer (which specifies the memory buffer location) to the first buffer memory

location ready for storing the F.I.D. of the selective PENDANT experiment. The statement, *st*, which is situated after the '*eoscnp*' statement, increments the memory block pointer to the next (in this case, the second and final) memory buffer location ready for storing the F.I.D. of the 1-D HOESY experiment.

After the NBLth memory buffer has been used, i.e., the 1-D HOESY buffer, the memory block pointer is reset to the first buffer memory location ready for storing the next F.I.D. of the selective PENDANT experiment. The data writing statement, *wr*=, situated at the end of the pulse sequence writes the separate NBL F.I.D.s to separate files for subsequent processing in the normal way.

A4.6 Hard Pulse Calibration

Pulse calibration is required for each nuclide that is manipulated by *r.f.*pulses. Pulse calibrations are also specific to the channel that is utilised, i.e., the particular pulse amplifier and the positioning of the coil in the probe etc. The work detailed in this thesis utilise direct detection of insensitive nuclei, e.g., ^{13}C and therefore pulses applied to the insensitive nuclei need only be calibrated for the transmitter channel, f1. However, protons are manipulated using both channels, i.e., f1 for direct-detect proton spectra and f2 (decoupler) for heteronuclear experiments.

NMR spectrometer manufacturers provide standard pulse programs and tests in order to suitably calibrate all pulses required for routine performance of NMR experiments. Most calibrations involve steadily incrementing the pulse lengths at a constant power until nulling of a signal that is directly on-resonance occurs. Since the null condition is equal to an inversion (provided the pulse lengths have been incremented in small enough amounts to ensure that a rotation multiple of π has not occurred), nutation angles and hence their equivalent pulse lengths are easily calculated. Calibrations are usually, and more preferably performed on air-saturated samples to ensure that nulling is a result of the pulse, rather than attributed to lengthy longitudinal relaxation times.

Proton pulses applied using channel f2 are usually calibrated indirectly by observing the insensitive nucleus spectrum of a proton-insensitive nuclear doublet, e.g., the ^{13}CH. A simple pulse sequence experiment [1] is performed whereby insensitive nuclear single quantum coherence is excited and the scalar coupling allowed to evolve by exactly 1/2**J**. At

the end of the evolution delay a proton pulse is applied and the doublet observed. Nulling of the doublet occurs when the nutation angle of the proton pulse is a multiple of $\pi/2$ corresponding to the complete conversion of single quantum coherence to unobservable multiple quantum coherence. Subsequently, the proton pulse durations for a given nutaion angle can be easily calculated.

A4.7 Calibration of shaped soft selective pulses

The calibration of shaped soft selective pulses is somewhat more complicated, owing to the requirement of the selective pulse to be phase coherent with hard pulses applied to the same nuclei in the same pulse sequence: a soft x-phase pulse must be equivalent to a x-phase hard pulse.

After an appropriate shaped pulse had been selected a software routine is invoked in order to calculate the pulse power and duration corresponding to the desired excitation bandwidth. Since the f1 and f2 pulse calibrations are identical for the Avance 300, the selective pulse calibration was simply carried out by the usual nulling method of an entire homonuclear coupled proton multiplet directly on-resonance.

After, the pulse had been calibrated, a normal phase corrected spectrum was obtained for a proton hard pulse on-resonance for the same proton multiplet. A selective pulse of same overall nutation angle was executed on resonance for the same multiplet. The resulting spectrum was phased to the same phase correction as that used previously for the hard pulse and any small zero and/or first order phase correction that was required was added to the acquisition parameters: the Bruker Avance 300 spectrometer enables the specification of a selective pulse phase correction, which is specified by the pulse program statement ":r", e.g., (p12:sp2 ph16:r):f2. The zero and first order phase correction is taken from the corresponding acquisition parameter.

All pulses were calibrated accurately and regularly throughout investigative work reported in this thesis.

Appendix A5 Two-dimensional spectroscopy

The term *dimension* in NMR actually refers to the number of frequency dimensions or domains present in a spectrum. For example, a one-dimensional spectrum has one frequency domain but actually contains a second dimension depicting intensity of the signal. Two-dimensional NMR spectra are presented on two orthogonal frequency axes, each analogous to a one-dimensional spectrum with the final third orthogonal dimension depicting intensity. They may be presented in different formats, often as contour plots rather than illustrating the intensity dimension, which sometimes complicates their view. As the name suggests, the contours represent the intensity and shape of the peak in the two frequency dimensions by concentric lines that are analogous to that drawn on a map (Figure A5.1).

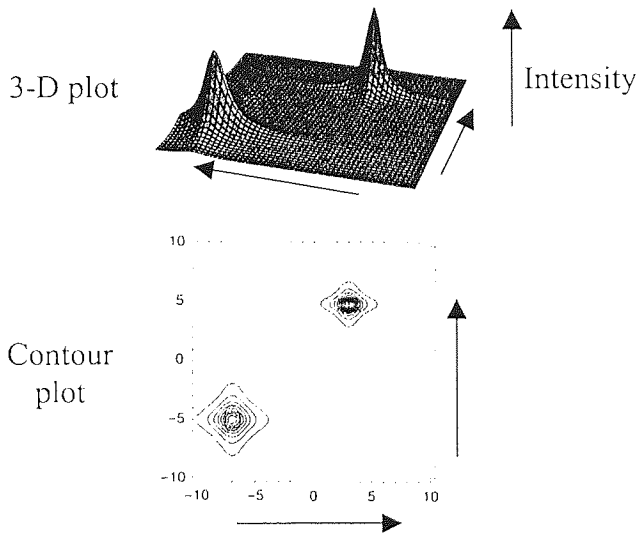

Figure A5.1 Schematic diagram of a two-dimensional spectrum modified from Levitt [52]

The spectral resolution of two-dimensional spectra is superior to one-dimensional spectra in that the noise of the spectrum is spread out over a plane without degrading the intensity of the signal. It was this advantage that was first realised by Jeener in 1971, the inventor of the technique, who proposed the pulse sequence and methodology for producing two-dimensional spectra (Figure A5.2).

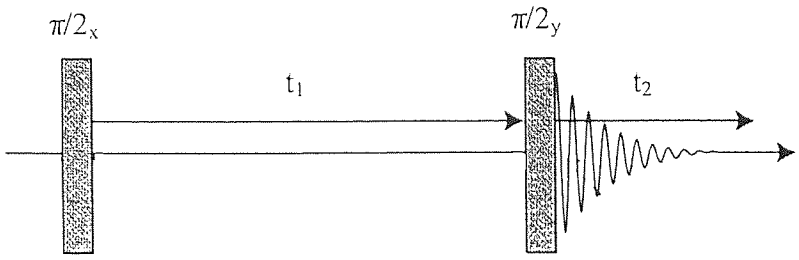

Figure A5.2 Basic pulse sequence for a two-dimensional experiment

A5.1 The second dimension

The effect of the pulse sequence is described in terms of the product operators (Appendix A8) for a simple two spin **I** = ½ system I and S that does not exhibit scalar coupling. Only the terms leading to observable single quantum coherence are presented in the final product operators.

$$
\begin{aligned}
&I_z + S_z \xrightarrow{\pi/2_x} -I_y - S_y \xrightarrow{\Omega I_z S_z t_1} -I_y\cos(\Omega I_z t_1) + I_x \sin(\Omega I_z t_1) \\
&-S_y\cos(\Omega S_z t_1) + S_x \sin(\Omega S_z t_1) \xrightarrow{\pi/2_y} -I_y\cos(\Omega I_z t_1) - I_z \sin(\Omega I_z t_1) \\
&-S_y\cos(\Omega S_z t_1) - S_z \sin(\Omega S_z t_1) \xrightarrow{\Omega I_z S_z t_2} -I_y\cos(\Omega I_z t_1)\exp(i\Omega I_z t_2) \\
&-S_y\cos(\Omega S_z t_1)\exp(i\Omega S_z t_2)
\end{aligned}
\qquad \text{A5- 5.1}
$$

The final observable coherence is cosine modulated as a function of chemical shift evolution during t_1. The coherence is also modulated as a complex function of chemical shift evolution due to normal quadrature detection during t_2.

Neglecting phase cycling, the pulse sequence is repeated and the evolution delay t_1 is incremented by a fixed amount on every successive transient. Each F.I.D. is stored separately in computer memory. The only change in the observable coherence is due to a cosine amplitude modulation as a result of chemical shift evolution during t_1. Consequently if one were to plot the modulation of signal intensity in the 1-D spectrum one would find that the I and S signals were cosine modulated in intensity (amplitude) by their respective chemical shifts. The evolution period t_1 has lead to the *frequency labelling* of the observable coherence.

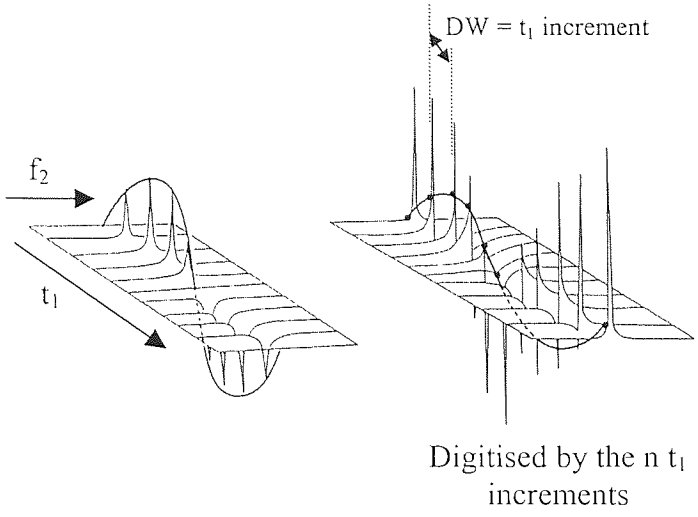

Figure A5.3 The interferrogram

With respect to the artificial time domain t_1, the I and S signals have been digitised according to a dwell time, **DW**, equal to the increment value of t_1 (Figure A5.3). The t_1 time domain signal is often referred to as the interferrogram since it is an artificially created F.I.D.. Two-dimensional Fourier transform with respect to t_1 and t_2 creates the two-dimensional frequency domain spectrum, f_1 and f_2. The I and S signals appear at their respective chemical shifts in each frequency dimension by analogy with that shown in figure A5.1.

A5.2 Correlation spectroscopy

Any experiment by which a property of the spin system can be modulated as a function of time permits the creation of another dimension. The simple experiment proposed by Jeener although providing greater spectral resolution, does not provide any extra information about the properties of the spin system. Ernst et al [4] realised the potential of the technique to provide more interesting information about the spin system while maintaining the signal-to-noise and resolution advantages. The idea stems from the realisation that signals that evolve with frequencies that are different during t_1 in comparison to t_2 may correlate two nuclei that share a mutual property like for example, scalar coupling. Indeed coherence transfer facilitates the correlation of scalar coupled nuclei by two-dimensional spectroscopy.

Multi-dimensional correlation spectroscopy is arguably the most versatile and informative of all pulse NMR experiments. The disadvantage of all multi-dimensional spectra is the inherently long experiment times due to the large number of transients required for adequate

digital resolution. Furthermore, extensive phase cycling routines extend even further the number of transients collected.

Appendix A6 Relaxation in liquids

During the course of NMR experiments radio frequency energy is applied to the spin system causing the excitation of coherence. Thereafter the spin system starts to return to thermal equilibrium via longitudinal and transverse relaxation, which serve to restore longitudinal magnetisation ($\pm\mathbf{M}_z \rightarrow \mathbf{M}_0$) and de-phase coherence ($\pm\mathbf{M}_{x,y} \rightarrow = 0$) over time periods T_1 and T_2 respectively.

Longitudinal relaxation is a purely enthalpic process: some of the magnetic nuclei of the sample have absorbed *r.f.* energy, which is subsequently dissipated via longitudinal relaxation mechanisms to the surrounding spin system. In contrast, coherence is a state of partial order of the magnetic nuclei, i.e., single quantum coherences exhibit phase coherence with each other and an external axis. Transverse relaxation is a purely entropic process as de-phasing coherence increases disorder, while the enthalpy of the system remains unchanged. Although the effects of longitudinal and transverse relaxation are quite different, their mechanisms are inextricably linked.

The random thermal motion of magnetic species of the sample produces a continuum of randomly fluctuating local magnetic fields of varying magnitude and frequencies. The local magnetic fields can be intra-molecular or inter-molecular in origin, caused by a variety of species. For example, nuclear dipoles, functional groups with magnetic moments and dissolved paramagnetic impurities, etc. The interaction of these local fluctuating magnetic fields with nuclei of the sample can give rise to longitudinal and transverse relaxation.

Both relaxation mechanisms processes are of central importance to the performance of NMR experiments. Longitudinal relaxation times largely determine the magnitude of most inter-pulse sequence relaxation delays and strongly influence experimental times. Transverse relaxation times determine the length of time that signals can be acquired before they decay to zero and also determines the observed line width in NMR spectra.

The treatment of relaxation given here adopts the following strategy:

- the general expressions for T_1 and T_2 are given.
- The fundamental mechanisms of longitudinal and transverse relaxation are described.

- A qualitative description of the length of T_1 and T_2 is given with respect to the physical properties of the liquids upon which they depend.

A6.1 General expressions for the longitudinal relaxation time T_1

For simplicity only the ensemble of one spin $\mathbf{I} = ½$ isotope that is assumed to be devoid of scalar coupling is considered for the derivation both relaxation time constants T_1 and T_2. Therefore one single quantum transition between the spin energy levels α and β each with component populations $\mathbf{P}_\alpha$ and $\mathbf{P}_\beta$ is considered. The probabilities of absorption, i.e., the transition $\alpha \rightarrow \beta$ and emission $\beta \rightarrow \alpha$ are given by the transition probabilities $\mathbf{W}_+$ and $\mathbf{W}_-$ respectively and the mean transition probability given by $\mathbf{W}$ figure A6.1

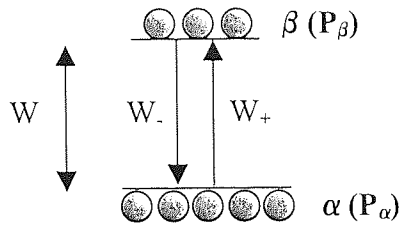

Figure A6.1 Single quantum transition for one spin I = ½ ensemble which is not scalar coupled

During the application of $\mathbf{B}_1$ the probability of absorption and emission is equal ($W_- = W_+$). After application of $\mathbf{B}_1$, the re-attainment of equilibrium begins and approaches the Boltzmann condition, which necessitates that $W_- > W_+$ by a factor proportional to the small population difference between the spin energy levels.

At equilibrium (eqm), the number of upward and downward transitions must be equal such that

$$P_{\beta eqm} W_- = P_{\alpha eqm} W_+ \qquad \text{A6- 6.1}$$

The Boltzmann condition requires that:

$$\frac{W_+}{W_-} = \frac{P_\beta}{P_\alpha} \exp(-2\mu B_0 / kT) \approx (1 - 2\mu B_0 / kT) = (1 - 2c) \qquad \text{A6- 6.2}$$

where **c** is a constant.

In relation to equation A6-6.2, $\mathbf{W}_+ = \mathbf{W}\exp(-\mathbf{c})$ and $\mathbf{W}_- = \mathbf{W}\exp(+\mathbf{c})$ i.e., $\mathbf{W}_+/\mathbf{W}_- = \exp(-2\mathbf{c})$
So $\mathbf{W}_+ = \mathbf{W}(1-\mathbf{c})$ and $\mathbf{W}_- = \mathbf{W}(1+\mathbf{c})$

then

$$W_+ + W_- = 2W \qquad \text{A6- 6.3}$$

So **W** is the mean transition probability. The factor of two is due to the transition of one nucleus changing the population difference by two.

The rate of change of the population difference across the transition is given by

$$\frac{d(P_\alpha - P_\beta)}{dt} = 2(W_- P_\beta - W_+ P_\alpha) \qquad \text{A6- 6.4}$$

By substituting for the transition probabilities shown above and the population difference across the transition, $\mathbf{P}_\alpha$-$\mathbf{P}_\beta$, which is proportional to the longitudinal magnetisation $\mathbf{M}_z$, equation A6-6.4 can be written:

$$\frac{dM_z}{dt} = 2W\left[(P_\beta - P_\alpha) + c(P_\alpha - P_\beta)\right]. \qquad \text{A6- 6.5}$$

The sum of the populations $\mathbf{P}_\alpha + \mathbf{P}_\beta$ is a constant and represents the total number of nuclei of this type so that equation A6-6.5 can be written:

$$\frac{dM_z}{dt} = -2W(M_z + const). \qquad \text{A6- 6.6}$$

At thermal equilibrium $d\mathbf{M}_z/dt = 0$ and $\mathbf{M}_z = \mathbf{M}_0$, so *const* = $-\mathbf{M}_0$ and because the longitudinal relaxation rate T_1^{-1} is 2W it is found that:

$$\frac{dM_z}{dt} = \frac{(M_0 - M_z)}{T_1} \qquad \text{A6- 6.7}$$

Upon integration equation A6-6.7 becomes

$$\ln(M_0 - M_z) = \frac{-t}{T_1} + \text{const} \qquad \text{A6- 6.8}$$

As **t** represents the elapsed time during which recovery takes place after an arbitrary state of perturbation, the constant of integration can vary between experiments. It is often more beneficial to consider the system immediately after perturbation i.e., at t = 0 and to assign an initial magnetisation, M_{zi}, from which recovery starts:

$$\ln(M_0 - M_z) = \frac{-t}{T_1} + \ln(M_0 - M_{zi}) \qquad \text{A6- 6.9}$$

Therefore, the recovery of $\mathbf{M_0}$ via longitudinal relaxation is characterised by a single exponential recovery. Unlike the isolated spin system treated above, in real multi-spin systems the longitudinal relaxation is usually a mutli-exponential process, due to the relaxation contribution of other spins. However, in most circumstances, deviation from single exponential behaviour is usually small and does not significantly change the value of T_1.

A6.2 The transverse relaxation time T_2

From a similar approach to that adopted for longitudinal relaxation given above, the transverse relaxation equation is written as

$$\ln(M_y) = \frac{-t}{T_2} + \ln(M_{yi}) \qquad \text{A6- 6.10}$$

because the equilibrium condition, corresponding to M_0 in this case is equal to zero, i.e., $M_x = M_y = 0$.

A6.3 Introduction of magnetic nuclei to B_0

Before being exposed to $\mathbf{B}_0$ the orientations of nuclear magnetic moments is isotropic. When exposed to $\mathbf{B}_0$, the magnetic moments begin to precess about $\mathbf{B}_0$ at angles according to their orientation prior to exposure to $\mathbf{B}_0$. Consequently, the orientations of the magnetic moments are still isotropic and no magnetisation exists. Over a period of time, T_1, longitudinal relaxation breaks down the isotropy and magnetisation develops. Even though the spin magnetic momentum is spatially and energetically quantised, the effect of the continuum of local fluctuating magnetic fields causes the orientation of $\boldsymbol{\mu}$ and hence its energy to *wander* between spin states. Indeed, the energy of the nucleus at a given time maybe a superposition of the α and β spin energy states, however, no phase coherence with an external axis or indeed another nucleus exists. The net population difference across the spin energy level transitions and hence M_0 remains the same.

A6.4 Longitudinal relaxation mechanisms

For a given nucleus to undergo longitudinal relaxation, a component of the randomly fluctuating magnetic field must exhibit a transverse (x/y) phase component with the correct rotational sense (relative to the precessional sense of the nucleus) and occur at the Larmor frequency of the nucleus. The latter criterion is required to invoke a single quantum transition between the corresponding spin energy levels, which causes a transfer of energy from the nucleus to the surrounding spin system. Subsequently the population of the lower spin energy state is increased contributing to the restoration of the equilibrium magnetisation M_0.

For spin $\mathbf{I}$ = ½ nuclei, of low viscosity liquids, there are four principal contributing mechanisms of relaxation and their importance in terms of their contribution to T_1 are; Dipole-Dipole relaxation > Chemical Shift Anisotropy (CSA) relaxation > Spin-Rotation relaxation > Scalar coupling relaxation.

Each is a separate relaxation mechanism in its own right and is defined separately. The summation of their effects and those from other lesser forms of relaxation not considered here, contribute to the empirical value of T_1.

A6.4.1 Intra-molecular Dipole-Dipole (Dipolar) relaxation

Dipole-dipole interactions are the magnetic interactions that occur between two magnetic dipoles or in the context of relaxation, dipolar nuclei of the sample. Intra-molecular dipolar relaxation is by far the most prominent source of dipolar relaxation due to the proximity of adjacent dipolar nuclei in the molecule.

Small magnetic fields loop in space around dipolar nuclei such that they may interact or couple with proximate magnetic nuclei in the sample. If one assumes that a molecule is rigid so that the inter-nuclear distance between two proximate dipolar nuclei, j and k is constant, and the molecule in which the dipoles exist is static; the magnitude and direction of the emanating fields at each nucleus is constant (Figure A6.2).

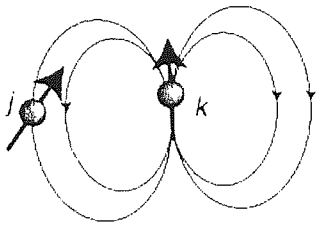

Figure A6.2 Dipolar magnetic field at spin j due to spin k. Reproduced from Levitt [52]

The dipolar magnetic field, $\mathbf{B}_{DD}$, at a nucleus due to a dipole of magnetic moment μ at a distance **r** and subtending an angle θ with respect to $\mathbf{B}_0$ is given by,

$$B_{DD} = \pm\left(\frac{\mu_0}{4\pi}\right)\mu\frac{\left(3\cos^2\theta - 1\right)}{r^3} \qquad \text{A6- 6.11}$$

where the term $\mu_0/4\pi$ is the vacuum permeability $4\pi \times 10^{-7}$ $JC^{-2}m^{-1}s^2$.

In an isotropic liquid the molecules undergo complex random thermal motion, comprised of translations, vibrations and rotations. Consequently, the relative positions of the dipoles change rapidly over time and the $3\cos^2\theta$-1 term averages to zero. Therefore, unlike the anisotropic *through-bond* scalar coupling that survives motional averaging (Appendix A3.2) dipolar *through-space* coupling does not give rise to splitting of NMR lines. However, the nuclear precession of dipolar nuclei coupled with the rotational motion of the molecule in

which they exist, produces fluctuating through-space dipolar magnetic fields at the Larmor frequencies of nuclei (Figure A6.3).

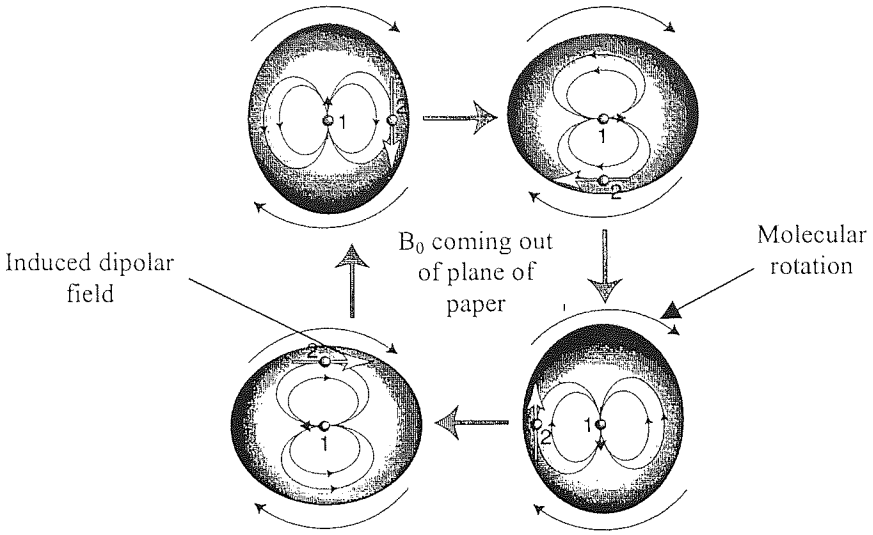

Figure A6.3 **The dipolar magnetic field induced at nucleus 2 by the combination of precession of spin 1 and molecular rotation. The dipolar magnetic field rotates at the Larmor frequency of spin k with the correct rotational sense (clockwise). Modified from Levitt [52].**

Consequently, these intramolecular through-space dipolar couplings can cause relaxation, the efficiency of which is proportional to the magnitude of $\mathbf{B_{DD}}$ and hence μ and the internuclear separation **r**. Therefore, proximate dipoles cause more efficient relaxation.

A6.4.1.1 The rotational correlation time τ_c

The rotational correlation time, τ_c, is used to characterise the rotational motion of molecules and is the time taken for a molecule to rotate through one radian. For example, in liquids, τ_c varies over the range of tens of picoseconds ($10x10^{-12}$) to tens of nanoseconds ($10x10^{-9}$).

Bloembergen, Purcell and Pound extended Debye's theory [59] of dielectric dispersion of polar liquids to determine the value of τ_c as a function of the physical properties of the liquid sample:

$$\tau_c = \frac{4\pi r^3 \eta}{3kT} \qquad \text{A6- 6.12}$$

where; η is the liquid viscosity of the solvent/solute mixture, related to the molecular weight of the species in solution, **T** is the temperature in Kelvin and **r** is the radius of the molecule assumed to be spherical. Therefore, τ_c increases with increasing viscosity as a result of a decrease in temperature and/or increase in molecular weight of the molecules in the liquid.

A6.4.2 Inter-molecular dipolar relaxation

Although intra-molecular dipolar relaxation is the most dominant and important source of relaxation, inter-molecular dipolar relaxation also contributes significantly. The fluctuating magnetic fields causing intermoleuclar dipolar relaxation originate from translation motions of molecules, which provide the necessary correlation times and hence frequencies for relaxation. The magnitude of the dipolar coupling and hence efficiency of intermolecular dipolar relaxation depends upon molecular diffusion and the minimum distance of approach of molecular species, which modulates the inter-dipole distance [28].

Intermolecular dipolar interactions may occur between solute molecules, or solute and solvent molecules, or between solute and paramagnetic species, the most prevalent of the latter being dissolved molecular oxygen and metal ions. Indeed, the removal of paramagnetic species and molecular oxygen from liquid analytical samples is crucial in some relaxation dependent experiments, namely nuclear Overhauser experiments (Appendix A7). Efficient, intermolecular dipolar relaxation also causes the broadening of resonance lines via transverse relaxation, which is described later.

Intermolecular relaxation tends to effect nuclei at the periphery of molecules, i.e., ^{1}H nuclei, which can lead to significant reductions in relaxation times. The relaxation times of ^{13}C nuclei in organic molecules that tend to be located away from the periphery are mainly dominated by intramolecular dipolar relaxation with protons.

A6.4.2.1 Characterising the fluctuating intramolecular dipolar magnetic field

The magnitude and sign, for example, of a transverse (x) component of the dipolar field B_x, at each dipole is modulated due to mutual rotational motion. Indeed the value of τ_c is also described as the time taken for the dipolar magnetic field to change sign. The time average magnitude of the transverse dipolar field is zero, however, the mean square dipolar magnetic field $<B_x^2> \neq 0$ is always positive and is used to characterise the field at a given time.

One can characterise more formally how rapidly the local dipolar magnetic field fluctuates according to τ_c by means of the autocorrelation function. The autocorrelation function, $\mathbf{G}_{(\tau)}$, assesses the value of the dipolar field at one time, **t**, compared to a later time, **t** + τ, and is assumed to decay exponentially at a rate that depends on τ_c:

$$G_{(\tau)} = \left\langle B_x^2 \right\rangle e^{-|\tau|/\tau_c} \qquad \text{A6- 6.13}$$

Figure A6.4 illustrates schematically the decay rate of the autocorrelation function for low and high values of τ_c, which correspond to low and high viscosity liquids respectively. The autocorrelation function at $\tau = 0$ is equal to the mean square dipolar magnetic field.

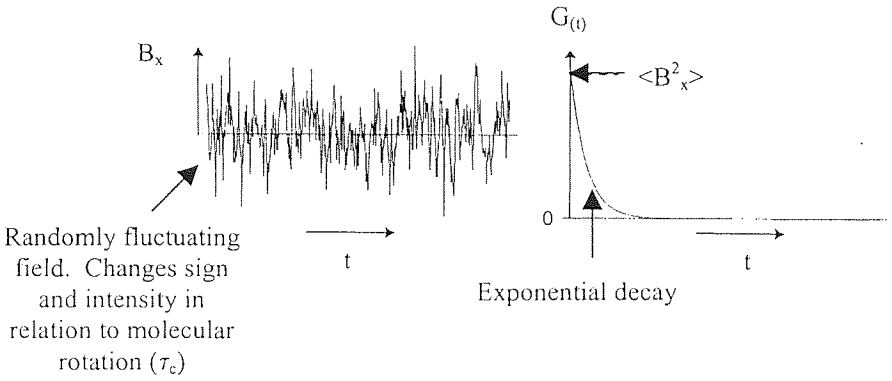

Figure A6.4 **The autocorrelation function and fluctuating local magnetic fields. Modified from publication by Levitt [52]**

One may illustrate the spectrum of fluctuating dipolar magnetic fields at a given τ_c, i.e., their intensity and frequencies by means of the spectral density $J_{(\omega)}$. As the intensity of the fluctuating fields is directly proportional to the relaxation time, a qualitative assessment of the magnitudes of relaxation times relating to τ_c and the corresponding physical properties of the liquid is obtained.

A6.4.3 Spectral density $J_{(\omega)}$

The spectral density is twice the Fourier transform of the autocorrelation function given by:

$$J_{(\omega)} = 2\int_0^{\infty} G(\tau)\exp\{-i\omega\tau\}. \qquad \text{A6- 6.14}$$

In terms of the mean square dipolar magnetic field and τ_c, $J_{(\omega)}$ is given by:

$$J(\omega) = 2\left\langle B_x^2 \right\rangle \frac{2\tau_c}{1+\omega^2 {\tau_c}^2}. \qquad \text{A6- 6.15}$$

The spectral density in this form is a Lorentzian function, however, the intensity of the fluctuating dipolar magnetic field components is usually plotted as a function of logarithmic frequency for a given constant correlation time τ_c. Therefore, one may assess the efficiency of relaxation at a given nuclear Larmor frequency for a given value of τ_c with corresponding physical properties of the liquid. Figure A6.5 gives a schematic representation of spectral density curves for three separate qualitative values of τ_c: short, medium and long correlation times, corresponding to fast, intermediate and slow molecular rotations respectively.

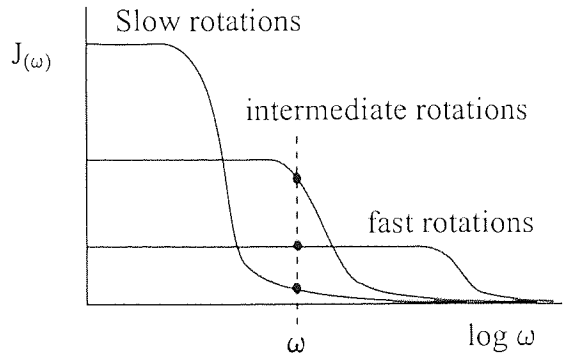

Figure A6.5 Spectral density curves for dipolar relaxation. Modified from Claridge [23]

The spectral density can also be considered the probability of finding a particular fluctuating magnetic field component at a given frequency. Therefore, all spectral density curves enclose the same area, thus the total power available to the spin system to cause relaxation by local fluctuating magnetic fields is the same. However, the intensity of the dipolar magnetic fields varies over a range of frequencies depending upon the value of τ_c and the properties of the liquid.

Low values of τ_c (fast motion), i.e., $1 >> \omega\tau_c$, which is generally indicative of small molecules in low viscosity liquids, have a low and constant power available to cause relaxation over a wide range of frequencies (flat region of curve). Therefore, T_1 tends to a similar value for nuclei of the same species for most nuclei found in e.g., organic molecules. This relaxation

behaviour is known as the extreme narrowing limit since NMR spectra exhibit narrow spectral lines. The width of NMR lines is actually dependent upon transverse relaxation times T_2 (see later), which tend to the same values as T_1 in the extreme narrowing limit.

As τ_c increases (intermediate motions) due to higher viscosity and/or higher molecular weight molecules, the spectral density increases for a smaller range of frequencies. For the Larmor frequency ω indicated in figureA6.5, the spectral density of the intermediate correlation time is the highest and T_1 will be the lowest, which corresponds to the condition $1 \approx \omega\tau_c$.

As τ_c further increases (slower motions) due to even higher viscosity and/or higher molecular weight molecules, the spectral density increases for an even smaller frequency range. Consequently the spectral density at the Larmor frequency given in figure A6.5 is near zero and the value of T_1 is higher than that of the moderate and small values of τ_c. Indeed as τ_c further increases the spectral density over the range of Larmor frequencies of nuclei found in most molecules becomes increasingly small, which increases the value of T_1 still further.

A6.4.4 Dipolar longitudinal relaxation time T_{1DD}

The longitudinal relaxation time exclusively for dipolar relaxation, T_{1DD}, expressed in terms of the spectral density and $\langle B_x^2 \rangle$ is given by

$$\frac{1}{T_{1DD}} = \gamma^2 \langle B_x^2 \rangle J(\omega) = 2\gamma^2 \langle B_x^2 \rangle \frac{\tau_c}{1 + (\omega\tau_c)^2}. \qquad \text{A6- 6.16}$$

Equation A6-6.16 is grossly simplified since in reality the dipolar magnetic fields have multiple transverse phase components that can potentially cause longitudinal relaxation.

In the extreme narrowing limit ($1 >> \omega\tau_c$) equation A6-6.16 simplifies to

$$\frac{1}{T_{1DD}} = 2\gamma^2 \langle B_x^2 \rangle \tau_c \qquad \text{A6- 6.17}$$

The minimum T_1, which occurs at $1 \approx \omega\tau_c$ is given by

$$\frac{1}{T_{1\min}} = \gamma^2 \frac{\left[B_x^2\right]}{\omega} \qquad \text{A6- 6.18}$$

Therefore, T_1 can vary considerably for the same sample between different strengths of $\mathbf{B_0}$ due to its proportionality with ω.

A6.4.5 Chemical Shift Anisotropy (CSA) relaxation

In isotropic liquids the shielding constant, σ, which is a tensor value, is time averaged due to molecular motions giving rise to an isotropic chemical shift (Appendix A3). However, at a given moment in time σ may be anisotropic ($\sigma_{xx} \neq \sigma_{yy} \neq \sigma_{zz}$), which produces a transient magnetic field that can couple with an adjacent nucleus. Consequently, a continuum of small fluctuating magnetic fields exist due to CSA, which can cause longitudinal and transverse relaxation.

As the magnitude of the chemical shift is $\mathbf{B_0}$ dependant, so is the magnitude of CSA relaxation. In the extreme narrowing limit the CSA contribution to T_1 is given by:

$$\frac{1}{T_1} = \frac{2}{15}\gamma^2 B_0{}^2 \left(\sigma_{\parallel} - \sigma_{\perp}\right)^2 \tau_c \qquad \text{A6- 6.19}$$

where, $\sigma_{\parallel}$ and $\sigma_{\perp}$ represent the shielding along and perpendicular to the axial symmetry axis of the molecule.

The impact of CSA relaxation obviously depends on the chemical shift range of the nuclei and therefore is not a major contributor to the T_1 of ^1H. At higher $\mathbf{B_0}$ strengths when the chemical shift range is increased, the effect of CSA relaxation may start to compete significantly with dipolar relaxation mechanisms. In circumstances where dipolar relaxation is not the dominant source of intra-molecular relaxation, CSA relaxation may be responsible for in excess of 50% of the total longitudinal relaxation. Indeed, this can be the case for sp^2 hybridised carbons, which are not directly bonded to protons [60].

A6.4.6 Spin-rotation relaxation (SRR)

Molecules possess a molecular magnetic moment derived from the distribution of electron density throughout the molecule. As a molecule rotates, the magnitude and direction of the molecular magnetic field is modulated at the site of a nucleus. At a given time, the molecular magnetic moment will have transverse phase components at the Larmor frequency and may interact with a magnetic nucleus causing spin-rotation relaxation. For isotropic liquids the contribution of spin-rotation relaxation to T_1, expressed as the relaxation rate, T_1^{-1} is given by:

$$\frac{1}{T_1} = \left[\frac{2\pi LkT}{h^2}\right] C_{eff}^2 \tau_J \qquad C_{eff}^2 = \frac{1}{3}\left(C_{\parallel}^2 + 2C_{\perp}^2\right) \qquad \text{A6- 6.20}$$

where **L** is the moment of inertia of the molecule, **k** is the Boltzmann constant and **T** is the temperature in Kelvin. $C_{\parallel}$ and $C_{\perp}$ represent the magnetic interaction due to spin-rotation along and perpendicular to the symmetry axis of the molecule.

The parameter, τ_J, is the molecular angular momentum correlation time and is related to the rotational correlation time, τ_c, by:

$$\tau_c \tau_J = \frac{I}{6kT}. \qquad \text{A6- 6.21}$$

Importantly, the magnitude of τ_J increases with increasing temperature, which is converse to that of τ_c. Consequently spin-rotation relaxation increases with decreasing temperature, which is opposite to that observed for all other relaxation mechanisms.

Spin-rotation can also occur within a molecule. For example, if a methyl group has a small energy barrier of rotation it is able to freely rotate about an sp^3 hybrid C-C bond. Consequently, the inherent magnetic moment of that group may provide the necessary frequencies and phases of magnetic field to cause spin-rotation relaxation of an adjacent nucleus. Spin-rotation relaxation is often only important in small molecules or molecules that contain freely rotating groups [60].

A6.4.7 Scalar coupling relaxation

Fundamentally, two nuclei, **j** and **k** that are mutually scalar coupled are dipolar coupled through chemical bonds. Fluctuations of the dipolar magnetic field at **j** due to **k**, (fluctuations of J_{jk}) with an appropriate phase at the Larmor frequency can cause relaxation. Fluctuations of the dipolar magnetic field can arise when J_{jk} is time-dependent, i.e., when **j** or **k** is involved in chemical exchange. Furthermore, the relaxation of **k** can produce time-dependent fluctuations in the dipolar field at **j**, however, is more pronounced when $I_k > ½$.

Indeed, if the longitudinal relaxation time T_{1k} for a spin **k** is short in comparison to $1/J_{jk}$, the local field produced at spin **j** by spin **k** fluctuates with a correlation time $\tau_k = T_{1k}$. Consequently, the longitudinal relaxation rate, T_{1j}^{-1}, of spin **j** is given by:

$$\frac{1}{T_{1j}} = \frac{2J^2}{3} I(I+1) \times \frac{\tau_k}{1+(\omega_j - \omega_k)^2 \tau_k^2} \qquad \text{A6- 6.22}$$

where **I** is the spin quantum number of spin **k** and ω_j and ω_k are the Larmor frequencies of spins **j** and **k** respectively. Fluctuations in the dipolar magnetic field that originate from relaxation and chemical exchange are referred to as scalar relaxation of the second and first kind respectively. Scalar coupling of the second kind only really becomes relevant when the Larmor frequencies of the spins involved are very similar, e.g., ^{13}C and ^{79}Br.

A6.5 Transverse (spin-spin) relaxation

Transverse relaxation is also caused by interaction of nuclei with random fluctuating magnetic fields of the same origin as that of longitudinal relaxation. However, in addition to transverse components, Z-components of the fluctuating magnetic fields may also cause transverse relaxation. Therefore, the value of T_1 and T_2 are inextricably linked however, their mechanisms and effects differ markedly.

Two nuclei may simultaneously induce a fluctuating dipolar magnetic field at the other as the molecule undergoes random thermal motion. If the induced fields are at the Larmor frequency of each nucleus, a mutual exchange in spin energy, corresponding to a flip in the spin state of each nucleus can occur. Therefore, in contrast to longitudinal relaxation,

transverse (or spin-spin relaxation as it is popularly termed) relaxation does not cause a change in enthalpy of the spin system, i.e., the populations of the spin energy levels and longitudinal magnetisations are not perturbed.

However, phase coherence that either of the two spins had with the ensemble prior to transverse relaxation is subsequently lost, causing de-phasing of coherence over time and the re-attainment of the equilibrium condition ($M_x = M_y = 0$) (Figure A6.6).

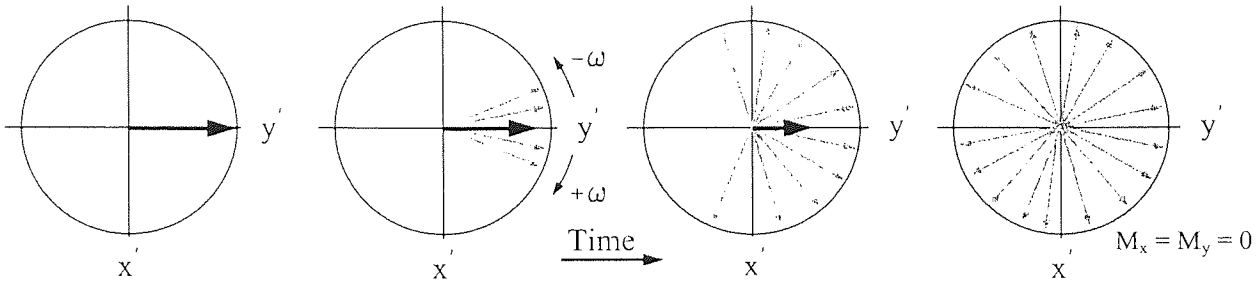

Figure A6.6 **Loss of phase coherence over time for a single quantum coherence on-resonance in the rotating frame. The precession frequency of individual nuclei is subtly modified (±ω) by transverse relaxation. Modified from Claridge [23].**

As coherence is a manifestation of partial order of the spin system, transverse relaxation serves to increase disorder and hence the entropy of the spin system.

In addition to the fluctuating magnetic fields at the Larmor frequency, transverse relaxation is also caused by very low-frequency magnetic fields represented by the spectral density $J_{(0\omega)}$. Expressed in terms of T_1 and $J_{(0\omega)}$, T_2 is given by

$$\frac{1}{T_2} = \frac{1}{T_1} + J_{(0\omega)}. \qquad \text{A6- 6.23}$$

Figure A6.7 illustrates schematically the variation of T_1 and T_2 as a function of correlation time, τ_c.

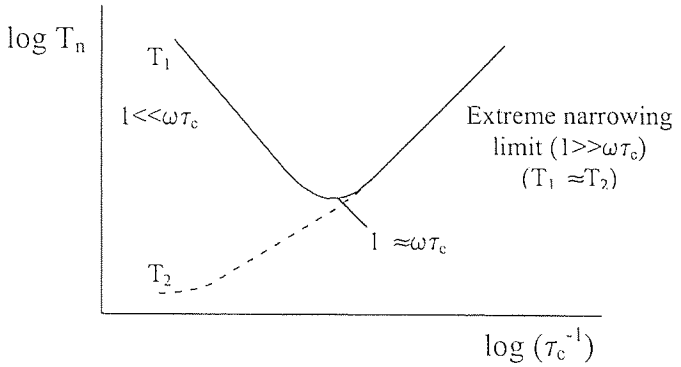

Figure A6.7 Variation of T_1 and T_2 with correlation time τ_c. Modified from Claridge [23].

In the extreme narrowing limit ($1>>\omega\tau_c$), which is indicative of low molecular weight molecules and/or liquids of low viscosity, T_2 tends to the same value as T_1. This is due to the small values of τ_c and hence small contribution of $J_{(0\omega)}$.

The value of T_2 differs from that of T_1 when $1>\omega\tau_c$ due to an increase in the spectral density of the low frequency fluctuating fields, $J_{(0\omega)}$. Indeed as τ_c increases due to higher viscosity and/or molecular weight of the molecules in the liquid, T_2 continues to decrease while T_1 increases. Consequently, the spectral line widths of nuclei in large molecules are characteristically broad.

When T_2 is single exponential, the spectral line width at half height is given by:

$$\Delta\nu_{1/2} = \frac{1}{\pi T_2}. \qquad \text{A6- 6.24}$$

A6.5.1 Inhomogeneous line broadening

Inhomogeneity of $\mathbf{B}_0$ across the sample volume causes a variation of the Larmor precession frequencies of identical nuclei in different parts of the sample, which causes the broadening of the spectral line. Therefore, the empirical line width is a summation of transverse relaxation and contributions due to inhomogeneous line broadening:

$$\frac{1}{T_2^*} = \frac{1}{T_2} + \frac{1}{T_{\text{in hom}}} \qquad \text{A6- 6.25}$$

The contribution of T_{inhom} can be significantly reduced by effective room temperature shimming to reduce $\mathbf{B_0}$ inhomogeneity. The contribution of T_{inhom} is significant in pulse sequence experiments of reasonable length, as T_2^* determines the lifetime of coherence, which is ultimately detected during signal acquisition. Consequently, pulse sequence experiments routinely incorporate refocusing elements, which counteract (refocus) the effects of T_{inhom} and, when applicable, the effects of chemical shift evolution (Appendix A8.2.8.2).

In this rudimentary treatment of relaxation only single quantum relaxation *pathways* have been considered. However, multiple quantum transitions ($\Delta m \neq 1$) provide valid longitudinal relaxation pathways, which contribute to the relaxation phenomenon know as the nuclear Overhauser effect (nOe), which is described in appendix A7.

Appendix A7 The nuclear Overhauser effect (nOe)

In 1953, A. W. Overhauser predicted that in paramagnetic samples, the intensity of a NMR signal could be greatly enhanced by saturating the electron spin resonance signal emanating from unpaired electrons in the sample. However, the electron-nuclear Overhauser effect did not receive widespread use due to its inherent complexity and the need to change the properties of diamagnetic samples, by the addition of free radicals.

Following work published on nuclear relaxation, Solomon [61] demonstrated the first example of the intra-molecular nuclear-nuclear Overhauser effect (nOe), which can be defined as: the net change in intensity of a NMR signal that has resulted from the perturbation of another related NMR transition. The origin of the nOe lies in specific dipolar longitudinal relaxation mechanisms, namely dipolar cross-relaxation, that occur between the perturbed spins and other dipolar coupled nuclei.

The cross-relaxation mechanism is unique in that is acts to restore thermal equilibrium across the perturbed spin transitions while adjusting the populations of the spin energy levels of the dipolar coupled nucleus or nuclei. This leads to a net change in the longitudinal magnetisation of the latter and hence a change in the intensity of its NMR signal when it is appropriately sampled.

The change in intensity may be positive or negative depending upon the particular cross-relaxation mechanism that is operative. This depends, as do all dipolar longitudinal relaxation mechanisms, on the physical properties of the sample, namely the rotational correlation time τ_c. The magnitude of the nuclear Overhauser enhancement (also given the acronym nOe) is dependant upon the strength of the dipolar coupling, which is directly proportional to the internuclear separation between the cross-relaxing nuclei. Analysis of the magnitudes of nOes can provide information on internuclear separation between the coupling dipoles when certain experimental requirements have been satisfied. Consequently, nuclear Overhauser experiments are used extensively as a means of intra-molecular (and in some circumstances intermolecular) structural analysis.

In circumstances when the nOe is positive, the effect has been used routinely to enhance signal intensities of insensitive nuclei e.g., ^{13}C in organic molecules. R.f. perturbation in the form of pulses or continuous irradiation of the spin energy level populations of protons, causes nuclear Overhauser enhancement of ^{13}C which exhibit dipolar coupling with the protons.

A number of different classes of nOe experiment exist, namely; the *steady-state* nOe, *truncated driven* nOe (TOE) and the *transient* nOe. The difference between each class of experiment lies in the method of perturbation of the spin system used, the way in which the nOe develops and the time over which the nOes are measured. The steady-state nOe is generally used for the qualitative determination of internuclear distances between the perturbed and enhanced spin, while TOE and transient nOe experiments can yield quantitative internuclear distances.

A7.1 Brief synopsis of longitudinal relaxation

Consider the spin energy level system of a non-scalar coupled two-spin system **I** and **S**, which are mutually dipolar coupled (Figure A7.1). The spins **I** and S are assumed to have different Larmor frequencies, however, for simplicity the schematic representation of the spin energy levels does not reflect this difference.

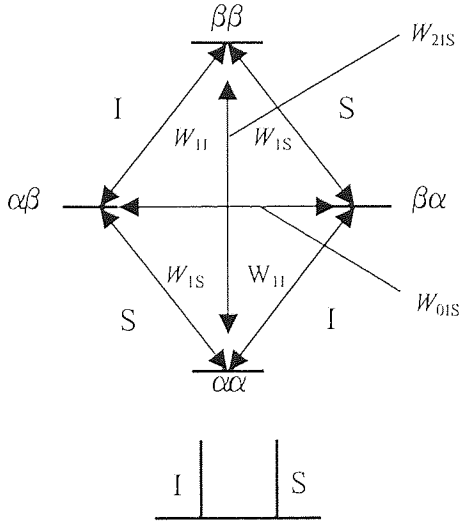

Figure A7.1 Spin energy level diagram for a two spin system I and S and corresponding spectrum

The time average dipolar coupling in isotropic liquids is zero so there is no difference in energy separation of the two single quantum transitions of **I** and **S**. The mean single quantum transition probabilities of I and S are given by W_{1I} and W_{1S} respectively.

The intra-molecular longitudinal dipolar relaxation described in Appendix A6, related to single quantum transitions, where the relaxing spin undergoes a change in spin energy by a single quantum ($\Delta m = -1$). Two other transitions exist, which involve the so-called spin *forbidden* transitions, i.e., $\Delta m \neq 1$. Although these transitions are incapable of causing observable coherence, they remain valid relaxation pathways and act in unison with the single quantum longitudinal relaxation *pathways* to restore thermal equilibrium. The double quantum transition (DQT), ($\Delta m=2$) given the mean transition probability (W_{2IS}) and zero quantum transition (ZQT), ($\Delta m=0$) given the mean transition probability (W_{0IS}) are the cross-relaxation pathways and are the sole relaxation transitions responsible for the nOe.
Double and zero quantum relaxation transitions result in the simultaneous flip of the spin states of both nuclei involved in the dipolar coupling, i.e., $\alpha\alpha \leftrightarrow \beta\beta$ and $\alpha\beta \leftrightarrow \beta\alpha$ respectively.

The origin of intramolecular dipolar cross-relaxation is identical to single quantum dipolar relaxation detailed in appendix A6: the coupling of the individual precession of nuclear magnetic moments with the rotational motion of the molecule in which it resides provides the necessary frequency, phase, and rotational sense of the fluctuating field at the site of a dipolar coupled nucleus. The only exceptions for cross-relaxation are:

- it is a mutually exclusive effect, i.e., the fluctuating magnetic field simultaneously produced at each nucleus is caused by the other dipolar coupled nucleus. This gives rise to the necessary simultaneous flip in spin states.

- The frequency of the dipolar magnetic field is different: double quantum relaxation (W_{2IS}) requires the frequency of the dipolar magnetic field to be the sum of the Larmor frequencies of the spins involved ($\omega_I + \omega_S$) i.e. two quanta. Zero quantum relaxation (W_{0IS}) requires the frequency of the field to be the difference of the Larmor frequencies of the spins involved ($\omega_I - \omega_S$), i.e., near zero quanta. Obviously the latter is rather inappropriately named, as a zero quantum transition would by definition be the same state. The use of the zero quantum term to indicate a small change in energy/frequency is universally adopted. It holds true in homonuclear systems,

however, in heteronuclear spin system the frequency difference may not be small and this convention is no longer entirely valid.

The operation of each cross-relaxation transition in a particular direction causes the spin populations of the two involved spin energy levels to change. As these spin energy levels are component to the single quantum transitions, it is evident that a population change due to cross-relaxation results in a change in the population difference across the single quantum transition and giving rise to a change in intensity of the NMR signal.

Before progressing to the theory of the nOe, a brief synopsis of the fundamentals of saturation, which is integral to the understanding of the *steady-state* experiment is presented.

A7.1.1 Saturation

Originally, the intra-molecular nuclear-nuclear nOe was observed by saturating the transition(s) of spin(s) dipolar coupled to others, which provided the necessary form of perturbation. $\mathbf{B}_1$ is applied at low power continuously and selectively at the Larmor frequency of a given transition, such that the population difference across that transition is maintained at zero. The transition is said to be saturated and the populations of the spin energy levels associated with that transition are equalised so that $\mathbf{M}_z = 0$.

In steady-state experiments selectivity of saturation is of paramount importance so that one may isolate the nOe due to saturation of another nucleus or group of nuclei. In most circumstances, the difference in chemical shift between the target transition and other transitions is small and achieving selectivity is often difficult. Consequently, the power of $\mathbf{B}_1$ needs to be significantly attenuated so that its effect does not "spill over" onto other nearby transitions hence maintaining selectivity. However, in these circumstances, only partial saturation of the transition may occur: a balance is struck between stimulated absorption and emission from the application of $\mathbf{B}_1$ and the effect of longitudinal relaxation mechanisms. The population difference across the transitions is constant, but non-zero and $\mathbf{M}_z \neq 0$.

Of more importance than the state of saturation achieved is the attainment of steady-state i.e. $d\mathbf{M}_z/dt = 0$ for both the perturbed and enhanced spin(s). This is crucial for the simplification of nOe theory in order that the analyses of experimental data can be used to determine

internuclear separation. Reaching steady state is a lengthy process requiring irradiation times usually of the order 5-10 T_1 of the irradiated nucleus.

Achieving partial saturation only effects the magnitude of the observed intensity change due to nOe. This is far less troublesome than potentially failing to reach steady-state, which may give rise to inaccurate internuclear distance measures. Partial saturation may be overcome by mathematical treatment of the equations, which is time consuming and complex [24], and may not be relevant for all irradiated transitions. Therefore, meaningful experiments are by definition lengthy but are required to reach steady-state.

A7.2 The steady-state nOe

If it is assumed that the Larmor frequencies of spins **I** and **S** are sufficiently close to one another, the difference in spin energy level populations across the single quantum transitions at thermal equilibrium of spins **I** and **S** can be assumed equal, so that $\mathbf{I}_0 = \mathbf{S}_0$.

At thermal equilibrium, the following equality holds true, where **n** is the population of each spin energy level

$$(n_{\alpha\alpha} - n_{\beta\alpha}) + (n_{\alpha\beta} - n_{\beta\beta}) = I_0$$

$$(n_{\alpha\alpha} - n_{\alpha\beta}) + (n_{\beta\alpha} - n_{\beta\beta}) = S_0$$

The population differences at thermal equilibrium across each of the **I** and **S** transitions including those multiple quantum transitions can be represented schematically by the following equalities. Where δ is the population excess or deficiency associated with a particular spin energy level.

I transitions: $\left.\begin{matrix}\alpha\alpha-\alpha\beta\\ \beta\alpha-\beta\beta\end{matrix}\right\}\delta$

S transitions: $\left.\begin{matrix}\alpha\alpha-\beta\alpha\\ \alpha\beta-\beta\beta\end{matrix}\right\}\delta$

$\Delta M = 2$: $\left.\begin{matrix}\alpha\alpha-\beta\beta\end{matrix}\right\}2\delta$

$\Delta M = 0$: $\left.\begin{matrix}\beta\alpha-\alpha\beta\end{matrix}\right\}0$

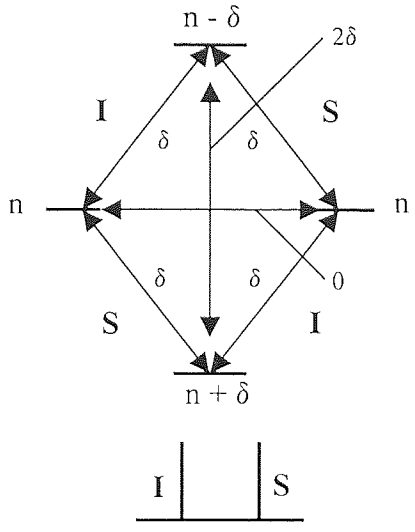

Figure A7.2 **Schematic representation of dipolar coupled two spin I = ½ system at thermal equilibrium**

If $\mathbf{B}_1$ is applied to cause the selective saturation of the **S** transitions, the following conditions hold.

I transitions: $\left.\begin{matrix}\alpha\alpha-\alpha\beta\\ \beta\alpha-\beta\beta\end{matrix}\right\}\delta$

S transitions: $\left.\begin{matrix}\alpha\alpha-\beta\alpha\\ \alpha\beta-\beta\beta\end{matrix}\right\}0$

$\Delta m = 2$: $\left.\begin{matrix}\alpha\alpha-\beta\beta\end{matrix}\right\}\delta$

$\Delta m = 0$: $\left.\begin{matrix}\beta\alpha-\alpha\beta\end{matrix}\right\}\delta$

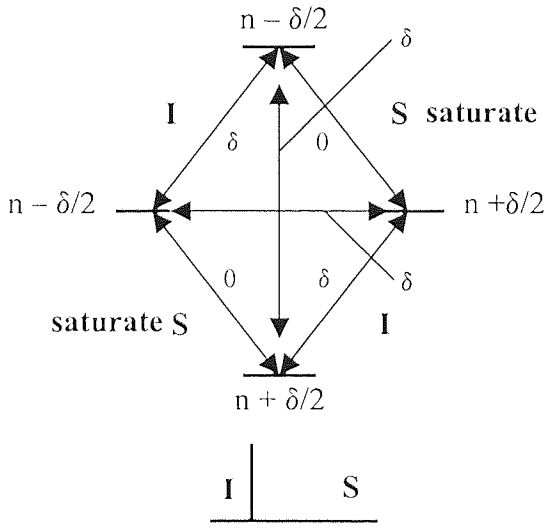

Figure A7.3 **Schematic representation of dipolar coupled two spin I = ½ system after saturation of S**

With the exception of the single quantum transitions of **I**, the population differences across all other transitions are perturbed from thermal equilibrium. As the S spin resonance is being continually saturated and is assumed to be at steady-state, the single quantum relaxation pathway of S (W_{1S}) is invalid in terms of being able to restore thermal equilibrium. As the **I** spin population differences across the corresponding **I** transitions are the same as at thermal

equilibrium, the system has no initial drive to relax due to the single quantum relaxation pathway of **I** (W_{1I}).

The spin system attempts to restore thermal equilibrium via the two remaining cross-relaxation pathways. The population difference across the DQT (W_{2IS}) is now δ compared to 2δ at thermal equilibrium. Therefore if relaxation occurs via the W_{2IS} cross-relaxation pathway, the population of the $\beta\beta$ spin state will be depleted hence increasing the population of the $\alpha\alpha$ spin state and approaching the thermal equilibrium condition. As the **I** transitions share the $\alpha\alpha$ and $\beta\beta$ spin energy levels, an increase in the population of $\alpha\alpha$ increases the population difference across the **I** transition $\alpha\alpha$-$\beta\alpha$, and a decrease in the population of $\beta\beta$ increases the population difference across the **I** transition $\beta\alpha$-$\beta\beta$. Consequently **I** has received a positive nuclear Overhauser enhancement due to DQ (W_{2IS}) cross-relaxation with spin **S** during its continued perturbation.

Similarly, the population difference across the ZQT (W_{0IS}) is now δ compared to 0 at thermal equilibrium. Therefore cross-relaxation via the ZQ pathway decreases the population of the $\beta\alpha$ spin state while increasing the population of the $\alpha\beta$ spin state and so approaches the thermal equilibrium condition. As the **I** transitions share the $\beta\alpha$ and $\alpha\beta$ spin energy levels, a decrease in the population of $\beta\alpha$ decreases the population difference across the **I** transition $\beta\alpha$-$\beta\beta$, whilst and an increase in the population of $\alpha\beta$ decreases the population difference across the **I** transition $\alpha\alpha$-$\alpha\beta$. Consequently, **I** has received a negative nuclear Overhauser enhancement due to ZQ (W_{0IS}) cross-relaxation with spin S during its continued perturbation.

The nOe has effectively perturbed the equilibrium populations of the spin energy levels of **I**. Consequently, the single quantum relaxation of spin **I** (W_{1I}) serves to simultaneously return the populations of the **I** spin energy levels to that of thermal equilibrium. Therefore, the total enhancement seen at **I** due to saturation of **S** will be a balance between all operative longitudinal dipolar relaxation mechanisms (W_{1I}, W_{0IS}, W_{2IS}).

Assuming that the relaxation of **I** occurs solely due to exclusive dipolar coupling with **S**, the two-spin Solomon equation [61] describes the change in longitudinal magnetisation of **I** as a function of the operative mean transition probabilities and is given by:

$$\frac{dI_z}{dt} = -(I_z - I_z^0)(W_{0IS} + 2W_{II} + W_{2IS}) - (S_z - S_z^0)(W_{2IS} - W_{0IS}) \qquad \text{A7- 7.1}$$

From the Solomon equation the fractional enhancement of **I** due to saturation of **S** ($f_I\{S\}$) at steady state can be derived. At steady state, $dI_z/dt = 0$ and $S_z = 0$, so that equation A7-7.1 becomes:

$$0 = -(I_z - I_z^0)(W_{0IS} + 2W_{II} + W_{2IS}) + S_z^0(W_{2IS} - W_{0IS}) \qquad \text{A7- 7.2}$$

Therefore,

$$\frac{I_z - I_z^0}{S_z^0} = \frac{W_{2IS} - W_{0IS}}{W_{0IS} + 2W_{II} + W_{2IS}} \qquad \text{A7- 7.3}$$

It is possible to quantify the magnitude of $S_z^0 = (\gamma_S/\gamma_I) I_z^0$ so that equation A7-7.3 becomes,

$$f_I\{S\} = \frac{I_z - I_z^0}{I_z^0} = \frac{\gamma_S}{\gamma_I} \frac{W_{2IS} - W_{0IS}}{W_{0IS} + 2W_{II} + W_{2IS}} \qquad \text{A7- 7.4}$$

where the factor 2 associated with W_{II} represents the two **I** single quantum transitions in the two spin system. The term ($W_{2IS} - W_{0IS}$) describes the cross-relaxation rate between spins **I** and **S**, which is referred to as the cross-relaxation rate constant σ_{IS}. The term ($W_{0IS} + 2W_{II} + W_{2IS}$) is the mutual dipolar relaxation rate constant, ρ_{IS}, of spin **I** by spin **S** (and vice versa).

Therefore, expressed in terms of σ_{IS} and ρ_{IS}

$$f_I\{S\} = \frac{\gamma_S}{\gamma_I} \frac{\sigma_{IS}}{\rho_{IS}} = \eta_{max} \qquad \text{A7- 7.5}$$

The fractional nOe derived from the two-spin Solomon equation given by equations A7-7.5 and A7-7.6 is the theoretical maximum nOe, η_{max}. This is because exclusive dipolar relaxation of **I** and **S** has been assumed, which does not consider the effect of external single

quantum relaxation sources of spin **I** that serve to reduce η_{max}. Such external relaxation sources, may be for example, Chemical shift anisotropy relaxation, spin rotation relaxation and intermolecular dipolar relaxation etc (Appendix A6.4). The effect of external relaxation and multi spin systems upon the empirical nOe is described later on.

It is evident that the magnitude and sign of the nOe depends upon the prevalence of either DQ or ZQ cross-relaxation in the system, which as are all dipolar relaxation mechanisms, dependent upon the spectral density of the dipolar magnetic field at those frequencies.

A7.2.1 Dependence of the nOe on τ_c and $J_{(\omega)}$

Derivation of the nOe enhancement factor in terms of the rotational correlation time provides a useful insight into its relationship with molecular properties of the liquid.

The mean transition probabilities expressed in terms of the rotational correlation times, τ_c and spectral density, $J_{(\omega)}$ are given by:

$$W_{0IS} = \frac{1}{20} K^2 J(\omega_I - \omega_S) = \frac{1}{10} K^2 \frac{\tau_c}{1 + (\omega_I - \omega_S)^2 \tau_c^2} \qquad \text{A7- 7.6}$$

$$W_{1I} = \frac{3}{40} = K^2 J(\omega_I) = \frac{3}{20} K^2 \frac{\tau_c}{1 + \omega_I^2 \tau_c^2} \qquad \text{A7- 7.7}$$

$$W_{1S} = \frac{3}{40} = K^2 J(\omega_S) = \frac{3}{20} K^2 \frac{\tau_c}{1 + \omega_S^2 \tau_c^2} \qquad \text{A7- 7.8}$$

$$W_{2IS} = \frac{3}{10} K^2 J(\omega_I + \omega_S) = \frac{3}{5} K^2 \frac{\tau_c}{1 + (\omega_I + \omega_S)^2 \tau_c^2} \qquad \text{A7- 7.9}$$

Where $K = (\mu_0 / 4\pi)\hbar\gamma_I\gamma_S r_{IS}^{-3}$ and r_{IS} is the internuclear distance between **I** and **S**

Therefore, expressed in terms of the correlation time τ_c, σ and ρ become

$$\sigma_{IS} = W_{2IS} - W_{0IS}$$
$$= \frac{1}{10} K^2 \tau_c \left[\frac{6}{1+(\omega_I + \omega_S)^2 \tau_c{}^2} - \frac{1}{1+(\omega_I - \omega_S)^2 \tau_c{}^2} \right] \qquad \text{A7- 7.10}$$

and

$$\rho_{IS} = W_{0IS} + 2W_{1IS} + W_{2IS}$$
$$= \frac{1}{10} K^2 \tau_c \left[\frac{1}{1+(\omega_I - \omega_S)^2 \tau_c{}^2} + \frac{3}{1+\omega_I^2 \tau_c^2} + \frac{6}{1+(\omega_I + \omega_S)^2 \tau_c{}^2} \right] \qquad \text{A7- 7.11}$$

By substituting equations A7-7.10 and A7-7.11 into equation A7-7.4, $f_I\{S\} = \eta_{max}$ after some cancellation of terms becomes

$$f_I\{S\} = \eta_{max} = \frac{5 + \omega^2 \tau_c^2 - 4\omega^4 \tau_c^4}{10 + 23\omega^2 \tau_c^2 + 4\omega^4 \tau_c^4} \qquad \text{A7- 7.12}$$

A7-7.12 holds true for $\gamma_I = \gamma_S$, i.e., a homonuclear system, and that $(\omega_I - \omega_S)\tau_c << 1$.
A schematic plot of η_{max} as a function of $\omega\tau_c$ and hence the physical properties of the sample is shown in figure A7.4.

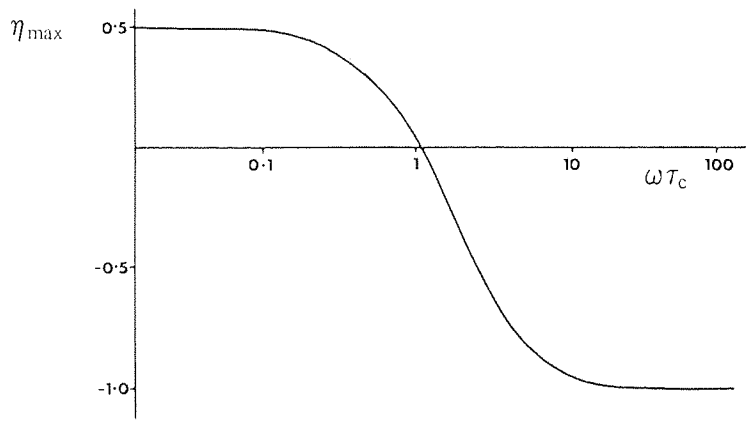

Figure A7.4 η_{max} **vs** $\omega\tau_c$ **for a** $^1H\{^1H\}$ **system. Reproduced from Neuhaus [24].**

When τ_c is small, which is indicative of low liquid viscosity and low molecular weight, i.e. in the extreme narrowing limit ($1 >> \omega\tau_c$), the spectral density of the dipolar magnetic fields is more or less even across the entire Larmor frequency range. Consequently the double

quantum dipolar magnetic fields are more prominent and hence W_{2IS} and the nOe is usually positive in the extreme narrowing limit. Indeed J(ω) becomes equal to $2\tau_c$ (Appendix B2) in the extreme narrowing limit and the ratios W_0:W_1:W_2 become 1:3/2:6. Therefore, η_{max} for a homonuclear spin system e.g., protons is given by:

$$\eta_{max}(\omega\tau_c << 1) = \frac{W_{2IS} - W_{0IS}}{W_{0IS} + 2W_{1IS} + W_{2IS}} = \frac{6-1}{1+3+6} = \frac{1}{2} \qquad \text{A7- 7.13}$$

As τ_c increases, which corresponds to an increase in liquid viscosity and molecular weight, the spectral density of the low-frequency dipolar magnetic fields are increased. Consequently W_{0IS} becomes more prevalent and the η_{max} decreases, passes through zero and becomes negative until reaching limiting value $\eta_{max} = -1$. The value of η_{max} is zero when $\omega\tau_c \approx 1.12$:

$$5 + \omega^2\tau_c^2 - 4\omega^4\tau_c^4 = 0 \qquad \text{A7- 7.14}$$

In this region of $\omega\tau_c$, η_{max} becomes sensitive to a variety of parameters upon which τ_c and the Larmor frequency ω of the nucleus depends, i.e., temperature, viscosity, and $\mathbf{B}_0$ etc.

The lack of a positive nOe in some samples may not be an indication of inefficient cross-relaxation as opposed to efficient single quantum relaxation, but may actually be the consequence of a negative nOe. This is a particular problem in large molecules since $\eta_{max} = -1$ entirely cancels the equilibrium magnetisation and renders the signal unobservable.

A7.2.2 Effects of external relaxation upon the magnitude of nOe.

In the *idealised* system described thus far, the rate constant ρ_{IS} represents the direct rate constant for the exclusive dipolar relaxation of spin **I** by spin **S** and vice versa. Consequently, the total relaxation rate constant, $\mathbf{R}_I$ (T_{1I}^{-1}) of spin **I** must be equal to ρ_{IS} as no other relaxation mechanisms have been considered.

In real systems the intra-molecular dipolar relaxation of spin **I** occurs as a result of mutual dipolar coupling with any number of spins **X** other than **S**. Consequently one may define the total intra-molecular dipolar longitudinal relaxation rate $\mathbf{R_I}^{DD}$, as a a pair-wise summation over all the two spin terms ρ_{IS} and ρ_{IX}:

$$R_I^{DD} = \rho_{IS} + \sum_X \rho_{IX} \qquad \text{A7- 7.15}$$

Furthermore, extra external relaxation mechanisms of **I**, e.g., intermolecular dipolar relaxation with paramagnetic impurities and dissolved molecular oxygen, chemical shift anisotropy relaxation and spin-rotation relaxation, all contribute to the total relaxation rate of **I** (R_I) and are represented by the rate ρ_I^*.

Therefore, $\mathbf{R_I}$ is the sum of $\mathbf{R_I}^{DD}$ and ρ_I^*:

$$\begin{aligned} R_I &= \rho_{IS} + \sum_X \rho_{IX} + \rho_I^* \\ &= R_I^{DD} + \rho_I^* \end{aligned} \qquad \text{A7- 7.16}$$

Consequently the total dipolar single quantum relaxation mean transition probability, W_{II}, is a pair-wise summation over all dipolar relaxation contributions:

$$W_{II}^{DD} = W_{IIS} + \sum_X W_{IIX} \qquad \text{A7- 7.17}$$

Therefore the empirically derived $f_I\{S\}$ for a two-spin system is given by:

$$f_I\{S\} = \frac{\gamma_S}{\gamma_I} \frac{\sigma_{IS}}{\rho_{IS} + \rho_I^*} \qquad \text{A7- 7.18}$$

The magnitude of the nOe is in part dependent upon the magnitude of the so-called *leakage* relaxation, ρ_I^* which causes the attenuation from η_{max}. Of the possible mechanisms of leakage relaxation, the contribution from intermolecular single quantum dipolar relaxation with paramagnetic impurities and dissolved molecular oxygen is the most prevalent

(Appendix A6.4.2). Therefore, the removal of these species from the analytical sample for nOe experiments is vitally important to maximise signal-to-noise ratios.

The correlation times of dissolved molecular oxygen do not vary considerably between samples of varying viscosity such that its contribution of ρ_I^* due to this relaxation mechanism remains more or less constant. However, the same cannot be said for τ_c associated with cross-relaxation, whereby the relative effect of ρ_I^* due to dissolved oxygen varies considerably between samples. Consequently molecules in the extreme narrowing limit, the magnitude of τ_c is low and the steady-state nOes observed are usually far short of the theoretical maximum due to the considerable effect of ρ_I^* relative to σ_{IS} and ρ_{IS}. However, away from the extreme narrowing limit, τ_c is high and the magnitudes of the steady-state nOes observed are usually closer to the theoretical maximum due to the considerable small effect of ρ_I^* relative to σ_{IS} and ρ_{IS}.

Finally the equations are adjusted once more to enable the description of the real empirical nOes that relate to multi-spin systems.

A7.2.3 Multi-spin systems

The multi-spin Solomon equation for the change in intensity of **I** is given by:

$$\frac{dI_z}{dt} = -\left(I_z - I_z^0\right)\left(R_I^{DD} + \rho_I^*\right) - \left(S_z - S_z^0\right)\sigma_{IS} - \sum_X \left(X_z - X_z^0\right)\sigma_{IX} . \qquad \text{A7- 7.19}$$

It is evident that the right-hand side of equation A7-7.19 includes a term for the cross-relaxation of **I** with any number of proximate spins **X** that may themselves be subject to perturbation as a result of saturation of **S**. The effect of this indirect cross-relaxation pathway is described later on.

The empirical steady-state nOe for a multi spin system (which includes the effect of $\mathbf{R_I}$), derived from the multiplspin Solomon equation is given by:

$$f_I\{S\} = \frac{\gamma_S}{\gamma_I}\frac{1}{R_I^{DD}+\rho_I^*}\left[\sigma_{IS} - \sum_X \frac{\left(X_z - X_z^0\right)}{S_z^0}\sigma_{IX}\right]$$
$$= \frac{\gamma_S}{\gamma_I}\frac{1}{R_I^{DD}+\rho_I^*}\left[\sigma_{IS} - \sum_X \frac{\gamma_X}{\gamma_S} f_X\{S\}\sigma_{IX}\right] \qquad \text{A7- 7.20}$$

The terms in the square brackets include the fractional enhancement at **X** due to saturation of **S** ($f_I\{S\}$) and the cross-relaxation of **X** with **I** (σ_{IX}), which account for the indirect cross-relaxation pathway in the multispin Solomon equation.

Expressed in terms of the mean transition probabilities, equation A7-7.20 becomes

$$f_I\{S\} = \frac{\gamma_S}{\gamma_I} = \left[\frac{(W_{2IS} - W_{0IS}) - \sum_X (\gamma_X/\gamma_S) f_X\{S\}(W_{2IX} - W_{0IX})}{2W_{1I} + W_{2IS} + W_{0IS} + \sum_X (W_{2IX} + W_{0IX}) + \rho_I^*}\right] \qquad \text{A7- 7.21}$$

By analogy with the two-spin system described previously, the mean transition probabilities can be defined in terms of τ_c, and ω to give:

$$W_{1I} = \frac{3}{20}K_I^2 \frac{\tau_c}{1+\omega_I{}^2\tau_c{}^2}$$

$$W_{2IS} = \frac{3}{5}K_{IS}^2 \frac{\tau_c}{1+(\omega_I+\omega_S)^2\tau_c{}^2}$$

$$W_{0IS} = \frac{1}{10}K_{IS}^2 \frac{\tau_c}{1+(\omega_I-\omega_S)^2\tau_c{}^2}$$

$$W_{2IX} = \frac{3}{5}K_{IX}^2 \frac{\tau_c}{1+(\omega_I+\omega_S)^2\tau_c{}^2}$$

$$W_{0IX} = \frac{1}{10}K_{IX}^2 \frac{\tau_c}{1+(\omega_I-\omega_S)^2\tau_c{}^2} \qquad \text{A7- 7.22}$$

where

$$K_I^2 = \left(\frac{\mu_0}{4\pi}\right)^2 \left(\hbar^2 \gamma_I^2 \gamma_S^2 r_{IS}^{-6} + \sum_X \hbar^2 \gamma_I^2 \gamma_S^2 r_{IX}^{-6}\right)$$

$$K_{IS}^2 = \left(\frac{\mu_0}{4\pi}\right)^2 \hbar^2 \gamma_I^2 \gamma_S^2 r_{IS}^{-6} \qquad \text{A7- 7.23}$$

$$K_{IX}^2 = \left(\frac{\mu_0}{4\pi}\right)^2 \hbar^2 \gamma_I^2 \gamma_S^2 r_{IX}^{-6}$$

Where **K** is the magnitude of the dipolar coupling interaction, **r** is the internuclear distance between the coupling dipoles, and μ_0 is the vacuum permeability.

In the extreme narrowing limit ($1 >> \omega\tau_c$), the motional dependent terms, i.e., the right hand side of equations A7-7.22 are constant and can be omitted. Subsequently equation A7-7.21 becomes:

$$f_I\{S\} = \frac{\gamma_S}{\gamma_S}\left[\frac{\left(\frac{3}{5} - \frac{1}{10}\right)K_{IS}^2 - \sum(\gamma_X/\gamma_S) f_X\{S\}\left(\frac{3}{5} - \frac{1}{10}\right)K_{IX}^2}{\frac{6}{20}K_I^2 + \left(\frac{3}{5} + \frac{1}{10}\right)K_{IS}^2 + \sum_X\left(\frac{3}{5} + \frac{1}{10}\right)K_{IX}^2 + \kappa_I}\right] \qquad \text{A7- 7.24}$$

where κ_I is an empirical correction factor proportional to ρ_I^*/τ_c, which in the extreme narrowing limit becomes an equality given by:

$$\kappa_I = \frac{\rho_I^*}{\gamma_I^2 \gamma_S^2 \hbar^2}\left(\frac{4\pi}{\mu_0}\right)^2 \frac{1}{\tau_c} \qquad \text{A7- 7.25}$$

Expressed in terms of internuclear distances between the coupling dipoles, **r**, the empirical steady-state multispin nOe for the extreme narrowing limit is given by:

$$f_I\{S\} = \eta_{\max}\left[\frac{r_{IS}^{-6} - \sum_X f_X\{S\} r_{IX}^{-6}}{r_{IS}^{-6} + \sum_X r_{IX}^{-6} + \kappa_I}\right] \qquad \text{A7- 7.26}$$

where r_{IS} and r_{IX} are the internuclear distances between **I** and **S** and **I** and **X** respectively.

Therefore, the steady-state nOe is not exclusively dependent upon the internuclear distance r_{IS} but additionally the internuclear distances r_{IX}. The contributions, $\sum_{X} r_{IX}$ are called *indirect effects,* which are derived from the terms mentioned previously: cross-relaxation of **S** may occur with spin(s) **X**, which causes non-equilibrium population differences across the **X** spin transitions. Consequently, spin(s) **X** will relax due to longitudinal relaxation, which can include cross-relaxation with proximate spin(s) **I**.

A7.2.3.1 Indirect (three-spin) effects

Indirect effects in some literature references are often referred to as *three-spin effects* i.e., (**S**→**X**→**I**). Indeed in the positive nOe regime i.e. extreme narrowing limit, three-spin effects are often manifested in steady-state nOe spectra either as; **I** signals with unexpected low intensity positive enhancements, no signals, or negative signals. This does not however, preclude, indirect effects being relayed over more than three spins. Indirect effects are strongly dependent upon the bonding geometry between the mutually dipolar coupled spins. Consequently, one can interpret indirect effects in a qualitative manner and draw inferences to molecular structure [24]

A7.2.4 The validity of the steady-state nOe for internuclear distance determination

The multi-spin steady –state nOe given by equation A7-7.25 does not exclusively depend upon the internuclear distance r_{IS} and depends on:

- the value of κ_I, which may vary between different **I** spins
- The value of $\sum_{X} r_{IX}$, which may similarly vary due to the variation in molecular structure about the **I** spins.

Consequently $f_I\{S\} \neq f_S\{I\}$. Therefore, in order to attempt to determine quantitative internuclear distances using the steady-state nOe, one must determine empirically the values of κ_I for each **I** spin. As this is extremely time consuming, or often not possible, the steady-state nOe is more commonly used for the qualitative determination of inter-nuclear distance. The analysis of the magnitudes and signs of enhancement provide indications of the effect of

direct and indirect nOe effects, which can then be used to confirm or question a proposed molecular structure.

Steady-state nOes whether used qualitatively or quantitatively, suffer from the ill effects of incomplete saturation of entire multiplets [24] and problems achieving selective perturbations in crowded spectral regions. Therefore, the steady-state nOe is usually only used when requiring only a few selective perturbations of spins that are well separated in the NMR spectrum. As such the technique is rarely used for large molecules for which spectral crowding is often exhibited and the extreme narrowing limit is also invalid.

Quantitative internuclear distance information is more accurately and readily obtained via transient nOe experiments, which are described in A7.3.

A7.2.5 The steady-state nOe outside the extreme narrowing limit: Spin-Diffusion

For large molecules in generally high viscosity liquids, the value of τ_c is large and so is the spectral density of dipolar magnetic fields at the ZQ cross-relaxation frequency. Indeed, the efficiency of ZQ cross-relaxation is so high that indirect cross-relaxation effects are prevalent regardless of molecular geometry. Consequently the nOe is relayed or diffused along the network of dipolar coupled spins. Hence the negative nOe regime is usually referred to as the spin-diffusion limit, and all nOes tend to the same value of -1. Therefore, steady-state nOes in the spin diffusion limit are not amenable to internuclear distance determinations.

A7.2.6 Heteronuclear steady state nOe

When the gyromagnetic ratios of spins **I** and **S** are different, as in heteronuclear systems, e.g., $^{13}C - {}^{1}H$, and the system exhibits extreme narrowing, the steady-state two-spin nOe is given by:

$$f_I\{S\} = \eta_{max} = \frac{\gamma_S}{2\gamma_I} \qquad \text{A7- 7.27}$$

Within the extreme narrowing limit, for the system $^{13}C\ \{^{1}H\}$, $\eta_{max} = 1.988$, and the signal becomes approximately 3 times as large ($\eta_{max} + 1$). The nOes of insensitive nuclei, e.g., ^{13}C

often approach η_{max} when the insensitive nucleus is directly attached to protons, as the relaxation of the insensitive nucleus is more or less entirely dependent upon dipolar relaxation with the protons. Indeed, the general enhancement of all insensitive nuclei by heteronuclear nOe is used routinely to increase the signal-to-noise ratio of their spectra.
It can be shown [24] that the nOe at an insensitive nucleus due to saturation of all protons (**M**) by broadband proton decoupling (Appendix A3.2.8) is equal to η_{max}, given in equation A7-7.27:

$$f_I\{M\} = \sum_M \frac{\gamma_M}{2\gamma_I} \frac{\sigma_{IM}}{R_I^{DD}} = \eta_{max} = \frac{\gamma_S}{2\gamma_I} \qquad \text{A7- 7.28}$$

Where it is assumed that relaxation of **I** occurs exclusively due to intramolecular dipolar relaxation with the saturated protons. For ^{13}C nuclei directly bonded to protons this assumption more or less holds true and η_{max} is often approached closely regardless of molecular geometry or the number of directly attached protons [60]. This is in part due to the fact that insensitive nuclei are generally less prone to intermolecular leakage effects (ρ_I^*) due to the fact that they are usually situated closer to the "centre" of the molecule. The longitudinal relaxation of isolated insensitive nuclei, i.e., ^{13}C quaternaries (which are not directly bonded to protons) is heavily influenced by external relaxation mechanisms, e.g., chemical shift anisotropy, which contribute to ρ_I^*. Consequently, the empirical nOe falls short of η_{max} and one should insert ρ_I^* as a denominator in equation A7-7.28. Of course polarisation transfer and exchange experiments, (Appendix A8.3.1) provide a maximum enhancement factor of 4.

Steady-state heteronuclear experiments suffer from the same shortcomings as in the homonuclear case and are seldom used in a quantitative manner. The use of the heteronuclear steady-state nOes is only useful for the study of isolated insensitive nuclei, e.g., ^{13}C quaternaries, which are not directly bonded to protons. Quantitative internuclear distances can be obtained using heteronuclear transient nOe experiments (Chapter 3), which are described from a homonuclear point of view in subsequent sections.

A7.2.6.1 The dependence of $f_I\{s\}$ on τ_c when γ_S/γ_I is positive.

By analogy with the homonuclear steady-state nOe, an increase τ_c the extreme narrowing condition no longer holds and the nOe starts to decrease. In contrast to the homonuclear nOe, the nOe at the insensitive nucleus, (**I**) only becomes negative when $\gamma_S/\gamma_I < 2.38$. The sign of the nOe can of course change due to three spin effects similar to that described in the homonuclear system.

The nOe is zero when

$$\tau_c = \left[\frac{5}{(\omega_I + \omega_S)^2 - 6(\omega_I - \omega_S)^2}\right]^{1/2} \qquad \text{A7- 7.29}$$

and by analogy with the homonuclear steady-state nOe described previously, is sensitive to parameters like, viscosity, temperature and $\mathbf{B_0}$.

A7.2.6.2 The dependence of $f_I\{s\}$ on τ_c when γ_S/γ_I is negative

When γ_S/γ_I is negative, ω_I is also negative. Werbelow, [62-63] determined that the relative signs of ω causes the magnitudes of the cross-relaxation frequencies to change. For two spins, which exhibit the same sign of γ, the following condition holds, $(\omega_I + \omega_S) > (\omega_I - \omega_S)$, i.e., the double quantum cross-relaxation mechanism occurs at a higher frequency than the zero quantum cross relaxation mechanism. Therefore, the derivations of $f_I\{\mathbf{S}\}$ are permuted and $f_I\{\mathbf{S}\}$varies with τ_c in a different manner to that of a hypothetical nOe due to the same value of γ_S/γ_I but which is positive. This observation is confirmed empirically and the following dependencies of the ratios γ_S/γ_I and τ_c hold.

When the ratio γ_S/γ_I falls between -3 and -1, enhancements of approximately -100% are observed for all values of $\omega\tau_c$. For large negative ratios, e.g., **I** = ^{29}Si and ^{15}N, the enhancements are approximately the inverse of that seen were the ratio positive.

By analogy with nOes in the spin diffusion limit for nuclei of positive ratios γ_S/γ_I, negative nOes in heteronuclear spin systems may completely cancel the equilibrium magnetisations of heteronuclei, which renders them unobservable.

A7.3 Transient nOe experiments

Unlike steady state experiments, transient experiments utilise pulses to rapidly achieve the necessary spin energy level population perturbation. As the method of perturbation of spin(s) **S** is not continuous, the enhancement seen at spin(s) **I** is transient: consequently longitudinal relaxation mechanisms of **S** work in unison with that of **I**, so competing simultaneously with cross-relaxation mechanisms between them. The competing relaxation processes dictate the total time over which enhancements can be observed before the restoration of thermal equilibrium.

Providing the *initial rate approximation* is valid, the build up of transient nOes is entirely dependant on cross-relaxation between the perturbed spin(s) **I** and **S** (σ_{IS}). As the efficiency of cross-relaxation is dependent upon the internuclear distance, the intensity of the nOe is directly proportional to the internuclear distance r_{IS}.

A7.3.1 The initial rate approximation

The Solomon equations for a two spin homonuclear system **I** and **S** relaxing exclusively due to dipolar coupling, and a multispin system **I**, **S** and **X** including external relaxation are given respectively by:

$$\frac{dI_z}{dt} = -\rho_{IS}\left(I_z - I_z^0\right) - \sigma_{IS}\left(S_z - S_z^0\right)$$
$$\frac{dI_z}{dt} = -R_I\left(I_z - I_z^0\right) - \sigma_{IS}\left(S_z - S_z^0\right) - \sum_X \sigma_{IX}\left(X_z - X_z^0\right) \qquad \text{A7- 7.30}$$

The initial conditions during a one-dimensional selective transient experiment, where perturbation is achieved via selective inversion of spin **S** by a selective pulse are:
$S_z = -S_z$, $I_z = I_z^0$ and $X_z = X_z^0$ so that the terms $(I_z - I_z^0)$ and $(X_z - X_z^0)$ are zero. Therefore the initial rate of change of I_z i.e., at a time $\tau_m = 0$ after the selective inversion of **S** is given by

$$\left.\frac{dI_z}{dt}\right|_{\tau_m=0} = 2\sigma_{IS}S_z^0 \qquad \text{A7- 7.31}$$

Which is also true of the enhancement of **S** due to perturbation of **I**. At $\tau_m = 0$, the enhancement of **I** due to perturbation of **S** is entirely dependent upon $2\sigma_{IS}$. The factor of two is due to the level of perturbation, i.e., inversion of **S**. If the selective perturbation of **S** had been caused by a $\pi/2$ pulse, i.e., half-inversion, the enhancement of **I** would be equal to σ_{IS}.

The effect of the relaxation rates of **I** and **S** ($\mathbf{R_I}$ and $\mathbf{R_S}$ respectively) only serve to modify the enhancement of **I** at much later times, i.e., when $\tau_m > 0 << R_S^{-1}$ and R_I^{-1} (T_1 and T_2 respectively) so that the enhancement builds up linearly and is entirely dependant upon σ_{IS}. This is the *initial rate approximation* and subsequently, the magnitude of the transient nOe is directly proportional to the internuclear distance r_{IS}^{-6}.

In contrast to the steady-state nOe where $f_I\{\mathbf{S}\} \neq f_S\{\mathbf{I}\}$, when the initial rate approximation is valid, $f_I\{\mathbf{S}\} = f_S\{\mathbf{I}\}$, because it does not depend upon the relaxation rates R_I and R_S, which are invariably different. Consequently, for the transient nOe experiment to be used to determine quantitative internuclear distances, i.e., for the initial rate approximation to remain valid, the experimenter must ensure that the enhancements are observed at times that are far less than the T_1's of the nuclei involved in cross-relaxation. At later times the when τ_m approaches the T_1's of the nuclei involved, the transient nOe development is no longer linear. For example, in the case of selective inversion of **S**, the longitudinal relaxation of **S** (T_{1S}) serves to restore thermal equilibrium population differences across the **S** transitions, thus reducing the nOe at **I**. Similarly, T_{1I} simultaneously serves to restore the equilibrium populations across the **I** transitions after nOe due to **S**. Therefore, knowledge of the T_1's of the nuclei involved in cross-relaxation is crucial.

In general, the nOe build up time, or mixing time, τ_m, as it is generally known, is usually of the order of milliseconds. Hence, transient nOes are generally small and so a large number of transients are required to provide adequate signal-to-noise ratios for their accurate measurement. Consequently, transient nOe experiments are generally long.

Finally, it is evident that the cross-relaxation rate and hence the initial rate of build-up of the transient nOe depends on the level of perturbation, which is in turn dependent upon the relaxation of the perturbed nuclei prior to the next transient. Therefore, to determine quantitative internuclear distances and directly compare the intensities of transient nOes from the same experiment, one must ensure that either of the following conditions:

- thermal equilibrium has been re-established
- The perturbed spins are perturbed to the same extent on every transient.

The time development of the transient nOe is shown schematically in figure A7.5.

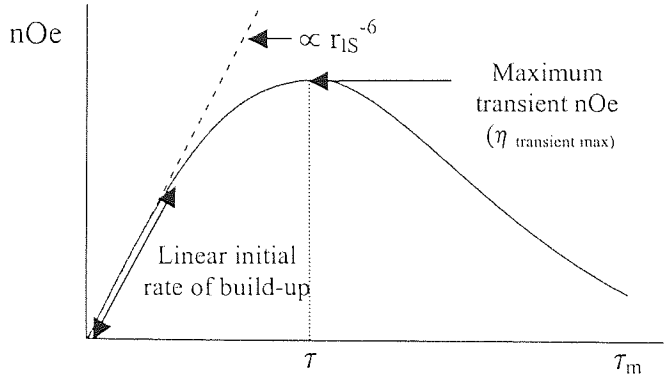

Figure A7.5 **Schematic representation of the time development of the transient nOe in the extreme narrowing limit. Modified from Claridge [23]**

A7.3.2 The development of the one-dimensional transient nOe for a two spin system I and S

To establish more formally the time development of the transient nOe for a two spin system **I** and **S**, the following simultaneous differential equations must be solved.

$$\frac{dI_z}{dt} = -R_I\left(I_z - I_z^0\right) - \sigma_{IS}\left(S_z - S_z^0\right)$$
$$\frac{dS_z}{dt} = -R_S\left(S_z - S_z^0\right) - \sigma_{IS}\left(I_z - I_z^0\right) \qquad \text{A7- 7.32}$$

The general solution of these equations expressed in terms of the fractional enhancement of **I** due to **S** ($f_I\{S\}$) have been given by Noggle and Schirmer [28]:

$$f_I\{S\}(\tau_m) = \frac{\left(I_z(\tau_m) - I_z^0\right)}{I_z^0} = C_1 e^{-\lambda_1 \tau_m} + C_2 e^{-\lambda_2 \tau_m} \qquad \text{A7- 7.33}$$

and

$$\frac{\left[S_z(t)-S_z^0\right]}{S_z^0}=C_1e^{-\lambda_1 t}\frac{(\lambda_1-R_1)}{\sigma}+C_2e^{-\lambda_2 t}\frac{(\lambda_1-R_2)}{\sigma} \qquad \text{A7- 7.34}$$

where the notation {S} has been preserved to denote the perturbed spin and $\sigma = \sigma_{IS} = \sigma_{SI}$. The constants C_1 and C_2 given by Noggle and Schirmer correspond to the method of perturbation and hence boundary conditions employed. In this circumstance where a selective pulse is used to invert the **S** spin populations, C_1 and C_2 are given by:

$$C_1=2\left(\frac{\lambda_2-R_s}{\lambda_1-\lambda_2}\right),C_2=-2\left(\frac{\lambda_1-R_s}{\lambda_1-\lambda_2}\right) \qquad \text{A7- 7.35}$$

where

$$\lambda_{1,2}=\frac{1}{2}\left\{(R_I-R_S)\pm\left[(R_I-R_S)^2+4\sigma^2\right]^{1/2}\right\} \qquad \text{A7- 7.36}$$

If it is assumed that $\mathbf{R_1} = \mathbf{R_S}$, the fractional nOe at **I** due to selective inversion of **S** is given by:

$$\begin{aligned} f_I\{S\}(\tau_m) &= -e^{-(R+\sigma)\tau_m}+e^{-(R-\sigma)\tau_m} \\ &\equiv e^{-(R-\sigma)\tau_m}\left(1-e^{-2\sigma\tau_m}\right) \\ &\equiv 2e^{-R\tau_m}\sinh(\sigma\tau_m) \end{aligned} \qquad \text{A7- 7.37}$$

where τ_m is the mixing time after which the transient nOe is observed. Differentiation of equation A7-7.37 at time t = 0 gives the initial rate of build-up of the transient nOe, i.e., equation A7-7.31. In the extreme narrowing limit, the form of $f_I\{S\}(\tau_m)$ is an exponential rise at a rate $e^{-2\sigma t}$ multiplied by a longitudinal relaxation decay function, which is shown schematically in figure A7.5 shown previously.

A7.3.2.1 Maximum transient nOe

The maximum transient nOe i.e., the point of inflection of the curve given in figure A7.5 is dependent upon the contribution of longitudinal relaxation rates other than dipolar cross-relaxation, i.e., $\mathbf{R_I}$ and $\mathbf{R_S}$ **(R)** and is given by:

$$\eta_{\substack{\text{transient}\\ \text{max}}} = \left(\frac{R+\sigma}{R-\sigma}\right)^{-\left[\frac{(R-\sigma)}{2\sigma}\right]} - \left(\frac{R+\sigma}{R-\sigma}\right)^{-\left[\frac{(R-\sigma)}{2\sigma}\right]}. \qquad \text{A7-7.38}$$

Which subsequently occurs at time τ given by

$$\tau = \left(\frac{1}{2\sigma}\right)\ln\left[\frac{(R+\sigma)}{(R-\sigma)}\right] \qquad \text{A7- 7.39}$$

For a homonuclear proton two spin system relaxing purely due to dipolar mechanisms i.e., $\rho_I^* = \rho_S^* = 0$, the value of maximum transient enhancement is 38.5% as opposed to 50% for a steady-state nOe. Consequently, external sources of relaxation reduce $\eta_{\text{transient max}}$ and the lifetime of the initial rate approximation. Therefore, one must make every effort to remove dissolved molecular oxygen and paramagnetic impurities from analytical samples (Appendix A4.3.2.1 and Appendix A6.4.2).

A7.3.3 The one-dimensional transient nOe experiment

Figure A7.6 shows the pulse sequence for a typical homonuclear selective one-dimensional transient nOe experiment.

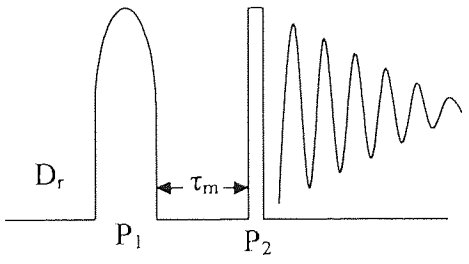

Figure A7.6 Basic One-dimensional homonuclear transient nOe pulse sequence.

The selective pulse, P_1, causes the selective inversion of an entire spin multiplet while all other spins remain unperturbed (Appendix A10) and the transient nOe is allowed to develop during τ_m. The final hard "*read*" pulse, P_2, applied to all nuclei allows the observation of the magnetisation that has built up during the inter-pulse sequence relaxation delay, D_r, and

mixing time τ_m. The experiment is then repeated, with the selective pulse applied to a spectral region devoid of signals (off-resonance). Consequently the magnetisation that has built-up from longitudinal relaxation during the inter-pulse sequence relaxation delay, D_r, and mixing time τ_m does not include contributions from cross-relaxation. The result of the off-resonance experiment acts as the "control" is subtracted from the on-resonance experiments so as to gain the absolute nOe due to the selected nucleus. The fractional enhancement $f_I\{S\}$ is determined by dividing the absolute nOe with the control.

A7.3.4 Two-dimensional transient nOe experiments

One-dimensional transient nOe experiments are particularly useful when the analysis of only a few transient nOes are required, and the inversion pulse can be applied selectivity to a given multiplet without affecting others in its vicinity. The latter property requires the chemical shift of the component signals in the spectrum to be well separated, similar to the requirement of the steady-state method.

In general larger and more complex molecules often exhibit crowded spectra such that selectivity of an inversion pulse cannot be achieved. Furthermore many selective perturbations may also be required to gain enough transient nOe data, so rendering the selective one-dimensional experiment a less attractive.

Two-dimensional transient nOe experiments overcome these shortcomings of one-dimensional transient nOe experiments. By the application of hard pulses, perturbation of the spin system is non-selective, so that all transient nOes are observed simultaneously in a single two-dimensional spectrum. The experiment benefits from the added spectral resolution inherent to two-dimensional spectra, facilitating easier analysis in crowded spectra and the resolution of inherently small transient nOes. When performed in a way that maintains the validity of the initial rate approximation, 2-D transient nOe data can be used to determine quantitative internuclear distance information in a similar way to that of one-dimensional experiments.

An example of a two-dimensional transient nOe experiment is the homonuclear NOESY (Nucelar Overhauser Effect SpectroscopY) experiment first proposed by Macura and Ernst

[29]. Figure A7.7 illustrates the simplest NOESY pulse sequence, which consists of three pulses separated by two delays.

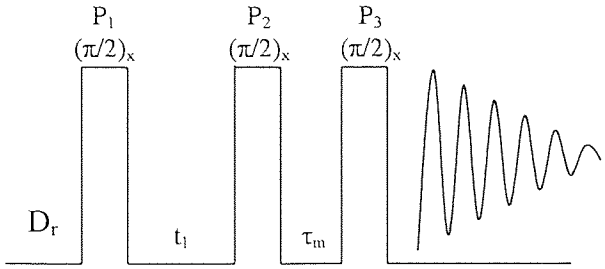

Figure A7.7 Basic NOESY pulse sequence

The first proton pulse, P_1, causes the excitation of single quantum coherence of all protons. During t_1, evolution due to chemical shift occurs such that at the end of t_1, the single quantum coherence of for example two protons **I** and **S**, which are not scalar coupled is given by:

$$-I_y \cos\Omega_I t_1 + I_x \sin\Omega_I t_1 - S_y \cos\Omega_S t_1 + S_x \sin\Omega_S t_1 \qquad \text{A7- 7.40}$$

See product operator formalism (Appendix A8). The value of t_1 is incremented over the entire course of the experiment, which provides the necessary frequency labelling and amplitude or phase modulation required for the second frequency dimension (Appendix A5).

Pulse P_2 (and subsequent mutual phase cycling of P_1 and P_2) converts the cosine components of single quantum coherence to Z-magnetisation:

$$-I_z \cos\Omega_I t_1 + I_x \sin\Omega_I t_1 - S_z \cos\Omega_S t_1 + S_x \sin\Omega_S t_1 \qquad \text{A7- 7.41}$$

The effect of the pulse sequence has lead to the perturbation of the longitudinal magnetisation of **I** and **S**, which have magnitudes proportional to the modulation of the chemical shifts during t_1, given by $-\cos\Omega_I t_1$ and $-\cos\Omega_S t_1$ respectively. Consequently, during τ_m, a transient nOe develops simultaneously at **I** and **S** due to mutual cross-relaxation. As σ_{IS} is constant, the magnitude of the transient nOe (by analogy with 1-D transient experiments) at **I** due to **S** and vice versa is proportional to the relative perturbation of $\mathbf{I}_z$ and $\mathbf{S}_z$, i.e., $-\cos\Omega_I t_1$ and $-\cos\Omega_S t_1$ respectively. Consequently, at the end of τ_m the magnitude of $\mathbf{I}_z$ and $\mathbf{S}_z$, which was

originally proportional to $-\cos\Omega_I t_1$ and $-\cos\Omega_S t_1$ now has additional dependence on $-\cos\Omega_S t_1$ and $-\cos\Omega_I t_1$ respectively.

The final *read* pulse, P_3, excites observable single quantum coherence originating from the $\mathbf{I}_z$ and $\mathbf{S}_z$ magnetisations, which is subsequently measured during signal acquisition. The interferrogram (Appendix A5) of **I** and **S**, exhibits a frequency modulation according to their own chemical shift and the chemical shift of the other due to the transient nOe. Consequently, 2-D Fourier transform gives rise to a 2-D spectrum, which comprises so-called cross-peaks and diagonal peaks figure A7.8.

Cross-peaks correlate the transient nOe that has resulted due to cross-relaxation between two dipolar coupled spins. The diagonal peaks represent the residual longitudinal magnetisation that has not been involved in cross-relaxation.

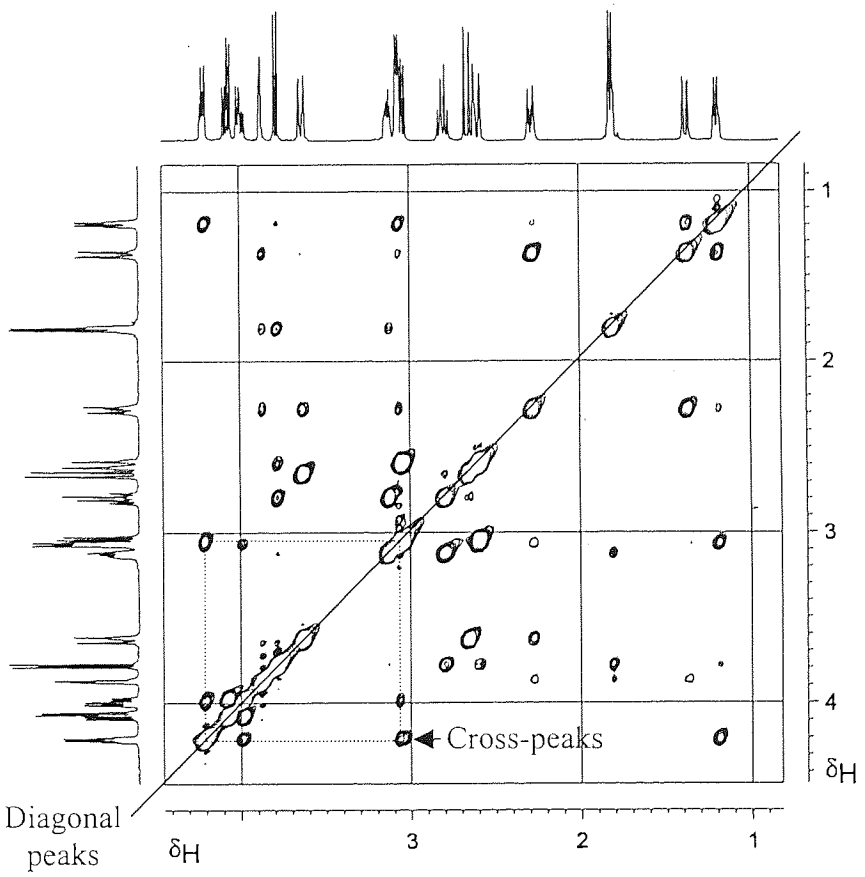

Figure A7.8 **Typical NOESY spectrum showing cross and diagonal peaks. (see text)**

The diagonal-peak terms and cross-peak terms are represented (a_{II} and a_{SS}) and (a_{IS} and a_{SI}) respectively.

$$I_y a_{II} \cos\Omega_I t_1 + S_y a_{SS} \cos\Omega_S t_1 + I_y a_{SI} \cos\Omega_S t_1 + S_y a_{IS} \cos\Omega_I t_1 \qquad \text{A7- 7.42}$$

Where the cross-peaks (a_{IS} and a_{SI}) = $a_{crosspeak}$ is given by:

$$a_{crosspeak}(\tau_m) = \frac{M_0}{2}\frac{\sigma}{D}\left(e^{-(R'+D)\tau_m} - e^{-(R'+D)\tau_m}\right) \qquad \text{A7- 7.43}$$

where M_0 is the intensity of the diagonal peak at $\tau_m = 0$. This corresponds to zero cross peak intensity, as no cross-relaxation can occur, and hence maximum diagonal peak intensity is observed for that experiment.

Differentiation of equation A7-7.43 at $\tau_m = 0$, by analogy with the one-dimensional transient nOe experiment gives the initial rate of transient nOe build-up:

$$\left.\frac{d\left(a_{crosspeak}\right)}{d\tau_m}\right|_{\tau_m=0} = -\sigma M_0 \qquad \text{A7- 7.44}$$

The initial rate of build-up is half that of the analogous one-dimensional experiment.
The difference in magnitude by the factor two is simply due to the method of perturbation employed in 2-D experiment. The NOESY experiment modulates the relative inversion between **I** and **S** due to the chemical shift difference between them. Over the complete number of transients in the NOESY experiment (each with a value of t_1 which has been incremented by a constant amount) it is assumed that the relative inversion between **I** and **S** is averaged and equal to halfway between complete inversion and no inversion (equivalent to the application of a $\pi/2$ pulse).

A7.3.5 Summary of the characteristics of 1-D and 2-D transient nOe experiments

When the initial rate approximation is valid 1-D and 2-D transient nOe experiments produce the same nOe except for the factor of two.

1-D and 2-D transient nOe experiments produce symmetrical enhancements i.e., $f_I\{\mathbf{S}\} = f_S\{\mathbf{I}\}$ for any value of $\mathbf{R_I}$ and $\mathbf{R_S}$, for all values of τ_m. The only exception to this occurs when the inter-sequence relaxation delay is inadequate to allow complete relaxation of all nuclei involved in cross-relaxation.

Cross-peaks in NOESY spectra exhibit the same intensity even if the number of equivalent spins between which a dipolar coupling exists is different. Macura and Ernst showed that if there are N_I spins **I** and N_S spins **S**, the cross-peak intensity is proportional to $N_IN_S/(N_IN_S)$. The same is true for absolute enhancements in 1-D experiments.

A7.3.6 Quantitative interpretation of transient nOe data

There are only a few methods routinely used for the quantitative determination of internuclear distances, of which the use of an internal calibrant and numerical integration of the Solomon equations are the most routinely employed. The former method allows the direct determination of internuclear distances by analysis of experimental data, as opposed to the latter which is used to predict the intensities of nOes, which are then compared to empirically derived values.

A7.3.6.1 Internal calibration

If the molecule under scrutiny contains two nuclei **a** and **b** of fixed and *known* internuclear distance, when the initial rate approximation is valid the transient nOe intensity is directly proportional to the internuclear distance r_{ab}. Providing the intital rate approximation is valid for all other dipolar coupled nuclei, e.g., **c** and **d**, a simple ratio of the cross-peak intensity with that of the internal calibrant yields r_{cd}.

$$\frac{f_a\{b\}}{f_c\{d\}} = \left(\frac{r_{ab}}{r_{cd}}\right)^{-6} \qquad \text{A7- 7.45}$$

Furthermore one can determine the value of τ_c, which is valuable as the direct determination of τ_c requires the execution of a number of experiments to completely characterise the relaxation of the spin system.

The accuracy of internuclear distance determinations using the internal calibrant method obviously depends upon the accuracy of the known internuclear distance. A small discrepancy in this distance will propagate larger errors in the determination of an unknown distance that is larger in magnitude than that of the calibrant. The calibrant should certainly be a fixed covalent bond length that should not be amenable to variation due to the local molecular structure in which it resides.

It is essential that τ_c in the area of the molecule containing the calibrant is the same as those areas in which unknown distances are being derived. It has been assumed throughout this treatment of the nOe that the value of τ_c remains constant for all cross-relaxing nuclei in the molecule. This assumption is quite misleading since molecules may not reorient isotropically, especially molecules of high molecular weight.

It is not uncommon that the value of τ_c vary by as much as 2 fold in larger molecules due to the effect of internal rigidity/mobility of particular chemical functions. When such internal mobility issues are not well characterised, a degree of caution is required when determining distances using this method.

It is important to realise that some internuclear distances that have been derived in flexible molecules may actually correspond to $\langle r^{-6} \rangle^{-1/6}$. Where $\langle\ \rangle$ represents conformational averaging of a chemical function or group, and the internuclear distance refers to the distance from a spin(s) outside the group, into spin(s) inside the group. In circumstances when the rotation of the chemical function or group is faster than τ_c^{-1}, the derived internuclear distance may correspond to $\langle r^{-3} \rangle^{-1/3}$. The effect of conformational averaging in this context is to derive minimum internuclear distances leading to a general underestimation of internuclear distances.

The only way to be sure that the initial rate approximation is valid for the calibrant and all unknown nOes is to perform a series of experiments incrementing the value of τ_m. A plot of nOe intensity versus τ_m should reveal the linear growth region and hence provide an indication of the correct experimental data to use that satisfies the initial rate approximation.

A7.3.6.2 Numerical integration of the Solomon Equations

Numerical integration of the multi-spin Solomon equations relevant to the spin system under scrutiny receives widespread use, as they are able to predict nOe intensities both within and beyond the initial rate approximation.

The technique requires the determination of the relevant relaxation matrix for the spin system, and the subsequent empirical determination of the values of **R** and σ for substitution into the Solomon equation. The theoretical transient nOes are then calculated by integration of the Solomon equations over small intervals of τ_m. The accuracy of this technique is adequate so long as the intervals over which integration is performed remain sufficiently small [24] and a full and accurate determination of **R**-values and σ has been achieved. Indeed in most circumstances the empirical determination of all the relevant **R**-values and σ proves to be impossible and one is forced to simplify the relaxation matrix at the expense of accuracy. Furthermore, one must rely upon the accuracy of experiments, integration of peaks, digital resolution etc such that at best one can only feasibly determine semi-quantitative internuclear distances.

Appendix A8 Product Operator Formalism

Most complex pulse sequences are not amenable to interpretation or analysis using classical vectors so more robust quantum mechanical methods of analysis are required. The quantum mechanical approach describes the state of the spin system under scrutiny by either a wavefunction or density operator, $\sigma(t)$. There exists two methods of quantum mechanical description of the state of an arbitrarily complex spin system during pulse sequence experiments, namely; the density matrix formalism [4, 53, 56] and more recently, the product operator formalism [12]. Both formalisms are based upon the density operator theory, however, the latter receives more widespread use since it marries semi-classical and quantum mechanical interpretations and hence provides a greater physical insight. Furthermore, the disadvantage of the density matrix approach is that it becomes cumbersome to implement in large spin systems. Indeed the product operator formalism has been utilised in this thesis for the description of NMR pulse sequences.

A8.1 The density operator

If relaxation is neglected, the time evolution of the density operator is described by the Liouville-von Neumann equation:

$$\dot{\boldsymbol{\sigma}}(t) = -i[\hat{\mathbf{H}}(t), \boldsymbol{\sigma}(t)] \qquad \text{A8- 8.1}$$

Where $\hat{\mathbf{H}}$ is the relevant Hamiltonian (Appendix A12) at a given instant in time. The density operator can be made time –independent within a finite period of time by the selection of an appropriate rotating frame. The time evolution of the density operator can then be expressed as a sequence of unitary transformations of the type:

$$\boldsymbol{\sigma}(t + \tau_1 + \tau_2) = \exp\{-i\hat{\mathbf{H}}_2 \tau_2\}\exp\{-i\hat{\mathbf{H}}_1 \tau_1\}\sigma(t)\exp\{+i\hat{\mathbf{H}}_1 \tau_1\}\exp\{+i\hat{\mathbf{H}}_1 \tau_2\}$$

A8- 8.2

with propagators $\exp\{-i\mathbf{H}_k \tau_k\}$. Equation A8-8.2 applies to any sequence of intervals, τ_k, with constant external fields or τ_k intervals where a time-independent average Hamiltonian can be defined.

The density matrix formalism expresses the density operator in terms of a matrix where the diagonal elements represent populations and the off-diagonal elements represent coherence.

A8.2 Product operator formalism

The density operator, σ, can be expressed as a linear combination of base operators $\mathbf{B}_s$.

$$\sigma(t) = \sum_s b_s(t)\mathbf{B}_s \qquad \text{A8- 8.3}$$

For spin systems that exhibit weak coupling (Appendix A3.2.5) the density operator can be described as a set of product operators:

$$\mathbf{B}_s = 2^{(q-1)} \prod_{k=1}^{N} (\mathbf{I}_{kv})^{a_{sk}} \qquad \text{A8- 8.4}$$

where N = the total number of $\mathbf{I} = ½$ nuclei in the spin system, k = index of the nuclei, v = x, y, or z, q = number of single spin operators in the product, $a_{sk} = 0$ for the N-q remaining nuclei. Product operators are orthogonal but are not normalised.

The complete base set $\{\mathbf{B}_s\}$ for a system with N spins of $\mathbf{I} = ½$ consists of 4^N product operators $\mathbf{B}_s$. Therefore, a weakly coupled two-spin system $\mathbf{I}$ and $\mathbf{S}$ comprises 16 product operators:

q = 0 ½ E (E = unity operator)

q = 1 I_z, I_x, I_y, S_z, S_x, S_y

q = 2 $2I_xS_z$, $2I_xS_y$, $2I_xS_x$

$2I_yS_z$, $2I_yS_y$, $2I_yS_x$

$2I_zS_z$, $2I_zS_y$, $2I_zS_x$.

Single spin operators represent entire spin multiplets, in this case a doublet, while multi-spin product operators represent multiple quantum coherence, which is described in the next section. Each product operator is equivalent to the corresponding density matrix for that particular state of the multiplet, however, each can be associated with a clear physical meaning.

Table A8.1 provides a qualitative description of each of the product operators, where SQC = Single quantum coherence, MQC = Multiple quantum coherence and the coherence order, **p**, is described in section A8.2.1. The x and y phases, which appear as subscripts adjacent to each operator, represent the corresponding phase in the rotating frame, i.e., x′ and y′ respectively. Table A8.1 illustrates the product operators that represent single quantum coherence in terms of semi-classical vectors. Figure 8.1 illustrates the single spin product operators in the semi-classical representation as introduced originally [12]. Where appropriate for means of clarity, a non-classical pictorial representation, which has been more recently proposed [64], will also supplement the semi-classical illustration. The former is clearly labelled (NC) to indicate the non-classical representation.

Product operator	**Description**	**Coherence Order, p**
½ **E**	Unit or Identity Operator	N/A
I_z	Longitudinal magnetisation of spin multiplet I	N/A
I_x	In-phase x'-coherence of spin multiplet I	SQC (**p** = 1)
I_y	In-phase y'-coherence of spin multiplet I	SQC (**p** = 1)
$2I_xS_z$	x'-coherence of spin I anti-phase with respect to *passive* spin S	SQC (**p** =1)
$2I_yS_z$	y'-coherence of spin I anti-phase with respect to *passive* spin S	SQC (**p** =1)
$2I_xS_x$, $2I_yS_y$, $2I_xS_y$ and $2I_yS_x$	Two-spin (double quantum coherence, DQC) of spins I and S	MQC (**p** = 2)
$2I_zS_z$	Longitudinal two-spin order (Zeeman order)	0

Table A8-1

The term *passive* spin describes the spins that are not involved in the coherence which are scalar coupled to the active spins. Those spins that are in a state of coherence are *active* spins.

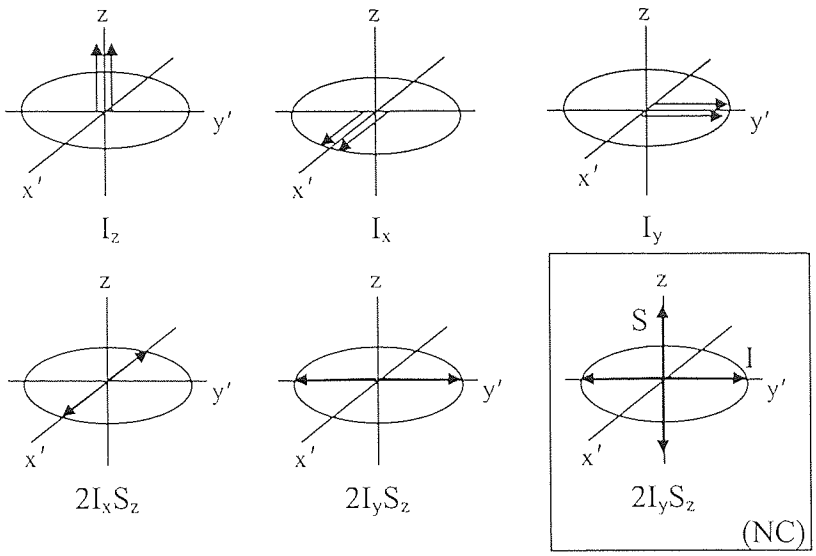

Figure A8.1 **Semi-classical and non-classical (NC) representations of single spin product operators**

A8.2.1 Multiple quantum coherences

Certain NMR pulse sequences can excite multiple quantum coherence of the spins involved in the scalar coupling. By analogy with the description of single quantum coherence given in appendix A1, multiple quantum coherence is considered to be a phase coherence between the spins, which are active in the coherence, i.e., those with transverse operators, e.g., I and S in $2I_xS_x$. However, in contrast to single quantum coherence, the spins of the ensemble involved in the coherence do not exhibit phase coherence with an external axis. Therefore, multiple quantum coherence is not observable since it does not constitute a resolvable magnetisation in the sample.

Quantum mechanically the individual spins that comprise the multiple quantum coherence are in a coherent superposition of Zeeman states where $\Delta m \neq \pm 1$. Therefore from a quantum mechanical standpoint it is obvious that MQC cannot give rise to observable signals. The order of coherence, **p**, is simply derived from the following equality:

$$\mathbf{p} = \sum_k \Delta m_k \omega_k \qquad \text{A8- 8.5}$$

Where Δm_k is the change in magnetic quantum number of spin k that occurs between two Zeeman states (α and β). Therefore, for **I** = ½ nuclei a **p**-quantum coherence can have

(**p** + 2n) active spins, where n is an integer. Qualitatively the order of coherence is simply given by the number of transverse operators in the product operator.

A8.2.1.1 Composition of multiple quantum coherence

The product operators given in table A8.1, which represent double quantum coherence, e.g., $2I_xS_x$ actually comprises a linear combination of pure double and pure zero quantum coherences: single product operators never represent pure **p**-quantum coherence. The composition of multiple quantum coherence is best illustrated in terms of raising and lowering operators (Appendix A12).

Shift operators describe the process of raising ($\hat{\mathbf{I}}^+$) or lowering ($\hat{\mathbf{I}}^-$) the magnetic quantum number m_z by one unit, equivalent to absorbing ($\alpha \rightarrow \beta$ through $\hat{\mathbf{I}}^+$) or emitting ($\beta \rightarrow \alpha$ through $\hat{\mathbf{I}}^-$) a single quantum respectively. When the composition of multiple quantum coherence is specified in terms of the shift operators it is possible to see the direction of coherence or the sense of population flow between the associated spin energy levels.

Expressed in terms of the shift operators $\hat{\mathbf{I}} = I$, the two spin multiple quantum coherence product operators are given by:

$$2I_xS_x = 1/2(I^+S^+ + I^+S^- + I^-I^+ + I^-S^-),$$
$$2I_yS_y = -1/2(I^+S^+ - I^+S^- - I^-I^+ + I^-S^-),$$
$$2I_xS_y = 1/2i(I^+S^+ - I^+S^- + I^-I^+ - I^-S^-),$$
$$2I_yS_x = 1/2i(I^+S^+ + I^+S^- - I^-I^+ - I^-S^-),$$

Pure multiple quantum coherences can be obtained via the linear combination of multiple quantum coherences:

$$1/2(2I_xS_x - 2I_yS_y) = 1/2(I^+S^+ + I^-S^-) = 2QT_x,$$
$$1/2(2I_xS_y + 2I_yS_x) = 1/2i(I^+S^+ - I^-S^-) = 2QT_y,$$
$$1/2(2I_xS_x + 2I_yS_y) = 1/2(I^+S^- + I^-S^+) = ZQT_x,$$
$$1/2(2I_yS_x - 2I_xS_y) = 1/2i(I^+S^- - I^-S^+) = ZQT_y,$$

Figure A8.2 illustrates schematically pure double and zero quantum coherence shown in terms of non-classical (NC) vector representations.

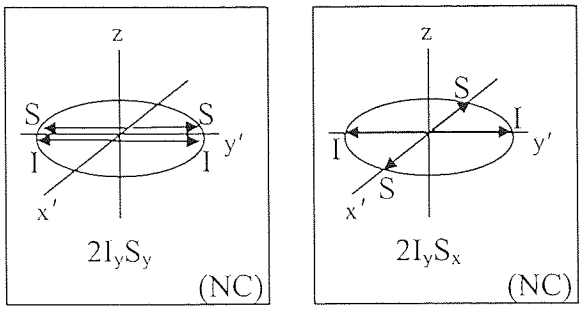

Figure A8.2 **Non-classical representation of multiple quantum coherence product operators. Note that the double-headed arrows indicate the net zero magnetisation**

A8.2.2 Three and four spin product operators

In larger spin systems, which exhibit mutual scalar coupling, some of the following product operators may be present in calculations. Three spin product operators:

$4I_{1x}S_zI_{2z}$:	SQC of spin I_1 of phase x, in anti-phase with respect to spins S and I_2.
$4I_{1x}S_xI_{2z}$:	DQC of spins I_1 and S of phase x, in anti-phase with respect to spin I_2
$4I_{1x}S_xI_{2x}$:	Triple quantum coherence (TQC) of all spins of phase x.
$4I_{1z}S_zI_{2z}$:	Longitudinal three-spin order (Zeeman order)

Spin I_2 is the *passive spin* in the DQC of spins I_1 and S and determines the relative phases of the active multiple quantum coherences. Passive spins can become *active spins* with the application of pulses of transverse phase. Figure A8.3 illustrates schematically the multiplet patterns indicative of two, three and four spin SQC product operators.

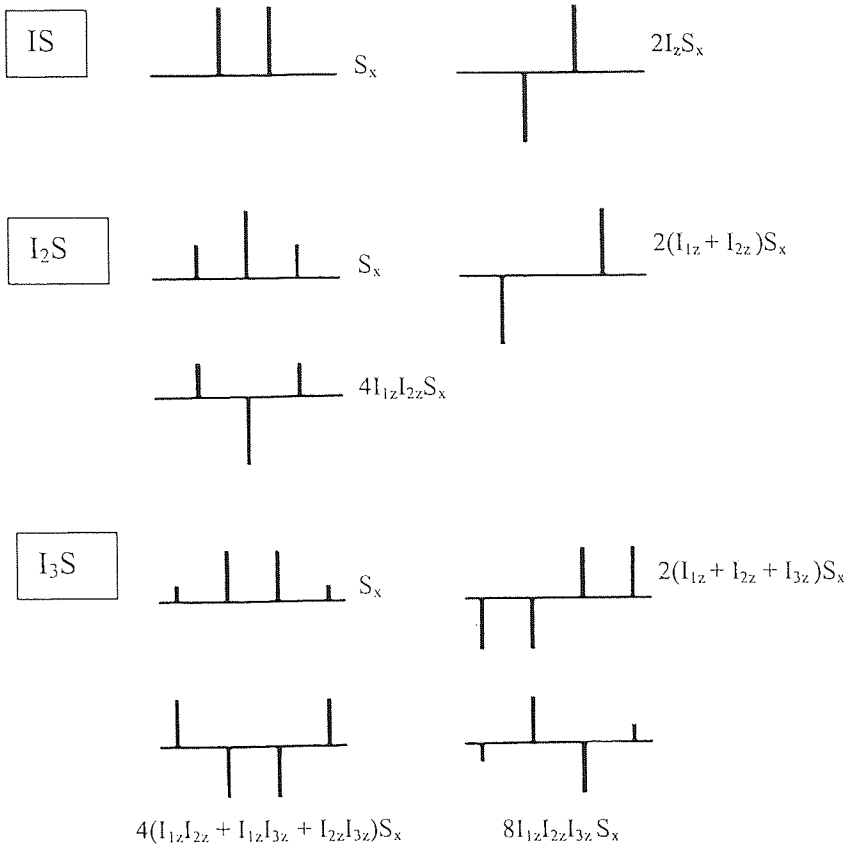

Figure A8.3 **Pictorial representation of SQC product operators of S where all spins I are magnetically equivalent**

A8.2.3 Longitudinal spin order (Zeeman order)

Longitudinal spin order refers to spin-correlated population of energy levels without net magnetisation and without coherence. Physically this corresponds to the exclusive correlation of z-components of the individual magnetic moment vectors of all the spins involved in the product operator. However, the correlation does not extend beyond the spins involved such that the net z-component of another group of spins maybe random. Consequently, there is no net magnetisation and the populations of the spin energy levels is assumed to adopt that shown in figure A8.4.

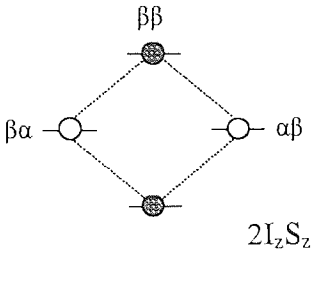

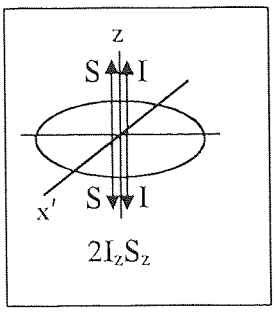

Figure A8.4 **Longitudinal spin-order. Shaded balls represent more population in comparison to those that are transparent.**

A8.2.4 Transformations of the product operators

Evolution of the density operator under the relevant Hamiltonians is expressed in a short hand version of equation A8-8.2 [12]:

$$\sigma(t) \xrightarrow{\mathcal{H}_1 \tau_1} \sigma(t+\tau_1) \xrightarrow{\mathcal{H}_2 \tau_2} \sigma(t+\tau_1+\tau_2) \qquad \text{A8- 8.6}$$

The Hamiltonians are written in terms of the product operators $\mathbf{B}_s$ instead of the usual notation given in Appendix A1. Therefore, the effective Hamiltonians are written:

$\mathcal{H}_{CS} = \sum_k \Omega_k I_{1z} =$ Chemical shift Hamiltonian

$\mathcal{H}_J = \sum_{i<k} \pi J_{kl}(2I_{1z}I_{2z}) =$ Scalar coupling Hamiltonian

$\mathcal{H}_{r.f.} = \sum_k \beta I_{1v} =$ *r.f.* pulse Hamiltonian

Where Ω_k is the evolution frequency of spin k in the rotating frame ($\omega_k - \omega_0$) where ω_k is the Larmor frequency corrected for chemical shift (Appendix A3.1).

The *r.f.* Hamiltonian is restricted to strong (Hard) *r.f.* pulses or selective pulses that manipulate evenly and entirely the whole spin multiplet (neglecting relaxation). The nutation angle of the pulses is given by β with phase v = x or y. The pulse acts exclusively on those I_1 spins. The transformations of the product operators are shown schematically in figure A8.5. and are described in the following sections.

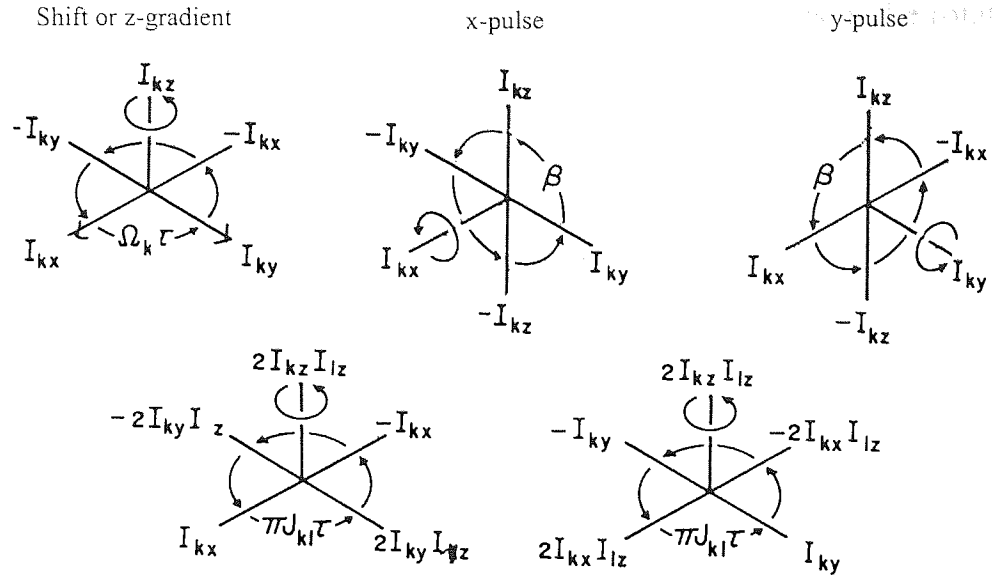

Figure A8.5 Transformations of the product operators under the various Hamiltonians for J > 0

A8.2.5 The effect of *r.f.* pulses

In relation to classical formalism, the transformation pertaining to a pulse results in a rotation of the operator in three-dimensional Cartesian space, according to the same principles as that described for classical vector manipulations. The accepted convention defining the sense of rotation for pulses and evolution is that given by Sorensen et al, which prescribes a positive rotation about the z'-axis leading from x'→ y'→ -x' → -y for nuclei of $\gamma > 0$. (Figure A8.5)

For single spin product operators

$$I_z \xrightarrow{\beta I_x} I_z \cos\beta - I_y \sin\beta$$

$$I_y \xrightarrow{\beta I_x} I_y \cos\beta + I_z \sin\beta$$

$$I_x \xrightarrow{\beta I_x} I_x$$

Operators with the same phase as the applied pulse are invariant to the transformation.
The effect of a pulse is considered separately for each single spin operator in the product operators. For multi-spin operators the transformations are treated separately, with the product of the former transformation becoming the starting product operator for latter transformations.

A8.2.6 The effects of evolution of single quantum coherences in the rotating frame

During pulse sequence delays coherences evolves in the rotating frame according to the Hamiltonians for chemical shift and scalar coupling. The Hamiltonians for both scalar coupling and chemical shift commute, such that transformations of the product operators during evolutions can be carried out sequentially and in an arbitrary order. Pulses are the exception to this rule and limit the periods of free precession.

A8.2.7 Chemical Shift

Transformation of the single spin product operators due to chemical shift are given by:

$$I_x \xrightarrow{\Omega I_z t} I_x \cos(\Omega I_z t) + I_y \sin(\Omega I_z t)$$

$$I_y \xrightarrow{\Omega I_z t} I_y \cos(\Omega I_z t) - I_x \sin(\Omega I_z t)$$

$$I_z \xrightarrow{\Omega I_z t} I_z$$

Chemical shift serves to modulate coherence cosinusoidally and sinusoidally as a function of Ω whereas longitudinal magnetisation is invariant to evolution. Evolution due to chemical shift always conserves the number **q** of single spin operators $\mathbf{U}_v$ with phase **v**. Figure A8.6 illustrates schematically the evolution due to chemical shift for a single quantum coherence.

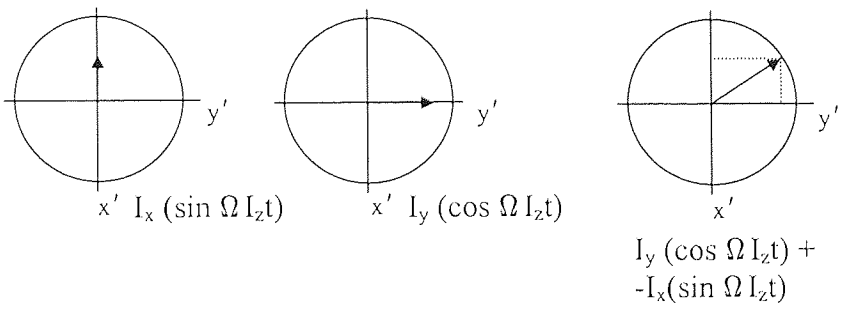

Figure A8.6 Evolution due to chemical shift

A8.2.8 Scalar coupling evolution

For a scalar coupled two-spin system IS, where the doublet I_x is exactly on-resonance (so there is no evolution due to chemical shift), the transformation of single quantum coherence of I due to scalar coupling evolution is given by:

$$I_x \xrightarrow{\pi J_{IS} t 2 I_z S_z} I_x \cos(\pi J_{IS} t 2 I_z S_z) + 2 I_y S_z \sin(\pi J_{IS} t 2 I_z S_z)$$

In contrast to evolution under chemical shifts and rotations due to pulses, evolutions due to scalar coupling *create* or *annihilate* product operators due to passive spins. The number of passive spins in the product operator e.g., S_z, depends on the number of nuclei with which the active spin e.g., I_x, is scalar coupled and which couplings are active during the evolution period. The transformation represents the conversion of in-phase single quantum coherence, I_x, to orthogonal anti-phase single quantum coherence I_y (Figure A8.7).

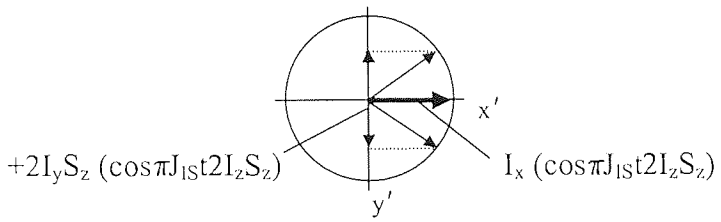

Figure A8.7 Single quantum coherence of I after evolution of scalar coupling in a two-spin system IS

Strictly speaking, the anti-phase coherence is said to be unobservable due to it having zero net integrated intensity. However, it can evolve under scalar coupling once again to give observable coherence:

$$2 I_x S_z \xrightarrow{\pi J_{IS} t 2 I_z S_z} 2 I_x S_z \cos(\pi J_{IS} t 2 I_z S_z) + I_y \sin(\pi J_{IS} t 2 I_z S_z)$$

It can be envisaged that with increasing complexity of the spin system due to extended spin coupling networks, the number of product operators that require computing as a result of evolution becomes very large. It is also evident that if the evolution period **t** is set so to $\mathbf{t} = 2\mathbf{J}_{IS}^{-1}$ the sine term becomes unity and pure anti-phase single quantum coherence will exist, similarly if $\mathbf{t} = \mathbf{J}_{IS}^{-1}$ the cosine term becomes unity and pure in-phase single quantum coherence of opposite sign exists.

A8.2.8.1 Refocusing the effects of evolution of single quantum coherences

Pulse NMR experiments can often be thought of as being made up of key building blocks of pulses and delays. The most important and frequently used building block is the spin-echo, which refocuses the effects of evolution due to chemical shift and inhomogeneous line

broadening. Furthermore it may also be used to refocus or modulate coherences as a function of scalar coupling.

A8.2.8.2 Refocusing the effects of chemical shift and B_0 inhomogeneity

It is assumed that all spins have attained a perfect state of x' phase coherence after a suitable pulse. A π pulse sandwiched between two evolution periods, $\mathbf{t}_1$ and $\mathbf{t}_2$ of the same duration ($\mathbf{t}_1 = \mathbf{t}_2$) constitutes a spin-echo sequence (Figure A8.8.).

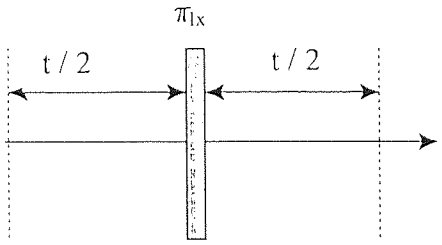

Figure A8.8 **Spin-echo sequence. Inversion pulse is placed at the centre of two identical evolution delays, t.**

For simplicity, the effect of the spin-echo sequence upon the refocusing of chemical shift and scalar coupling on one coherence is illustrated, however the result is applicable to any order of coherence.

$$I_x \xrightarrow{\Omega I_z t_1} I_x \cos(\Omega I_z t_1) + I_y \sin(\Omega I_z t_1) \xrightarrow{\pi I_x} I_x \cos(\Omega I_z t_1) - I_y \sin(\Omega I_z t_1)$$
$$\xrightarrow{\Omega I_z t_2} I_x$$

Application of the π_x pulse at the midpoint of the spin-echo nutates the $+\mathbf{I}_y$ component about the x' axis, while the $\mathbf{I}_x$ component remains invariant. The resultant vector now located in the opposite quadrant evolves due to chemical shift during $\mathbf{t}_2$, which causes the refocusing of the **I** coherence along +x' (Figure A8.9).

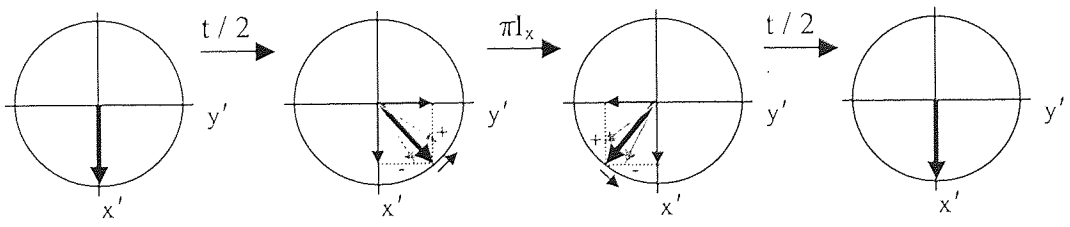

Figure A8.9 **Refocusing chemical shift and B_0 inhomogeneity. Arrows in grey indicate effects due to Inhomogeneous line broadening: + and – represent coherence with evolution frequencies faster and slower than the true Larmor frequency.**

The effect of inhomogeneous line broadening (Appendix A6.5.1) is simultaneously reversed or refocused by the application of the spin-echo sequence. The individual nuclear spins that have lost their phase coherence with one another precess at faster and slower frequencies, which de-phases the entire coherence. The effect of the refocusing pulse has been to reposition these vectors such that at the end of the spin-echo the effect due to inhomogeneous line broadening has been refocused. The refocusing of inhomogeneous line broadening during pulse sequences is essential to preserve coherence for its continued manipulation.

A8.2.8.3 Evolution of Heteronuclear scalar coupling only

The effect that the spin-echo sequence of figure A8.8 has upon the heteronuclear scalar coupling of a two-spin $\mathbf{I} = ½$ system, IS, is depicted for the I spin by the product operator transformations given below. The terms representing chemical shift are also included at each step.

$$I_x \xrightarrow{\pi J_{IS} t_1 2I_z S_z + \Omega I_z t_1} I_x \cos(\pi J_{IS} 2I_z S_z t_1)\cos(\Omega I_z t_1) + I_y \cos(\pi J_{IS} 2I_z S_z t_1)\sin(\Omega I_z t_1)$$
$$+ 2I_y S_z \sin(\pi J_{IS} 2I_z S_z t_1)\cos(\Omega I_z t_1) - 2I_x S_z \sin(\pi J_{IS} 2I_z S_z t_1)\sin(\Omega I_z t_1) \xrightarrow{\pi I_x}$$
$$I_x \cos(\pi J_{IS} 2I_z S_z t_1)\cos(\Omega I_z t_1) - I_y \cos(\pi J_{IS} 2I_z S_z t\ )\sin(\Omega I_z t_1)$$
$$- 2I_y S_z \sin(\pi J_{IS} 2I_z S_z t_1)\cos(\Omega I_z t_1) - 2I_x S_z \sin(\pi J_{IS} 2I_z S_z t_1)\sin(\Omega I_z t_1) \xrightarrow{\pi J_{IS} t_2 2I_z S_z + \Omega I_z t_2} I_x$$

Chemical shift and scalar coupling of the I coherence is refocused.

The effect of the spin-echo sequence upon the S spin coherence is given by the product operator transformations:

$$S_x \xrightarrow{\pi J_{IS} t_1 2I_z S_z + \Omega S_z t_1} S_x \cos(\pi J_{IS} 2I_z S_z t_1)\cos(\Omega S_z t_1) + S_y \cos(\pi J_{IS} 2I_z S_z t_1)\sin(\Omega S_z t_1)$$
$$+ 2S_y I_z \sin(\pi J_{IS} 2I_z S_z t_1)\cos(\Omega S_z t_1) - 2S_x I_z \sin(\pi J_{IS} 2I_z S_z t_1)\sin(\Omega S_z t_1) \xrightarrow{\pi I_x}$$
$$S_x \cos(\pi J_{IS} 2I_z S_z t_1)\cos(\Omega S_z t_1) + S_y \cos(\pi J_{IS} 2I_z S_z t_1)\sin(\Omega S_z t_1)$$
$$+ 2S_y I_z \sin(\pi J_{IS} 2I_z S_z t_1)\cos(\Omega S_z t_1) - 2S_x I_z \sin(\pi J_{IS} 2I_z S_z t_1)\sin(\Omega S_z t_1) \xrightarrow{\pi J_{IS} t_2 2I_z S_z + \Omega I_z t_2}$$
$$S_x \cos(\Omega S_z 2t) + S_y \sin(\Omega S_z 2t)$$

Chemical shift of S is not refocused due to application of the π pulse to I spins only.
The IS scalar coupling is refocused as a result of the inversion of the I spin system: the I spin states, α or β, associated with each S coherence (which define their evolution frequencies) are

interchanged by the π_{Ix} pulse. Consequently the components of the S coherence evolve with the opposite frequency during the second time period $\mathbf{t_2}$. The S spin coherences are said to have had their 'spins re-labelled' by the π_{Ix} pulse.

Insertion of a simultaneous π_x pulse to S in the same spin-echo sequence leads to refocusing due to chemical shift of both coherences at the end of $\mathbf{t_2}$. However, the simultaneous 'spin re-labelling' of I and S causes the coherence to continue to evolve due to scalar coupling during $\mathbf{t_2}$. Therefore, as evolution due to chemical shift is refocused for spins I and S, one may omit the chemical shift Hamiltonain for spin-echo sequences. The overall transformation of the product operators for coherences I and S due to the modified spin-echo sequence (simultaneous inversion pulses applied to I and S) is given by:

$$
\begin{aligned}
I_x + S_x \xrightarrow{\pi J_{IS} t_1 2I_zS_z} & S_x \cos(\pi J_{IS} 2I_zS_z t_1) + 2S_yI_z \sin(\pi J_{IS} 2I_zS_z t_1) + \\
& I_x \cos(\pi J_{IS} 2I_zS_z t_1) + 2I_yS_z \sin(\pi J_{IS} 2I_zS_z t_1) \\
\xrightarrow{\pi I_x + S_x} & S_x \cos(\pi J_{IS} 2I_zS_z t_1) + 2S_yI_z \sin(\pi J_{IS} 2I_zS_z t_1) + \\
& I_x \cos(\pi J_{IS} 2I_zS_z t_1) + 2I_yS_z \sin(\pi J_{IS} 2I_zS_z t_1) \\
\xrightarrow{\pi J_{IS} t_2 2I_zS_z} & S_x \cos(\pi J_{IS} 2I_zS_z 2t) + 2S_yI_z \sin(\pi J_{IS} 2I_zS_z 2t) + \\
& I_x \cos(\pi J_{IS} 2I_zS_z 2t) + 2I_yS_z \sin(\pi J_{IS} 2I_zS_z 2t)
\end{aligned}
$$

The spin-echo has served to phase and amplitude modulate I and S coherence, as a function of **J** and the total evolution period 2**t**.

A8.2.8.4 Evolution of Homonuclear scalar couplings only

The effect of a spin-echo sequence applied to on a homonuclear two-spin scalar coupled system, I_1 I_2, is exactly analogous to that described for the effect of the spin-echo, with simultaneous π pulses applied to I and S in heteronuclear systems. The π pulse is applied to all I spins of the system simultaneously, causing refocusing of chemical shift and continued evolution of scalar coupling. The latter is due to the simultaneous spin re-labelling of both I spins.

If it were possible to execute a frequency selective π pulse to one of the I spin multiplets, the effect of the chemical shift for the I spin to which the pulse was applied would be refocused.

Furthermore scalar coupling evolution of both spins would be refocused. However, evolution due to chemical shift of the other I spin would not be refocused.

A8.2.9 Excitation of multiple quantum coherence

The product operator description of a simple pulse sequence for the excitation of multiple quantum coherence in a two-spin scalar coupled system IS is given below

$$
\begin{aligned}
I_z \xrightarrow{(\pi/2)I+S_x} -I_y \xrightarrow{t} &\left\{\begin{array}{r} -I_y\cos(\Omega I_z t)\cos(\pi J_{IS} t 2I_z S_z) \\ I_x\sin(\Omega I_z t)\sin(\pi J_{IS} t 2I_z S_z) \\ 2I_x S_z\cos(\Omega I_z t)\cos(\pi J_{IS} t 2I_z S_z) \\ 2I_y S_z\sin(\Omega I_z t)\sin(\pi J_{IS} t 2I_z S_z)\end{array}\right\} \xrightarrow{(\pi/2)I+S_x} \\
&-I_z\cos(\Omega I_z t)\cos(\pi J_{IS} t 2I_z S_z) \\
&I_x\sin(\Omega I_z t)\sin(\pi J_{IS} t 2I_z S_z) \\
&-2I_x S_y\cos(\Omega I_z t)\cos(\pi J_{IS} t 2I_z S_z) \\
&-2I_z S_y\sin(\Omega I_z t)\sin(\pi J_{IS} t 2I_z S_z)
\end{aligned}
\qquad \text{A8- 8.7}
$$

The amplitude of multiple quantum coherence depends on $\mathbf{J}_{IS}$ and the delay t. For example, neglecting chemical shift, the amplitude of coherence $2I_{1x}I_{2y}$ from above is modulated according to $\sin(\pi \mathbf{J}_{IS}t)$. Since the extent of coupling and range of coupling constants varies considerably between spin systems, the amplitude and order of multiple quantum coherences excited is often not uniform. Multiple quantum coherences can be reconverted into single quantum coherence for detection by suitably phased pulses.

A8.2.9.1 Evolution of multiple quantum coherence due to chemical shift

Evolution of multiple quantum coherence due to chemical shift is given by the general rule,

$$
\{q-\text{spin}-\text{pQC}\}_x \xrightarrow{\sum \Omega_k I_{kz} t} \{q-\text{spin}-\text{pQC}\}_x \cos\Omega_{\text{eff}} t + \{q-\text{spin}-\text{pQC}\}_y \sin\Omega_{\text{eff}} t
$$

Where **q** is the total number of product operators and **p** is the coherence order

$$
\mathbf{p} = \Delta m = \sum_k \Delta m_k \quad \text{and} \quad q = \sum_k |\Delta m_k|, \Omega_{\text{eff}} = \sum_k \Delta m_k \Omega_k
$$

and $\Delta m_k = \pm 1$ depending on the change in quantum number of spin k.

For example, evolution due to chemical shift of the double quantum coherence $2I_xS_x$ during a time **t** is given by:

$$2I_xS_x \xrightarrow{(\Omega I_z+\Omega S_z)t} 2\left[I_x \cos\Omega I_z t + I_y \sin\Omega I_z t\right]\left[S_x \cos\Omega S_z t + S_y \sin\Omega S_z t\right]$$

Pure double and zero quantum coherences evolve at the sum and difference of the of the chemical shifts respectively, given by:

$$\{2QC\}_x \xrightarrow{(\Omega_I I_z+\Omega_S S_z)t} \{2QC\}_x \cos(\Omega_I + \Omega_S)t + \{2QC\}_y \sin(\Omega_I + \Omega_S)t$$

$$\{ZQC\}_x \xrightarrow{(\Omega_I I_z+\Omega_S S_z)t} \{ZQC\}_x \cos(\Omega_I - \Omega_S)t + \{ZQC\}_y \sin(\Omega_I - \Omega_S)t$$

Therefore, pure homonuclear zero quantum coherence is said to be invariant to evolution due to chemical shift since the difference in Larmor frequencies is negligible.

A8.2.9.2 Phase properties of multiple quantum coherence

The effect upon multiple quantum coherence due to a shift in phase of Φ radians caused by e.g., a Z-gradient pulse or the rotation of the detection axis, can be summarised by the following transformation, which amounts to a rotation about the Z-axis.

$$\{q-\text{spin}-\mathbf{p}QC\}_x \xrightarrow{\Phi I_z} \{q-\text{spin}-\mathbf{p}QC\}_x \cos\mathbf{p}\Phi + \{q-\text{spin}-\mathbf{p}QC\}_y \sin\mathbf{p}\Phi$$

Therefore, in general, multiple quantum coherence exhibits a **p**-order sensitivity to phase shifts. Therefore, a $\pi/2$ phase shift would rotate homonuclear pure double quantum coherence twice as far as single quantum coherence, while leaving zero quantum coherence invariant. The difference in evolution and phase characteristics provides the means to separate coherence in terms of its order.

One may specify the effect of a spatially dependent magnetic field inhomogeneity or a Z-gradient, $\Delta\mathbf{B_0}(r)$, in terms of the precessional frequency, ω_{MQC}, of multiple quantum coherence by:

$$\omega_{MQC} = \sum_k \Delta m_k [\omega_k + \gamma_k \Delta B_0(r)] \qquad \text{A8- 8.8}$$

A8.2.9.3 Evolution of multiple quantum coherence due to scalar coupling

By analogy with evolution due to the effective chemical shift, Ω_{eff}, a linear combination of all spin couplings $\mathbf{J}_{km}$ between active spins **k** and passive spins **m** is given by $J_{eff} = \sum_k \Delta m_k J_{km}$.

Evolution due to $\mathbf{J}_{eff}$ is given by:

$$\{q-spin-pQC\}_x \xrightarrow{\sum_k \pi J_{km} t 2I_{kz} I_{mz}} \{q-spin-pQC\}_x \cos \pi J_{eff} t + 2I_{mz} \{q-spin-pQC\}_y \sin \pi J_{eff} t$$

For example, in a three-spin system I S M, where spins I and S share scalar coupling but only S couples to M, the multiple quantum coherence $2I_xS_y$, will develop scalar coupling between the active spin S and passive spin M during a suitable evolution period.

$$2I_xS_y \xrightarrow{\pi J_{km} t 2I_zS_z} 2I_xS_y \cos(\pi J_{IS} t) - 4I_xS_xM_z \sin(\pi J_{IS} t)$$

When the maximum order of coherence has been excited, for example $2I_xS_x$ in a two-spin system, so that it can not evolve with passive spins, the product operator remains invariant under the transformation of scalar coupling.

A8.2.9.4 Refocusing the effects of evolution of multiple quantum coherence

The behaviour of multiple quantum coherence to a spin echo is exactly analogous to that of single quantum coherence, with the exception of **p** order sensitivity to evolution.

A8.3 Coherence Transfer

As well as exciting multiple quantum coherence, the pulse sequence of expression A8-8.7 also caused the transformation of anti-phase single quantum coherence of I ($2I_yS_z$) into anti-phase single quantum coherence of S ($2I_zS_y$). This phenomenon is just one example of coherence transfer and during a suitable time period, the transferred anti-phase coherence (S) can evolve under the influence of scalar coupling into observable coherence.

The example given above belongs to the generic set of experiments utilising the evolution of coherence due to scalar coupling using non frequency-selective, or hard pulses. The transfer is said to occur via a **J**-ordered state, which corresponds to longitudinal (Zeeman) spin-order. Coherence transfer underpins many of the more complex and informative pulse NMR experiments because the nature of the transfer invokes certain important properties upon the phase and magnitude of the observable coherence.

The magnitude and phase of the transferred coherence will depend not only upon the properties of the destination coherence (in this case, S) but also the magnitude and phase of the coherence from which it originated (in this case, I). Specifically, these properties will be for the originating coherence, (neglecting effects due to imperfect pulse etc) where those properties effecting phase as well as magnitude are highlighted in italics:

- γ
- The isotopic abundance
- The absolute abundance in the sample volume
- T_1 and the inter-pulse sequence relaxation delay
- *The modulation of the coherence due to chemical shift and scalar coupling*
- The degree of transverse relaxation during evolution period(s) (T_2)

And for the single quantum coherence of the destination spin:

- *the modulation of the coherence due to chemical shift and spin coupling*
- The degree of transverse relaxation during that evolution period (T_2)

The coherence transfer as described by equation A8-8.7 has modulated the frequency of the destination coherence as a function of chemical shift and/or spin coupling of the original spin. Indeed coherence transfer of this type underpins multi-dimensional NMR spectra used to correlate spins that exhibit scalar coupling with one another.

A8.3.1 Polarisation Transfer: The refocused INEPT experiment

The INEPT (Insensitive Nuclei Enhanced by Polarisation Transfer) pulse sequence [1, 4, 43] was designed to enhance the signal-to-noise ratios of the of *insensitive* nuclei, e.g., ^{13}C,

which suffer from low γ and low natural isotopic abundance (dilute spins). The sequence utilises polarisation transfer, a form of coherence transfer, whereby the polarisation of a *sensitive* spin (^{1}H) with high γ and high isotopic abundance is transferred to an *insensitive* nucleus via scalar coupling. The refocused INEPT pulse sequence [1, 43, 4] incorporates an extra refocusing period after polarisation transfer, which refocuses anti-phase coherence of the insensitive nuclei, into in-phase coherence prior to acquisition. Consequently, broadband decoupling of protons (Appendix A3.2.8) during acquisition can be used to further increase the signal-to-noise ratio of the insensitive nuclei.

Consider a two-spin scalar coupled system I and S where I is the sensitive spin (^{1}H) and S is the insensitive spin, e.g., ^{13}C. At equilibrium the difference in magnetisation or polarisation between the individual transitions of the I and S spins exhibits a weighting proportional to the ratio of the two gyromagnetic ratios [4]. Therefore, the density operator describing the equilibrium condition maybe written:

$$\sigma_{eq} \approx I_z + \frac{\gamma_S}{\gamma_I} S_z$$

The refocused INEPT sequence is shown in figure A8.10. The product operators are given for the points labelled σ_n in the pulse sequence.

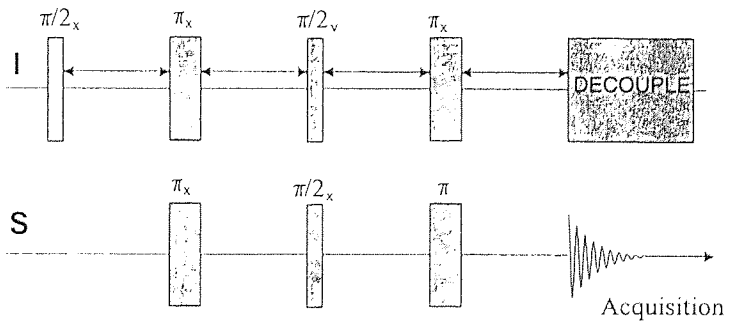

Figure A8.10 Refocused INEPT pulse sequence

$$\sigma_1 \approx -I_y + \left(\frac{\gamma_S}{\gamma_I}\right) S_z$$

During t_1, chemical shift and inhomogeneous line broadening is refocused while scalar coupling. The overall transformation is given by:

$$\sigma_2 \approx -I_y + \left(\frac{\gamma_S}{\gamma_I}\right)S_z \xrightarrow{\pi I_y} \xrightarrow{\pi S_y} \xrightarrow{\pi J_{IS} t_1 2I_z S_z} I_y \cos \pi J_{IS} t_1 - 2I_x S_z \sin \pi J_{IS} t_1 - \left(\frac{\gamma_S}{\gamma_I}\right)S_z$$

The ($\pm \pi/2_y$) and ($\pi/2_x$) pulses applied to I and S respectively are cycled over two transients such that the I pulse phase is alternated (as above) with respect to a constant S pulse phase. This phase cycling routine has the effect of cancelling the contribution of the longitudinal magnetisation of S spin on the right hand side of σ_4.

$$\sigma_3 \approx I_y \cos \pi J_{IS} t_1 - 2I_z S_z \sin \pi J_{IS} t_1 - \left(\frac{\gamma_S}{\gamma_I}\right)S_z$$

$$\sigma_4 \approx I_y \cos \pi J_{IS} t_1 - 2I_z S_x \sin \pi J_{IS} t_1 + \left(\frac{\gamma_S}{\gamma_I}\right)S_y$$

σ_3 illustrates the **J**-ordered state, i.e., longitudinal two-spin (Zeeman) order, which is a pre-requisite of all polarisation transfer experiments.

By analogy with the first evolution period, t_1, the final refocusing period, t_2, leads to the same overall transformation of the product operators, however, with the modulation of scalar coupling according to 3/8**J**. Assuming no broadband decoupling during acquisition, the following coherence exists:

$$\sigma_5 \approx -2I_x S_z \sin \pi J_{IS} t_1 \cos \pi J_{IS} t_2 - S_y \sin \pi J_{IS} t_1 \sin \pi J_{IS} t_2$$

As opposed to the native polarisation of the S spin (as indicated on the right hand side of equation $\sigma 4$ $(\gamma_S / \gamma_I)S_y$) the S spin has attained an enhancement by a factor γ_I / γ_S, which for a I = ^{1}H and S = ^{13}C equates to an enhancement factor of 4. The added advantage of polarisation transfer experiments is that the inter-pulse relaxation delay need only depend upon the generally much shorter T_1 of I.

A8.3.1.1 Multiple couplings and spectral editing in refocused INEPT

It can be shown [11] that for broadband decoupled spectra the magnitude and sign of S coherence for a number (n) of scalar couplings (I_nS) is given by the general transfer function:

$$-n\gamma_I S_x \sin \pi J_{IS} t_1 \sin \pi J_{IS} t_2 \cos^{n-1} \pi J_{IS} t_2$$

The transfer functions for short-range scalar couplings, n = 1,2 and 3, i.e., protons directly bonded to S are:

$$\sigma_5(IS) \approx -S_x \sin \pi J_{IS} t_1 \sin \pi J_{IS} t_2$$
$$\sigma_5(I_2S) \approx -2S_x \sin \pi J_{IS} t_1 \sin \pi J_{IS} t_2 \cos \pi J_{IS} t_2$$
$$\sigma_5(I_3S) \approx -3S_x \sin \pi J_{IS} t_1 \sin \pi J_{IS} t_2 \cos^2 \pi J_{IS} t_2$$

The transfer functions illustrate the magnitude dependence of S on t_1 and t_2 and also the sign dependence (phase) on t_2 due to the cosine dependence. Since a variance in scalar coupling constants exist in the spin system, a compromise value of t_1 is sought to maximise polarisation transfer. The value of t_2 is set to 3/8**J**, which facilitates the *spectral editing* of the S coherence according to scalar coupling multiplicity: CH and CH_3 multiplicities have the same phase, which is opposite to CH multiplicities. Spectral editing is useful for the rapid assignment of multiplicity and remains successful providing extreme coupling constants do not exist.

S nuclei may exhibit scalar coupling that occurs over multiple intervening bonds (long-range), i.e., n > 1. However, the magnitude of heteronuclear long-range couplings are a fraction of short-range couplings, such that the evolution of the former is considered ineffective during the short-range optimised evolution periods.

Appendix A9 Compensation of Off-resonance and *r.f.* inhomogeneity effects by composite pulses

NMR pulse sequence experiments are designed to manipulate the nuclear spin system in a precise fashion so as to provide specific information. The success of the experiments critically depend upon the precision of pulses in terms of their phase and nutation angles and experiments are often designed with this ideality in mind.

When the precision of pulses is compromised, the utility of the experiment can be similarly compromised, and may be manifested in the spectrum as attenuated signals, adverse phase properties or unwanted signals. Beyond the ability of the spectrometer to produce accurate pulse powers, durations and phases, and the experimenter to accurately calibrate pulse nuatation angles, off-resonance and *r.f.* inhomogeneity effects are the two primary sources of pulse imprecision.

r.f. inhomogeneites arise due to variations in the intensity of the *r.f.* field across the analytical sample volume. Neglecting sample dependent effects, *r.f.* inhomogeneites are in part dependent on the quality of *r.f.* transmitter coils in the NMR probe and their orientation relative to the sample. Indeed, as NMR hardware advances, *r.f.* inhomogeneites are becoming less of a problem in high-resolution liquid NMR experiments. The *r.f.* inhomogeneites cause inaccurate nutation angles, which vary across the sample volume and therefore are similar in effect to pulse miscalibration.

Off-resonance effects have been described in appendix A1.8.3 and cause both nutation angle and phase discrepancies, which, increase in severity with greater offset from the carrier frequency.

Composite pulses are a series of hard pulses of possibly different durations and phases that can be designed to achieve the same overall transformation as a single hard pulse while compensating for *r.f.* inhomogeneity and/or off-resonance effects. Therefore, a suitable composite pulse may be substituted for a normal hard pulse (usually a $\pi/2$ or π pulse) in a pulse sequence experiment.

Levitt and Freeman [22, 43] were the first to propose composite pulses for the replacement of single hard pulses. Previously composite pulses had been successfully applied to cause frequency selective excitation for solvent suppression purposes and for broadband decoupling (Appendix A3.2.8).

The concept of using composite pulses originated from the realisation that; a specific nutation cased by a single hard pulse can be equally achieved by any number of combinations of nutations by a composite pulse. If each possible combination is subject to the same effects, one combination will be better at compensating for *r.f.*inhomogeneity and off-resonance effects.

The design of composite pulses has evolved considerably since the early simplistic "geometrical approach"[22] (tracking of magnetisation vectors in 3-D space) to more complex computer aided design using average Hamiltonian theory and Magnus expansions [22]. Consequently, an enormous array of composite pulses have been designed, however, the choice of which one to employ is not a trivial task and requires consideration of the following factors.

Some composite pulses are only suitable for the transformation of a particular initial state, i.e., inversion of Z-magnetisation as opposed to the inversion of coherence for the purpose of refocusing. More recent methods of design [23] yield composite pulses that cause a given transformation regardless of the initial state of the spin system. Consequently, the composite pulse can be applied universally to for example, inversion of magnetisation as well as refocusing of coherence.

Some composite pulses impart phase shifts upon the final transformation, the severity of which may depend upon the extent of the *r.f.* inhomogeneity and/or off-resonance effect, which varies from spin to spin. In most circumstances such phase shifts are unwelcome since the composite pulses must be phase coherent with other pulses in the sequence.

Generally, the longer and more complex composite pulses tend to yield the best compensation efficiencies. Consequently long composite pulses may lead to unacceptable attenuation of signals due to detrimental relaxation effects and may be inappropriate for use in many multi-pulse experiments. Therefore, in general, composite pulses are more

frequently used in less complex and short pulse sequences that can better tolerate an increase in pulse sequence length.

Most composite pulses only sufficiently compensate for either *r.f.* inhomogeneity or off-resonance effects but rarely for both. Those composite pulses that do compensate simultaneously for both *r.f.* inhomogeneity and off-resonance effects, i.e., those invented by Tycko [26] are usually complex and lengthy and also suffer from the disadvantageous relaxation effects as described above. Therefore, one usually chooses a composite pulse that favours the compensation of off-resonance effects over the less severe effects of *r.f.* inhomogeneity.

Finally, the choice of composite pulse employed in a pulse sequence may be further restricted by the capabilities of the NMR spectrometer. Some of the component pulses of the more efficient composite pulses utilise nutation angles and phases that are not multiples of $\pi/2$. Subsequently, they may not be amenable on older spectrometers, which do not possess modern pulse generators and phase shifters. As the thrust of work detailed in this thesis is aimed towards experimenters that do not have access to modern NMR spectrometers, only composite pulses that utilise nutation angles and phase shifts in multiples of $\pi/2$ have been used.

Levitt has conveniently classified common composite pulses [22] according to their compensation efficiencies (determined qualitatively) while simultaneously classifying them in terms of their transformation properties as highlighted above. Furthermore, Claridge [23] has usefully summarised the important properties of a selection of available composite pulses for the compensation of off-resonance effects for pulse sequences of short duration. Both literature resources have proven useful during experimental work.

An example of the composite pulse analogue of a single hard inversion (π_x) pulse is the ($90°_x$ – $240°_y$ – $90°_x$) sequence, which compensates for off-resonance effects over a 40% larger frequency bandwidth than the single pulse. Figure A9.1 a and b illustrate the trajectories taken by 5 magnetisations, which correspond to resonance offsets between $\Delta B_1/B_1 = 0.4$ to 0.6 for the single hard inversion pulse and the composite pulse respectively.

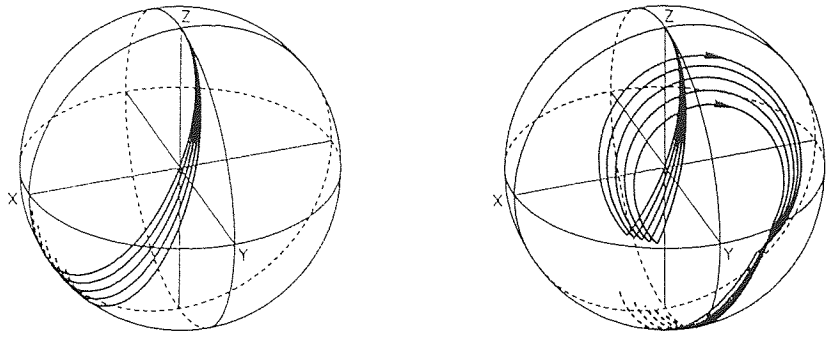

Figure A9.1 a) Hard Pulse b) Composite pulse

Reproduced from Freeman [43]

The composite pulse achieves a high level of phase and nutation angle compensation with respect to the hard pulse analogue, however, does not appreciably compensate for *r.f.* inhomogeneity at larger offsets. This composite pulse can also be used for refocusing of coherence, however, not without incurring disadvantageous phase errors [23].

Finally, the efficiency of composite pulses obviously relies upon the stability and accuracy of pulses generated by the NMR spectrometer and accurate pulse calibrations. The simple substitution of composite pulses into pulse sequences may in fact lead to detrimental effects due to the points highlighted above and it is always advised to compare compensated versions of experiments with the original. Indeed, some complex pulse sequences involving multiple quantum coherences will be intolerant to composite pulses. Although a vast number of composite pulses exist, after careful consideration of the factors described above and restrictions due to NMR spectrometer hardware, the choice of composite pulse can be quite limited.

Appendix A10 Selective Pulses

In some instances it is useful to apply pulses to a selected region of a spectrum perhaps encompassing an entire multiplet or its individual component lines while leaving all other spins unaffected. The development of such selective pulses has received widespread attention since they are central to important experimental techniques such as solvent suppression, reducing dimensionality (1-D analogues of 2-D techniques) [64] and selective coherence and magnetisation transfer techniques [44, 65-66].

A10.1 Soft selective pulses

The easiest way to produce a selective pulse is simply to significantly attenuate the power of a normal hard square wave pulse and increase its duration. In common with hard pulses, the approximate selectivity of the so-called soft rectangular pulse, or excitation bandwidth over which the pulse is effective (ν), is proportional to the inverse of the pulse length, τ_p.

Important factors that must be considered for all selective pulses are:

1) The pulse must act purely over the desired excitation bandwidth without perturbing other transitions.
2) The frequency response should ideally be uniform in terms of phase and intensity across the excitation bandwidth.
3) The increased duration of soft pulses, as opposed to hard pulses, implies that the magnetisation or coherence for which it is acting upon becomes more sensitive to T_2 relaxation.

The frequency response of a selective pulse is given by the Fourier transform of the excitation profile. The frequency response of a soft square wave pulse is similar to that of a hard pulse and exhibits a sinc-like oscillation (Appendix A1.7), with the principle pulse amplitude and phase being non-uniformly distributed over the excitation bandwidth (ν). Additionally, side lobes modulating in phase and intensity extend outward from the edge of the bandwidth (Figure A10.1).

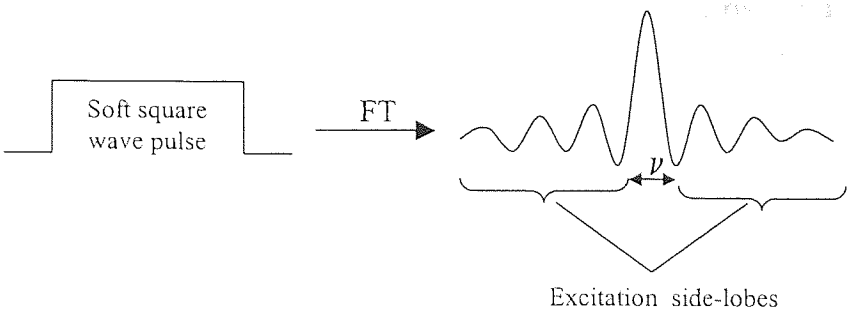

Figure A10.1 Excitation profile of a soft square wave pulse

It is evident that the soft pulse would perform poorly in terms of selectivity due to the excitation side-lobes that extend from the principal excitation bandwidth, ν. The side lobes could potentially perturb transitions outside the desired frequency range with differing phases and intensity.

The uneven intensity and phase response across the excitation bandwidth can potentially cause the component lines of a multiplet would be tantamount to peripheral lines experiencing severe off-resonance effects (Appendix A1.8.3) proportional to their offset from carrier and their location in the excitation profile. Potentially this could cause severe phase and intensity distortions of the component lines during the course of the pulse. This property would render the soft pulse as inappropriate for use in pulse sequence experiments, which often demand precise pulses in terms of phase and intensity across entire multiplets.

It is evident that the ideal excitation profile of a soft pulse would be rectangular or "top hat" shape across the excitation bandwidth. Consequently the frequency responses across the excitation bandwidth would be of constant (pure) phase and of equal intensity, while also being devoid of excitation side lobes, which would maintain selectivity.

A10.2 Shaped Soft pulses

In response to the deficiencies of soft rectangular selective pulses, soft shaped pulses were devised which had already received successful use in Magnetic Resonance Imaging (MRI). The pulse envelope or the propagation of amplitude for the duration of the pulse is shaped according to a particular profile that affords a more suitable excitation profile.

The earliest example of the use of shaped pulses was the Gaussian pulse [66], so-called due to its Gaussian pulse envelope producing an approximate Gaussian excitation profile. The

Gaussian pulse further approaches the "top hat" condition, giving rise to a more uniform distribution of amplitude and phase across the excitation bandwidth while its intensity falls more quickly to zero. However Gaussian pulses cause some phase distortions of multiplet lines within the principal excitation bandwidth but away from the exact carrier frequency. Furthermore the Gaussian pulse exhibit undesirable oscillatory behaviour at the periphery of the excitation bandwidth, which includes negative side-lobes, which induce inverted responses in these regions [23].

When Gaussian pulses are used in simple *pulse and collect* experiments these phase errors can be compensated for reasonably easily by simple phase correction of the final spectrum, since the phase distortions increase linearly with increasing offset. However, Gaussian pulses may not necessarily be appropriate for application in multipulse experiments where careful control of phase is required.

Purged half-Gaussian pulses [23] correct for phase distortions across the excitation bandwidth but requires the implementation of hard pulses directly after execution of the shaped pulse. Consequently purged half-Gaussian pulses may not be appropriate for inclusion in pulse sequences.

A10.2.1 Pure Phase shaped pulses

As the name suggests these more elaborate pulse shapes are designed to give close to pure phase and uniform amplitude across the entire excitation bandwidth derived from their "top hat-like" excitation profiles. They also give rise to better selectivity due to their minimal excitation profiles beyond the principle bandwidth.

Pure phase pulses are technically more demanding in their implementation since they require computer software control to drive the waveform generator necessary to shape the complex pulse envelopes. The first family of pure phase shaped pulses to be designed were the BURP (Band-selective, Uniform, Response, Pure phase pulse) [23]. By analogy with composite pulses (Appendix A9), the shape envelopes induce the magnetisation(s) or coherence(s) to take complex trajectories. For example the trajectories taken by magnetisation over a range of off-sets from the carrier frequency is shown schematically for the IBURP2 selective inversion pulse in figure A10.2

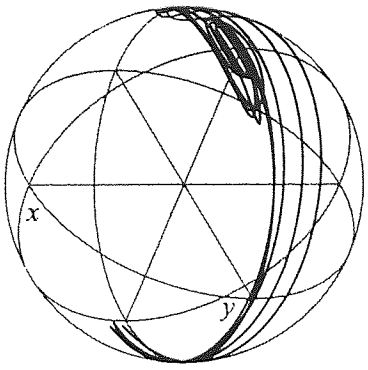

Figure A10.2 **Schematic diagram of the trajectories taken by single magnetisations for the IBURP2 selective inversion pulse. Reproduced from publication by Claridge [23].**

Another example of pure phase pulses belong to the Gaussian cascade family [23]. As the name suggests their pulse envelopes are composed of a cascade of different gaussian pulses, which are designed to invoke a particular set of nutations with the overall effect of achieving the pure phase analogue of a single gaussian pulse.

Pure phase pulses are therefore suitable for the direct replacement of hard pulses in pulse sequences without the need for compensation methods such as purging. However, they are not completely devoid of disadvantages because they are generally of longer duration than other selective pulses, which may cause detrimental T_2 relaxation effects.

In analogy to composite pulses (Appendix A9), most pure phase pulses are designed to perform a particular function on a given initial state of magnetisation or coherence. For example, a π pulse may be effective for inversion of coherence, however, may not be suitable for the inversion of longitudinal magnetisation. Some pulses are designed to act on any initial state and are thus termed "universal" pure phase selective pulses.

In experimental work detailed in this thesis, the pure phase pulses, SNEEZE, Q5 Gaussian cascade and Q3 Gaussian cascade [23] were used to affect excitation of coherence ($\pi/2$ pulse) from magnetisation, manipulation of coherence ($\pi/2$ pulses), and refocusing of coherence (π pulse) respectively. A schematic representation of their excitation profiles (and for the IBURP2 pulse given previously) is given in figure A10.3.

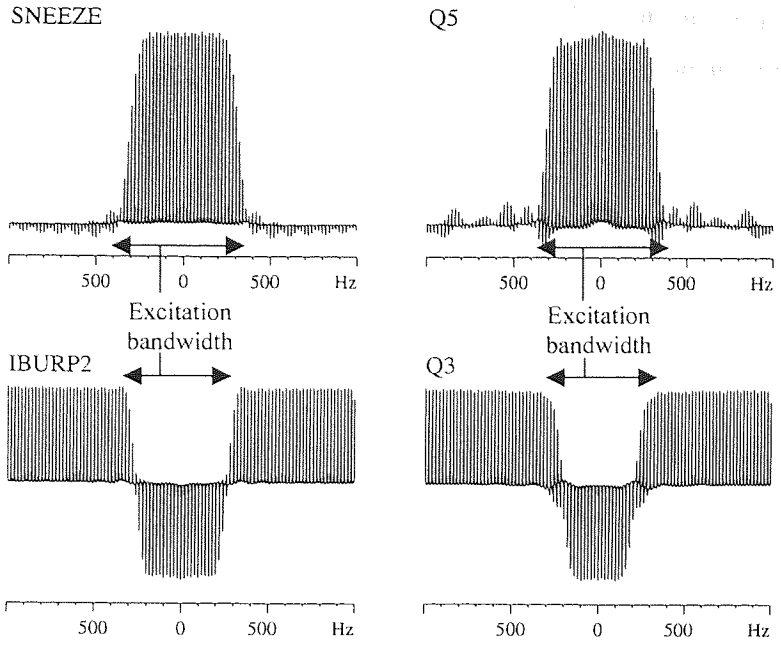

Figure A10.3 **Schematic diagram of excitation profiles for the labelled pulses. The 'top-hat' character can be easily seen which gives rise to pure phase responses across the principal excitation bandwidth. Reproduced from publication by Claridge [23].**

Soft rectangular pulses can be implemented on most spectrometers since they simply require attenuation of the pulse power, however, shaped soft pulses and pure phase pulses require software control and a waveform generator so as to appropriately shape the pulse envelope. The latter system is commonly found as standard on most modern spectrometers however, for spectrometers of lesser specification, the implementation of shaped pulses is not possible.

A10.3 The DANTE sequence

Prior to the advent of shaped pulses, and the technology to drive them, a selective excitation scheme called DANTE [25, 43-44] (Delays Alternating with Nutation for Tailored Excitation) was invented that required only the implementation of hard pulses. Therefore one is able implement selective pulses on all commercially available spectrometers with ease.

The DANTE sequence is comprised of a train of N short hard pulses of total nutation angle β, which are each separated by fixed delays τ:

$$\text{DANTE sequence : } [\beta\text{- t -}]_N.$$

The total nutation angle of the DANTE pulse is given by the sum of the pulses β and in common with soft rectangular pulses, the excitation bandwidth approximates to the inverse of the overall duration of the sequence ($[\beta\text{- t -}]_N^{-1}$s).

The effect of the DANTE pulse train at steadily increasing offsets from the carrier frequency (a to i) for single magnetisations is shown diagrammatically in Figure A10.4.

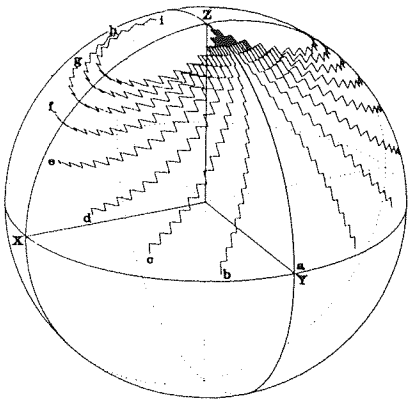

Figure A10.4 Diagram of the DANTE pulse sequence upon single magnetisations. (see text) Reproduced from publication by Freeman [43].

Magnetisations exactly on-resonance (a) experience the cumulative effect of the N pulses and effect a complete nutation in the ZY'. Those magnetisations slightly off-resonance (a-g) trace out zig-zag paths due to chemical shift evolution during the τ delays. For large offsets from the carrier (h-i), magnetisations experience small approximately circular trajectories near the Z-axis and so contribute little to the finally observed spectrum.

The excitation profile, which is given by the Fourier transform of the DANTE sequence, according to linear approximation [25] is given in figure A10.5. An interesting feature of the DANTE excitation is the presence of excitation sidebands that are symmetrically disposed about the carrier at a frequency τ^{-1}.

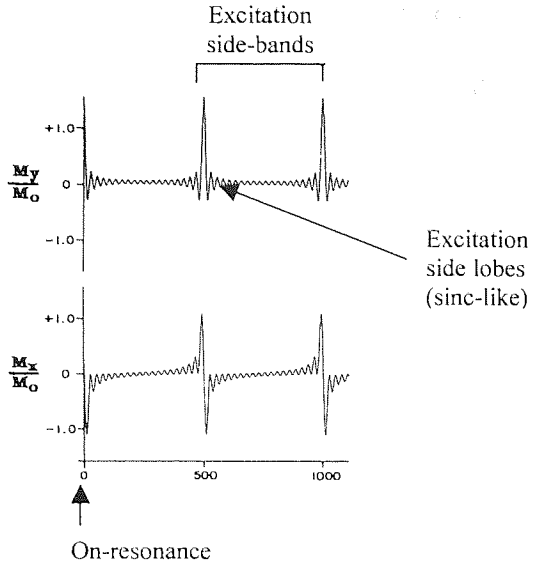

Figure A10.5 **Excitation profiles for DANTE pulse indicating excitation side-lobes and excitation side-bands. Reproduced from original DANTE publication [25]**

Maintaining selectivity over a particular region requires judicious choice of the value of τ or positioning of the carrier frequency so as not to cause unwanted excitations at the sideband frequencies.

It is evident that the DANTE excitation profile exhibits the same sinc-like oscillation side lobes as single hard-pulses, which extend outward from the excitation bandwidth decreasing to a minimum at $1/2\tau^{-1}$. Consequently, DANTE pulse trains invoke the same unfortunate phase and intensity distortions of the component lines of a multiplet over the excitation bandwidth and may not be suitable for implementation in multipulse sequences.

A10.3.1 Shaped DANTE

It is possible to shape the pulse envelope of the DANTE sequence by modulation of the duration of the component pulses producing a shaped excitation profile similar to that achieved via soft shaped pulses [44]. Shaped DANTE has received wide spread use as it its easily implemented on most NMR spectrometers without the necessity for specialist waveform generators.

A10.3.2 Implementation of shaped pulses in pulse sequences

In principal the choice of selective pulse employed in a multipulse sequence should attempt to satisfy the following criteria:

A10.3.2 Implementation of shaped pulses in pulse sequences

In principal the choice of selective pulse employed in a multipulse sequence should attempt to satisfy the following criteria:

- optimum selectivity
- Pure phase and Intensity across the excitation bandwidth (top-hat)
- Phase coherence with any other hard pulses present in the pulse sequence
- Easy implementation via existing hardware and software
- Minimum pulse duration to minimise detrimental T_2 relaxation effects
- Use of the correct type of pulse for the purpose required.

Appendix A11 Z-Gradients

The dephasing of coherence using Z-gradients [67-68] (B_0 gradients) has been used extensively in one and multi-dimensional pulse NMR experiments. Indeed, Z-gradients have received popular use for the dephasing of coherence in NOESY experiments (Z-filtering) to obtain a similar state of pure magnetisation to that required in selective PENDANT-1-D HOESY.

Application of a Z-gradient pulse causes coherence to be rotated, or de-phased about the Z-axis in addition to that caused by inherent chemical shifts and scalar couplings. The angle through which single quantum coherence is dephased by a Z-gradient of magnitude, $B_{g(z)}$ applied for a duration, t_g, is given by:

$$\phi_{(z)} = \gamma B_0 \tau_g + \gamma \epsilon B_{g(z)} \tau_g \qquad \text{A11- 11.1}$$

Where ϵ is a spatially dependent term, i.e., the abscissa of the molecule containing the nuclear spins. Therefore, dephasing of coherence also depends linearly on the spatial location of the nuclei in the sample at the time of application of the Z-gradient. The spatial dependence is represented pictorially in figure A11.1.

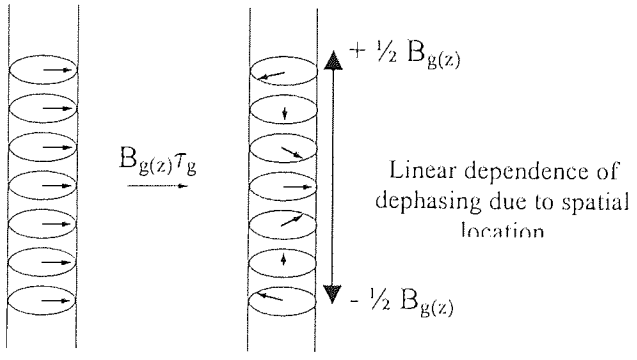

Figure A11.1 **Dephasing of single quantum coherence (depicted by single vectors) by a Z-gradient pulse. Modified from Claridge [23]**

Z-gradients invoke phase shifts that are proportional to coherence order **p**:

$$\phi = B_{g(z)} \tau_g \sum_I \mathbf{p}_I \gamma_I$$

It can be approximated that for spin systems that exhibit weak scalar coupling that a Z-gradient of sufficient duration and strength leads to the complete dephasing of coherence, while magnetisation remains invariant.

A11.1 Experimental considerations of applying Z-gradients

The application of Z-gradient pulses involves the following well-known factors

- Perturbation of the field –frequency lock system (Appendix A4.3) – The degradation of $\mathbf{B}_0$ homogeneity during the Z-gradient pulse obviously adversely affects the deuterium lock signal leading to a momentary loss in the field-frequency lock. Since the lock signal is typically integrated over longer time scales than the gradient pulse, the resolution of the experiment is maintained. However, one must incorporate gradient recovery periods into pulse sequences, which are minimum time delays that are required for the recovery of the lock system and other important functions (Appendix A4.5.6).

- On application of a Z-gradient pulse, eddy currents are induced in hardware components, which are in proximity to the z-gradient coils. Subsequently, the eddy currents induce spurious magnetic fields in the analytical sample potentially leading to artefacts in the spectrum. The Z-gradient coils in the NMR probe used in experimental work are *actively shielded* [23], which greatly attenuates the eddy currents. Furthermore, a shaped gradient pulse with a half sine wave profile was used. The gentle rise and fall of the Z-gradient due to the shaped profile further reduces the potential for inducing eddy currents [23]

In common with the effects of chemical shift and $\mathbf{B}_0$ inhomogeneity, the effects of Z-gradient pulses can be similarly refocused. Indeed pulsed field gradient spin echo (PGSE) experiments (which comprise *r.f.* refocusing pulses and two identical Z-gradient pulses of opposing polarity) [67] can be used to selectively refocus coherences due to their particular orders **p**. Consequently one must ensure that unfortuitous refocusing of coherence does not occur as a result of the pulse/gradient sequence construction. One

way to ensure this is to scramble the Z-gradient amplitudes and polarities as recommended by Freeman [43].

A11.2 Homospoil pulses

Investigative work into selective PENDANT 1-D-HOESY was performed using a Z-gradient probe on a spectrometer equipped with shaped gradient capacity. However, those users that do not have access to Z-gradient probes and modern NMR instruments (for which the thrust of this work is largely dedicated) can achieve a similar effect by implementing a *homospoil* pulse. One can purposely invoke a large perturbation in the current of one of the Z (Spinning shims) with a specified duration and polarity by analogy with a Z-gradient pulse. Consequently, the momentary loss in $\mathbf{B}_0$ inhomogeneity causes dephasing of coherence, however, without the accuracy that is inherent to the more formally applied z-gradient pulses. However, for the purpose of purely dephasing coherence, these homospoil pulses are clearly sufficient.

The significant disadvantages of homospoil pulses are the significant induction of eddy currents and long recovery times of the field-frequency lock system. Indeed the latter may take up to one hundred times longer than that of Z-gradient pulses and approach or even extend greater than one second. In the context of selective PENDANT-1-D HOESY, this extra recovery time does not constitute a problem for the following reasons:

- the longitudinal relaxation times T_1 of ^{13}C are long. Therefore, for half the number of transients (whereby the ^{13}C magnetisation during the preparation element is –Z (chapter 4.)), there will be a negligible loss in available magnetisation, which is subsequently read for selective PENDANT acquisition. Furthermore this is offset against advantageous longitudinal relaxation that occurs for the other half of transients where ^{13}C magnetisation is positive.

- The homospoil pulse (and subsequent recovery time) at the end of the 1-D HOESY mixing time (selective PENDANT acquisition time) will generally be accommodated: The 1-D HOESY mixing time is nominally optimised to $1.5T_1$ of the protons. In small organic molecules in a deoxygenated sample the mixing time will be of the

order of the typical acquisition time of selective PENDANT and homospoil pulse and corresponding recovery time.

- The only real disadvantage is in relation to extended experimental times. However, in comparison to the summation of the two separate experiments a time-saving will still be realised.

Appendix A12 Basic Quantum Mechanics and NMR Hamiltonians

In quantum mechanics the system under scrutiny is described by a set of wavefunctions, which are complex functions that in general, vary with time. In NMR the wavefunctions of concern are those that define the nuclear spin states. Indeed the wavefunctions, or basis states of the spin system have already been introduced in a simplified notation. For example, the spin states α and β represent the angular momentum and hence the magnetic moment vector along the z-axis ($\mathbf{B}_0$) for individual nuclei. However, when used to describe the spin states of an ensemble of nuclei, they represent the product of the wavefunctions (basis states) of the individual nuclei or product basis. The product basis are denoted more appropriately by the *bra-ket* notation introduced by Dirac: where the *ket* notation of α and β is given by $|\alpha>$ and $|\beta>$ and the complex conjugate ($|\alpha>^*$) or *bra* notation is given by $<\alpha|$. The wavefuntions are orthonormal, i.e., they are orthogonal ($<\alpha|\beta> = <\beta|\alpha> = 0$) and normalised ($<\alpha|\alpha> = <\beta|\beta> = 1$).

For predicting the *observables* (outcome) of operations in NMR experiments, e.g., the effect of $\mathbf{B}_0$ on the wavefunctions or the effect of pulses, one must a apply the corresponding operator, $\hat{\mathbf{A}}$, to the wavefunction (*ket*) and complete the integral with the *bra*:

$$<\alpha|\hat{\mathbf{A}}|\alpha> = \oint \alpha^* \hat{\mathbf{A}}\, \alpha\, dt = <\hat{\mathbf{A}}> \qquad \text{A12- 12-1}$$

where $<\hat{\mathbf{A}}>$ is the observable or expectation value. However, one usually needs to determine the observables or *expectation values* over the entire ensemble of the spin system, i.e., the ensemble average, which is simply given by a bar over the terms of equation C1.1.

Wavefunctions are said to be *eigenfuctions* of the operator being used when the result of operating on the wavefunction by the operator, $\hat{\mathbf{A}}$, generates a number or *eigenvalue* but leaves the original function unchanged. The wavefunctions $|\alpha>$ and $|\beta>$ are eigenfunctions of the nuclear spin angular momentum operators $\hat{\mathbf{I}}$ hereafter referred to simply as angular momentum operators. Indeed the eigenvalues of $|\alpha>$ and $|\beta>$ have already been seen previously (Appendix A1.4) when operated on by the longitudinal angular momentum operator $\hat{\mathbf{I}}_z$ due to the magnetic field $\mathbf{B}_0$. For example, the eigenvalues $|\alpha>$ and $|\beta>$ are +1/2

and –1/2, which correspond to the magnitudes of the 2I+1 observable values of the magnetic quantum number, m for I = ½ nuclei. (Appendix A1). The expectation value of the of longitudinal angular momentum operator $\hat{I}_z$ is therefore given by,

$$\begin{aligned} <\hat{I}_z> &= <\alpha|\hat{I}_z|\alpha> \\ &= <\alpha|\tfrac{1}{2}|\alpha> \\ &= \tfrac{1}{2}<\alpha|\alpha> \\ &= \tfrac{1}{2} \end{aligned}$$ A12- 12-2

Similarly, $<\hat{I}_z> = -\tfrac{1}{2}$ for the wavefunction $|\beta>$.

In addition $\hat{I}_z$, on can define the transverse angular momentum operators, $\hat{I}_x$ and $\hat{I}_y$ whose expectation values are the x and y components of angular momentum respectively. The operation of all the angular momentum operators on the wavefunctions gives the well-known relations:

$$\hat{I}_x|\alpha> = \tfrac{1}{2}|\beta>, \qquad \hat{I}_x|\beta> = 1/2|\alpha>$$
$$\hat{I}_y|\alpha> = \tfrac{1}{2}\,i|\beta>, \qquad \hat{I}_y|\beta> = -1/2i|\alpha>$$
$$\hat{I}_z|\alpha> = \tfrac{1}{2}|\alpha>, \qquad \hat{I}_z|\beta> = -1/2|\beta>$$

The angular momentum operators $\hat{I}_x$ and $\hat{I}_y$, can be decomposed into shift operators, ($\hat{I}^+$ and $\hat{I}^-$), which raise ($\hat{I}^+$) or lowering ($\hat{I}^-$) the z-angluar momentum (m_z) by one quanta:

$$\hat{I}^+ = \hat{I}_x + i\,\hat{I}_y$$
$$\hat{I}^- = \hat{I}_x - i\,\hat{I}_y$$

Therefore:

$$\hat{I}_x = \tfrac{1}{2}(\hat{I}^+ + \hat{I}^-)$$
$$\hat{I}_y = \tfrac{1}{2}\,i(\hat{I}^+ - \hat{I}^-)$$

It is evident from the shift operator representation that the transverse angular momentum vectors are superpositions of longitudinal spin angular momenta. Indeed, it illustrates the concept of coherence in terms of angular momentum.

The spin angular momentum operators are integral to the description of the NMR Hamiltonians, which are the energy operators that account for the relevant *internal* and

external interactions of the spin system under scrutiny. The prediction of observables, (expectation values) throughout NMR pulse sequence experiments, is facilitated by the operation of the relevant NMR Hamiltonians on the relevant wavefunctions (product functions) of the spin system. The product operator formalism is used to describe the observables and state of the spin system in the pulse sequence experiments reported in this thesis (Appendix A8). In this instance the relevant Hamiltonians at a given instant in time operate on a set of *product operators* that represent the state of entire spin multiplets.

A12.1 The NMR Hamiltonians

The nuclear spin Hamiltonian, $\mathcal{H}$, which is operative at a given time in NMR experiments is composed of some or all of the following Hamiltonians.

$$\mathcal{H} = \mathcal{H}_z + \mathcal{H}_{r.f.} + \mathcal{H}_{CS} + \mathcal{H}_J + \mathbf{H}_D + \mathbf{H}_{SR} + \mathbf{H}_Q$$

Where

$\mathcal{H}_z$ represents external magnetic fields, i.e., B_0 (Zeeman Hamiltonian)

$\mathcal{H}_{r.f.}$ represents external *r.f.* magnetic fields, e.g., pulses. (*r.f.* Hamiltonian)

$\mathcal{H}_{CS}$ represents induced magnetic fields due to orbital electronic motions (Chemical shift Hamiltonian)

$\mathcal{H}_J$ represents electron mediated (indirect (through-bond)) nuclear coupling (Scalar coupling Hamiltonian)

$\mathcal{H}_D$ represents direct (through-pace) magnetic dipolar coupling (Dipolar Hamiltonain)

$\mathbf{H}_{SR}$ represents moment associated with molecular angular momentum (Spin-rotation Hamiltonian)

$\mathcal{H}_Q$ represents electric field gradients (Quadrupolar coupling Hamiltonian), which is not relevant to this work and is therefore not considered.

A12.1.1 Zeeman Hamiltonian, $\mathcal{H}_z$

With B_0 considered to be oriented along the z-axis:

$$\mathcal{H}_z = \sum_i \omega_i \hat{I}_{zi}$$

Where ω_i is the Larmor frequency of spin $\mathbf{I}$ and the sum extends over all spins.

A12.1.2 Radiofrequency Hamiltonian $\mathcal{H}_{r.f.}$

The *r.f.* field is usually applied perpendicular to B_0. If the *r.f.* field is applied along the x' axis of the rotating frame, i.e., x-phase then:

$$\mathcal{H}_{r.f.} = B_1(t)\cos(\omega t + \varphi(t)) \sum_i \gamma_i \hat{\mathbf{I}}_{xi}$$

Where spins **i** are homonuclear. $B_1(t)\cos(\omega t + \varphi(t))$ signifies that the *r.f.* field can be modulated in magnitude and phase respectively at a constant carrier frequency ω. Neglecting off-resonance effects (Appendix A1.8.3), for a *r.f.* pulse of constant amplitude and phase (+x), $\mathcal{H}r.f.$ is given by:

$$\mathcal{H}r.f. = \beta / t_p \sum_i \hat{\mathbf{I}}_{xi}$$

Where the nutation angle, $\beta = -\gamma_i B_1 t_p$, where t_p is the pulse length.

A12.1.3 Chemical shift Hamiltonian, $\mathcal{H}_{CS}$

The chemical shift Hamiltonian in an isotropic liquid (for which work detailed in this thesis relates) can be written:

$$\mathcal{H}_{CS} = \sum_i -\gamma_i \mathbf{B}_0 \sigma \hat{\mathbf{I}}_{zi}$$

Where spins **i** are homonuclear and σ is the chemical shift shielding tensor (Appendix A3.1.1).

A12.1.4 Scalar coupling Hamiltonian

The isotropic weak scalar coupling (Appendix A3.2) Hamiltonian (which relates to the work detailed in this thesis) is given by:

$$\mathcal{H}_J = \sum_{i<k} 2\pi \mathbf{J}_{ik} \hat{\mathbf{I}}_{zi} \hat{\mathbf{I}}_{zk}$$

Where J_{ik} is the scalar coupling constant (Appendix A3.2) measured in 2π radians s^{-1}.

A12.1.5 Dipolar Hamiltonian, $\mathcal{H}_D$

The dipolar Hamiltonian can be written:

$$'H_D = \frac{1}{2}\sum_{j=1}^{N}\sum_{k=1}^{N}\left[\frac{\mu_j.\mu_k}{r_{jk}^3} - \frac{3(\mu_j.r_{jk})(\mu_k.r_{jk})}{r_{jk}^5}\right] \qquad \text{A12- 12-3}$$

where $\mu_i = \gamma_i\hbar\hat{\mathbf{I}}_i$ and r_{jk} is the average internuclear distance between dipoles j and k, $|r_j - r_k|$. In isotropic liquids (which relates to the work detailed in this thesis), the angular momentum terms, e.g., $\hat{\mathbf{I}}_j = (\hat{\mathbf{I}}_{xj}, \hat{\mathbf{I}}_{yj}, \hat{\mathbf{I}}_{zj})$, which are spatially modulated due to molecular re-orientation are time averaged to zero. Hence, dipolar coupling in isotropic liquids is not observed.

A12.1.6 Spin-rotation Hamiltonian, $'H_{SR}$

The spin-rotation Hamiltonian can be written:

$$'\mathbf{H}_{SR} = \sum_m \sum_i \hat{\mathbf{I}}_i \,.\, \mathbf{C}_{i,m} \,.\, \mathbf{J}_m$$

Where $\hat{\mathbf{I}}_j = (\hat{\mathbf{I}}_{xj}, \hat{\mathbf{I}}_{yj}, \hat{\mathbf{I}}_{zj})$, $\mathbf{C}_i$ is the spin-rotation interaction tensor and $\mathbf{J}_m$ is the molecular angular momentum. The Hamiltonian describes the mutual coupling of spins **i** of a molecule **m** with a molecular magnetic moment that is a consequence of molecular angular momentum.

Appendix A13 Selective PENDANT pulse program.

See Appendix A4.5 for pulse programming.

See pulse sequence diagram in Chapter 2.2 figure 2.2.

Hard pulse lengths

Proton pulses from pulse sequence

($\pi/2$) - $P_{1 \text{ and } 2}$ = 10μ seconds

(π) - P_3 = 20μ seconds

Pulse program key:

p3 = $P_{1 \text{ and } 2}$, p4 = P_3

Carbon pulses from pulse sequence

($\pi/2$) - $P_{4 \text{ and } 7}$ = 6.5μ seconds

(π) - $P_{5,6 \text{ and } 8}$ = 13.0μ seconds

Pulse program key:

p1 = P_4, p2 = $P_{5,6 \text{ and } 8}$,

Selective pulses from pulse sequence

($\pi/2$) - $P_{a \text{ and } b}$ = 0.1454 s (SNEEZE)

(π) - P_c = 0.08628 s (Gaussian Q3 cascade)

Pulse program key: **p11 = $P_{a \text{ and } b}$, p12 = P_c**

Evolution delays key: **τ_a = d3** **τ_b = d4** **τ_c = (d3 + τ_1)**

τ_1 = τ_3 (d5+d15) **τ_2 = d6**

Pulse program in proper syntax.

Highlighted text in bold and boxes are present for labelling purposes and are not part of the proper pulse program. All other statements are part of the actual program used.

Delays given by e.g. nμ, where n is a number, indicates delays in microseconds that are appended to correct for timing overheads due to pulse power switching (pl:) etc. This is to maintain accurate refocusing etc.

```
#include <avance.incl>
#include <delay.incl>

"d6=1s/(cnst1*4)"          ;defines evolution delay by cnst1= (JCH short-range) in acquisition parameters
"d5=1s/(cnst2*4)"          ;cnst2= (JCH short-range) in acquisition parameters
"d3=1s/(cnst3*4)"          ;cnst3= (JCH long-range) in acquisition parameters
"d4=1s/(cnst3*cnst4)"
"d8=(p12/2)-(p1+p6+p1/2)";defines delay prior to execution of P6 and 7 at midpoint of selective 1H pulse.
"d15=(d5-6.5u)"            ;d5 compensated for timing of pulses
"p6=2.666*p1"              ;pulse length multiplier for composite pulses
```

```
1 ze
2 d1 do:f2
  d12 pl0:f2
  d12 fq1:f2
  (p11:sp1 ph11:r):f2
  d5
  d15
  p1:f1 ph1          Staggered carbon pulse (P4) by (d5+d15) = τ1
  3u
  d3 pl0:f2
  (p12:sp2 ph16:r):f2 (d8 p1 ph7):f1
  3u
  d3 pl2:f2
  d5 fq1:f2
  d5
  (p3 ph4 d6):f2
  (p4 ph6 d6):f2 (15.15u p1 ph7):f1
  (p3 ph0):f2        (Polarisation exchange pulse 1H          (J FILTER ELEMENT)
  d5 fq1:f2
  d5
  p1:f1 ph10         (Polarisation exchange pulse 13C)
  3u
  d4 pl0:f2
  (p12:sp2 ph16:r):f2 (d8 p1 ph7):f1
  3u
  d4
3 go=2 ph29
  wr #0
  exit

ph0=1 1 3 3
ph1=0 0 2 2 1 1 3 3
ph4=0
ph5=0 1 2 3
ph6=1 1 3 3
ph7=0 2 0 2 1 3 1 3
ph10=1 1 1 1 2 2 2 2
     3 3 3 3 0 0 0 0
ph11=0 0 0 0 0 0 0 0
     2 2 2 2 2 2 2 2
ph16=0 2
ph17=1 3 1 3 0 2 0 2
ph29=1 1 3 3 2 2 0 0        Receiver phase cycle
```

A13.1 Selective PENDANT pulse program with composite pulse 1 (Chapter 2.9)

;selective PENDANT with composite pulse 180 13C pulses: 90-240-90

```
#include <avance.incl>
#include <delay.incl>

"d6=1s/(cnst1*4)"          ;defines evolution delay by cnst1= (J_CH short-range) in acquisition parameters
"d5=1s/(cnst2*4)"          ;cnst2= (J_CH short-range) in acquisition parameters
"d3=1s/(cnst3*4)"          ;cnst3= (J_CH long-range) in acquisition parameters
"d4=1s/(cnst3*cnst4)"
"d8=(p12/2)-(p1+p6+p1/2)";defines delay prior to execution of P6 and 7 at midpoint of selective 1H pulse.
"d15=(d5-6.5u)"            ;d5 compensated for timing of pulses
"p6=2.666*p1"              ;pulse length multiplier for composite pulses


1 ze
2 d1 do:f2
  d12 pl0:f2
  d12 fq1:f2
  (p11:sp1 ph11:r):f2
  d5
  d15
  p1:f1 ph1
  3u
  d3 pl0:f2
  (p12:sp2 ph16:r):f2 (d8 p1 ph7 p6 ph17 p1 ph7):f1
  3u
  d3 pl2:f2
  d5 fq1:f2
  d5
  (p3 ph4 d6):f2
  (p4 ph6 d6):f2 (15.15u p1 ph7 p6 ph17 p1 ph7):f1
  (p3 ph0):f2
  d5 fq1:f2
  d5
  p1:f1 ph10
  3u
  d4 pl0:f2
  (p12:sp2 ph16:r):f2 (d8 p1 ph7 p6 ph17 p1 ph7):f1
  3u
  d4
3 go=2 ph29
  wr #0
  exit

ph0=1 1 3 3
ph1=0 0 2 2 1 1 3 3
ph4=0
ph5=0 1 2 3
ph6=1 1 3 3
ph7=0 2 0 2 1 3 1 3
ph10=1 1 1 1 2 2 2 2
     3 3 3 3 0 0 0 0
ph11=0 0 0 0 0 0 0 0
     2 2 2 2 2 2 2 2
```

Composite pulse

Composite pulse

Composite pulse

ph16=0 2
ph17=1 3 1 3 0 2 0 2
ph29=1 1 3 3 2 2 0 0

A13.2 Selective PENDANT pulse program with composite pulse 2 (Chapter 2.9)

```
;selective PENDANT with composite pulse 180 13C pulses: 336-246-10-74-10-246-336

#include <avance.incl>
#include <delay.incl>

"d6=1s/(cnst1*4)"
"d5=1s/(cnst2*4)"
"d3=1s/(cnst3*4)"
"d4=1s/(cnst3*cnst4)"
"d8=(p12/2)-(p5+p6+p7+p8+p7+p6+p5/2)"
"d15=(d5-6.5u)"
"p5=p1*3.73"
"p6=p1*2.73"
"p7=p1*0.11"
"p8=p1*0.82"


1 ze
2 d1 do:f2
  d12 pl0:f2
  d12 fq1:f2
  (p11:sp1 ph11:r):f2
  d5
  d15
  p1:f1 ph1
  3u
  d3 pl0:f2
  (p12:sp2 ph16:r):f2 (d8 p5 ph7 p6 ph18 p7 ph17 p8 ph19 p7 ph17 p6 ph18 p5 ph7):f1
  3u
  d3 pl2:f2
  d5 fq1:f2
  d5
  (p3 ph4 d6):f2
  (p4 ph6 d6):f2 (p5 ph7 p6 ph18 p7 ph17 p8 ph19 p7 ph17 p6 ph18 p5 ph7):f1
  (p3 ph0):f2
  d5 fq1:f2
  d5
  p1:f1 ph10
  3u
  d4 pl0:f2
  (p12:sp2 ph16:r):f2 (d8 p5 ph7 p6 ph18 p7 ph17 p8 ph19 p7 ph17 p6 ph18 p5 ph7):f1
  3u
  d4
3 go=2 ph29
  wr #0
  exit

ph0=1 1 3 3
ph1=0 0 2 2 1 1 3 3
ph4=0
ph5=0 1 2 3
ph6=0 0 2 2
ph7=0 2 0 2 1 3 1 3
ph10=1 1 1 1 2 2 2 2
```

Composite pulse

Composite pulse

Composite pulse

3 3 3 3 0 0 0 0
ph11=0 0 0 0 0 0 0 0
2 2 2 2 2 2 2 2
ph16=0 2
ph17=1 3 1 3 0 2 0 2
ph18=2 0 2 0 3 1 3 1
ph19=3 1 3 1 2 0 2 0
ph29=1 1 3 3 2 2 0 0

A13.3 Selective PENDANT with DANTE proton pulses

```
;selective PENDANT with DANTE proton pulses

#include <avance.incl>
#include <grad.incl>
#include <delay.incl>

"d6=1s/(cnst1*4)"
"d5=1s/(cnst2*4)"
"d3=1s/(cnst3*4)"
"d4=1s/(cnst3*cnst4)"
"d8=(p12/2)-(p2/2)"
"d15=(d5-6.5u)"
"p6=2.666*p1"


1 ze
2 d1 do:f2
  d12 pl13:f2
  d12 fq1:f2
  p1:f1 ph1
3 d25                ;start of DANTE pulse (90)
  p5:f2 ph11
  d25                ;end of DANTE pulse (90)
  lo to 3 times l0
  3u
  2.5u               ;overhead for n+1 loops
  d3
  (p2 ph7):f1
4 d27                ;start of DANTE pulse (180)
  p7:f2 ph16
  d27                ;end of DANTE pulse
  lo to 4 times l1
  3u
  d3
  d5 fq1:f2
  d5 pl2:f2
  (p3 ph4 d6):f2
  (p4 ph6 d6):f2 (3.5u p2 ph7):f1
  (p3 ph0):f2
  d5 fq1:f2
  d5 pl13:f2
  p1:f1 ph10
  d4
5 d27                ;start of DANTE pulse (180)
  p7:f2 ph16
  d27                ;end of DANTE pulse
  lo to 5 times l1
  (p2 ph7):f1
  0.025s
  2.5u               ;overhead for n+1 loops
  d4
  go=2 ph29
  wr #0
  exit

ph0=1 1 3 3
```

```
ph1=0 0 2 2 1 1 3 3
ph4=0
ph5=0 1 2 3
ph6=1 1 3 3
ph7=0 2 0 2 1 3 1 3
ph10=1 1 1 1 2 2 2 2
     3 3 3 3 0 0 0 0
ph11=0 0 0 0 0 0 0 0
     2 2 2 2 2 2 2 2
ph16=0 2
ph17=1 3 1 3 0 2 0 2
ph29=1 1 3 3 2 2 0 0
```

Appendix A14 Selective PENDANT –1-D HOESY pulse program

Correct pulse program syntax as interpreted from Bruker Avance guide and confirmed by Bruker UK (Coventry).

See Appendix A4.5 for pulse programming.

See pulse sequence diagram in Chapter 2.2 figure 2.2.

Hard pulse lengths

Proton pulses from pulse sequence

(π/2) - $P_{1 \text{ and } 2}$ = 10μ seconds

(π) - P_3 = 20μ seconds

Pulse program key:

p3 = $P_{1,2 \text{ and } 3}$, p4 = $P_{4 \text{ and } 5}$

Carbon pulses from pulse sequence

(π/2) - $P_{4 \text{ and } 7}$ = 6.5μ seconds

(π) - $P_{5,6 \text{ and } 8}$ = 13.0μ seconds

Pulse program key:

p1 = $P_{11,16,18,19,20}$. p2 = $P_{12,13,14,15, \text{ and } 17}$

Selective pulses from pulse sequence

(π/2) - $P_{6 \text{ and } 10}$ = 0.1454 s (SNEEZE)

P_8 = 0.214s (Gaussian Cascade Q5)

(π) - $P_{7 \text{ and } 9}$ = 0.08628 s (Gaussian Q3 cascade)

Pulse program key: **p11 = $P_{6 \text{ and } 10}$, p12 = $P_{7 \text{ and } 9}$, p14 = P_8**

Evolution delays key: τ_a = d4 τ_b = d3

$\tau_1 = \tau_3$ d5 τ_2 = d6

Pulse program in proper syntax.

Highlighted text in bold and boxes are present for labelling purposes and are not part of the proper pulse program. All other statements are part of the actual program used.

Delays given by e.g. nμ, where n is a number, indicates delays in microseconds that are appended to correct for timing overheads due to pulse power switching (pl:) etc. This is to maintain accurate refocusing etc.

```
;selective PENDANT-1-D HOESY.  NBL = 2.

#include <avance.incl>
#include <grad.incl>
#include <delay.incl>


"p2=p1*2"
"p4=p3*2"
"d6=1s/(cnst1*4)"
"d5=1s/(cnst2*4)"
"d3=1s/(cnst3*4)"
"d4=1s/(cnst3*8)"
"d12=20u"
"d11=30m"
"d13=4u" ;default delays prior to and after selective pulses
"d16=1m"
"d17=3.5u"
"d18=(p14-p11)" ;compensatory delay for difference in selective pulse lengths to refocus 13C
"d8=(p12/2)-(p2/2)"

1 ze
2 d1 do:f2
  d11 st0
  d11 fq1:f2        ;Frequency set to centre of 1H chemical shift range for execution of the J-filter
  d11 pl2:f2
 (p3 ph0 d5):f2 (d17 p1 ph1):f1
 (p4 ph6 d5):f2 (d17 p2 ph7):f1
 (p3 ph4 d6):f2                          Low-pass J-filter
 (p4 ph18 d6):f2 (d17 p2 ph7):f1
 (p3 ph0):f2
  d12 fq1:f2        ;Switch between on-resonance and off resonance frequencies on concurrent transients
  (p2 ph7):f1
  d12 pl0:f2
 p11:sp1:f2 ph11:r
 d18
 d13
 d4 pl0:f2
 d13
 (p12:sp2 ph16:r):f2 (d8 p2 ph7):f1
 d13
 d4 pl0:f2                               Selective PENDANT
 p14:sp4:f2 ph0:r
 d13
 (p1 ph10):f1
 d13
 d3 pl0:f2
 (p12:sp2 ph16:r):f2 (d8 p2 ph7):f1
 d13
 d3
 (p1 ph20):f1
 50u UNBLKGRAD                           Preparation element
 p16:gp1          ; Z-GRADIENT
 d16                                          |
 d13 BLKGRAD                             Cont.
 d12 pl0:f2
```

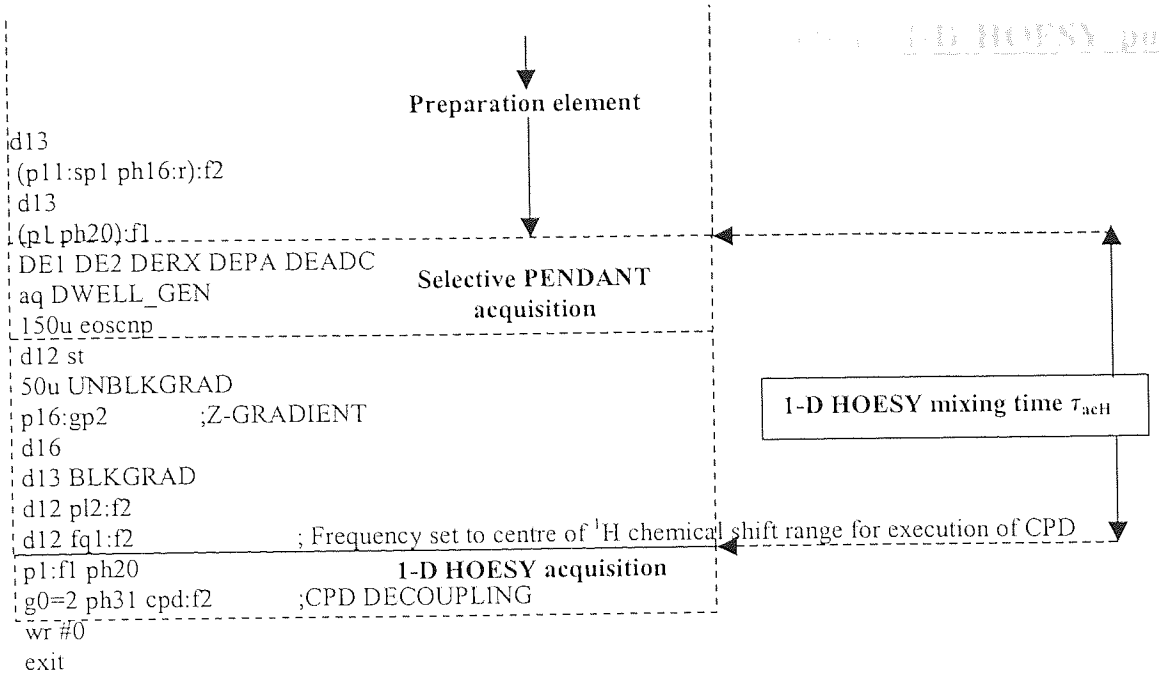


```
ph0=1 1 3 3
ph1=0 0 2 2 1 1 3 3
ph4=0
ph6=0 0 2 2
ph7=0 2 0 2 1 3 1 3
ph10=1 1 1 1 2 2 2 2
   3 3 3 3 0 0 0 0
ph11=0 0 0 0 0 0 0 0
   2 2 2 2 2 2 2 2
ph16=0 2
ph17=1 3 1 3 0 2 0 2
ph18=1 3
ph20=0 2 0 2 1 3 1 3
ph31=1 1 3 3 2 2 0 0
```

A14.1 Selective PENDANT experiment from selective –1-D HOESY pulse program

```
;selective PENDANT from selective PENDANT-1-D HOESY.

#include <avance.incl>
#include <grad.incl>
#include <delay.incl>


"p2=p1*2"
"p4=p3*2"
"d6=1s/(cnst1*4)"
"d5=1s/(cnst2*4)"
"d3=1s/(cnst3*4)"
"d4=1s/(cnst3*8)"
"d12=20u"
"d11=30m"
"d13=4u" ;default delays prior to and after selective pulses
"d16=1m"
"d17=3.5u"
"d18=(p14-p11)" ;compensatory delay for difference in selective pulse lengths to refocus 13C
"d8=(p12/2)-(p2/2)"

1 ze
2 d11 fq1:f2
  d11 pl2:f2
  50u UNBLKGRAD
  p16:gp2
  d16
  d13 BLKGRAD
  p1:f1 ph20
  d30 cpd:f2
  df do:f2
  d11
  (p3 ph0 d5):f2 (d17 p1 ph1):f1
  (p4 ph6 d5):f2 (d17 p2 ph7):f1
  (p3 ph4 d6):f2
  (p4 ph18 d6):f2 (d17 p2 ph7):f1
  (p3 ph0):f2
  d12 fq1:f2
  (p2 ph7):f1
  d12 pl0:f2
  p11:sp1:f2 ph11:r
  d18
  d13
  d4 pl0:f2
  d13
  (p12:sp2 ph16:r):f2 (d8 p2 ph7):f1
  d13
  d4 pl0:f2
  p14:sp4:f2 ph0:r
  d13
  (p1 ph10):f1
  d13
  d3 pl0:f2
  (p12:sp2 ph16:r):f2 (d8 p2 ph7):f1
  d13
```

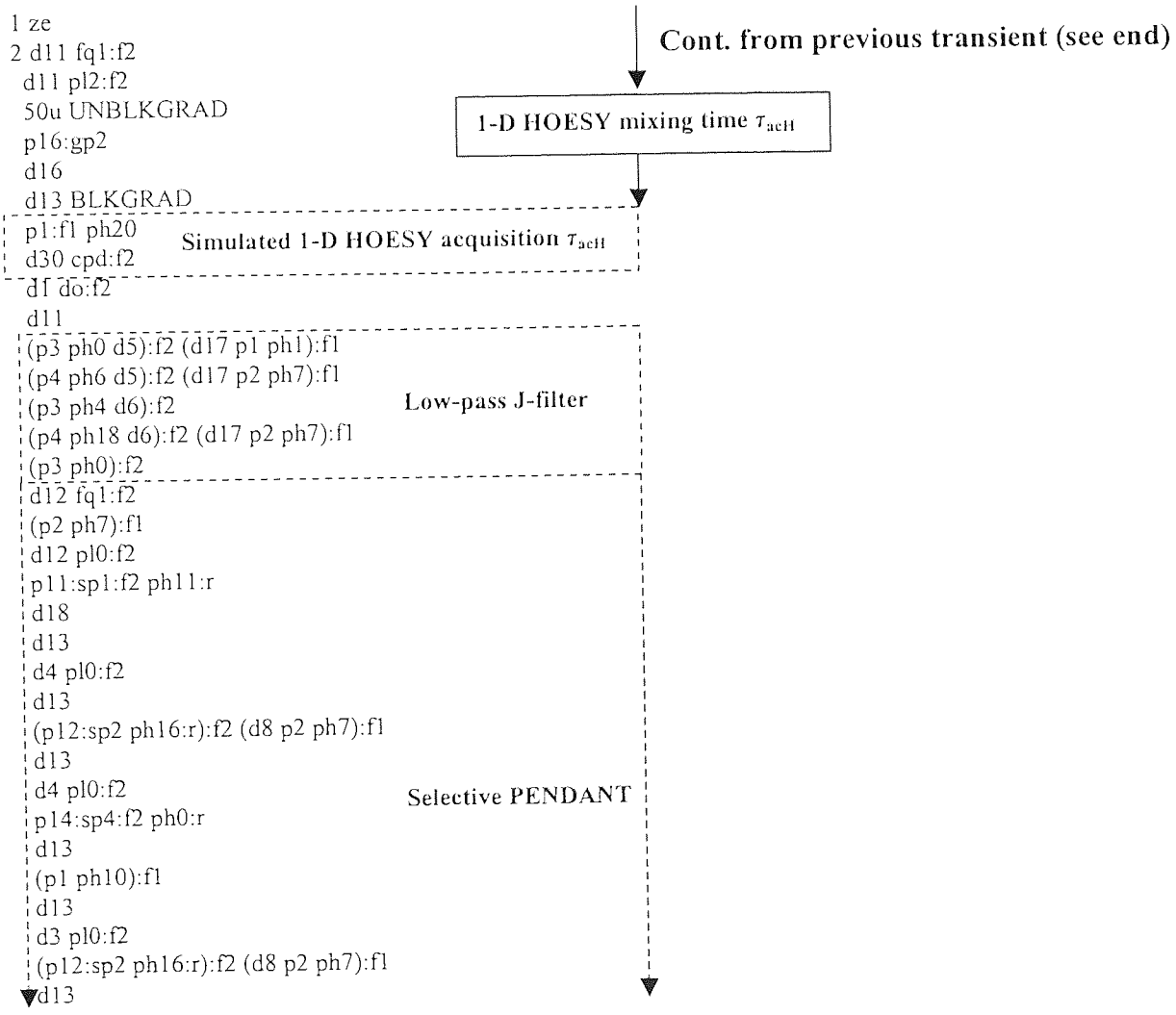

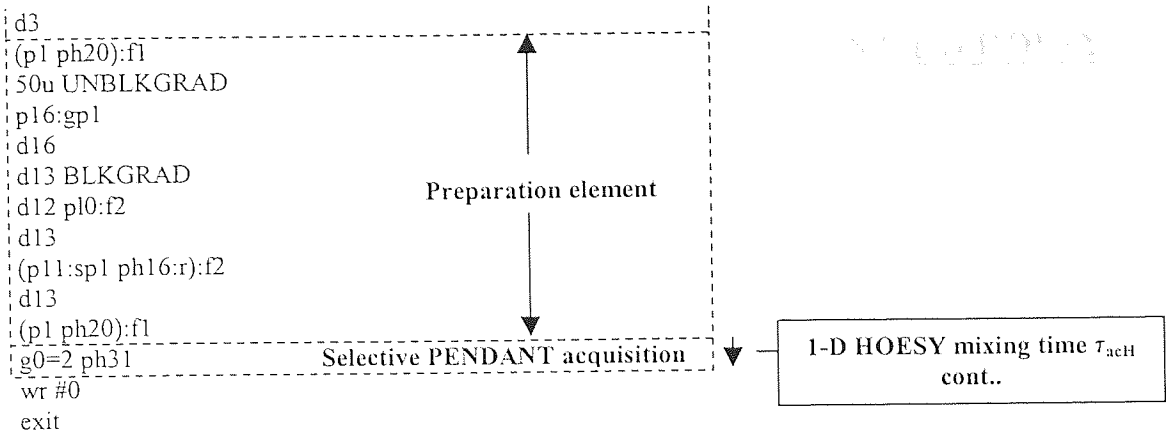

ph0=1 1 3 3
ph1=0 0 2 2 1 1 3 3
ph4=0
ph6=0 0 2 2
ph7=0 2 0 2 1 3 1 3
ph10=1 1 1 1 2 2 2 2
3 3 3 3 0 0 0 0
ph11=0 0 0 0 0 0 0 0
2 2 2 2 2 2 2 2
ph16=0 2
ph17=1 3 1 3 0 2 0 2
ph18=1 3
ph20=0 2 0 2 1 3 1 3
ph31=1 1 3 3 2 2 0 0

A14.2 1-D HOESY acquisition from selective PENDANT-1-D HOESY

```
;1-D HOESY acquisition  from selective PENDANT-1-D HOESY.

#include <avance.incl>
#include <grad.incl>
#include <delay.incl>


"p2=p1*2"
"p4=p3*2"
"d6=1s/(cnst1*4)"
"d5=1s/(cnst2*4)"
"d3=1s/(cnst3*4)"
"d4=1s/(cnst3*8)"
"d12=20u"
"d11=30m"
"d13=4u" ;default delays prior to and after selective pulses
"d16=1m"
"d17=3.5u"
"d18=(p14-p11)" ;compensatory delay for difference in selective pulse lengths to refocus 13C
"d8=(p12/2)-(p2/2)"

1 ze
2 d1 do:f2
  d11
  d11 fq1:f2
  d11 pl2:f2
  (p3 ph0 d5):f2 (d17 p1 ph1):f1
  (p4 ph6 d5):f2 (d17 p2 ph7):f1
  (p3 ph4 d6):f2                          Low-pass J-filter
  (p4 ph18 d6):f2 (d17 p2 ph7):f1
  (p3 ph0):f2
  d12 fq1:f2
  (p2 ph7):f1
  d12 pl0:f2
  p11:sp1:f2 ph11:r
  d18
  d13
  d4 pl0:f2
  d13
  (p12:sp2 ph16:r):f2 (d8 p2 ph7):f1
  d13
  d4 pl0:f2                               Selective PENDANT
  p14:sp4:f2 ph0:r
  d13
  (p1 ph10):f1
  d13
  d3 pl0:f2
  (p12:sp2 ph16:r):f2 (d8 p2 ph7):f1
  d13
  d3
  (p1 ph20):f1
  50u UNBLKGRAD
  p16:gp2                                 Preparation element
  d16
  d13 BLKGRAD                             Cont.
  d12 pl0:f2
```

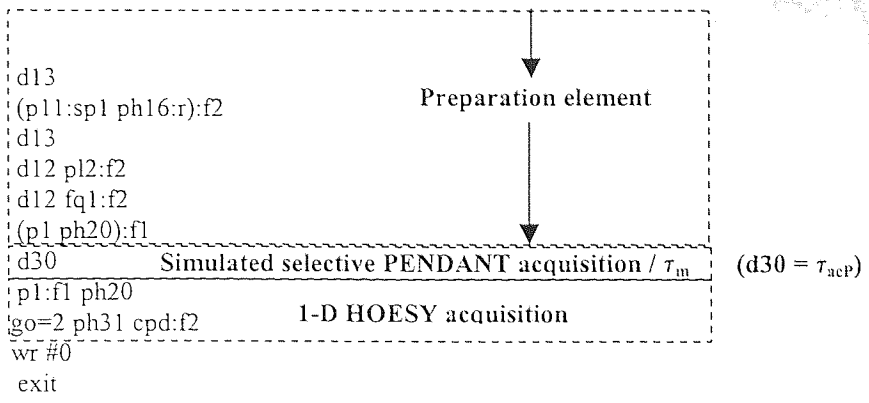


```
ph0=1 1 3 3
ph1=0 0 2 2 1 1 3 3
ph4=0
ph6=0 0 2 2
ph7=0 2 0 2 1 3 1 3
ph10=1 1 1 1 2 2 2 2
   3 3 3 3 0 0 0 0
ph11=0 0 0 0 0 0 0 0
   2 2 2 2 2 2 2 2
ph16=0 2
ph17=1 3 1 3 0 2 0 2
ph18=1 3
ph20=0 2 0 2 1 3 1 3
ph31=1 1 3 3 2 2 0 0
```